Chair of Drilling and Completion Engineering

Master's Thesis

Relief Well Profile Analysis and Evaluation of a Passive Seismic Method for Relief Well Placement in the Shallow Wisting Discovery

Manuela Kurz, BSc

Leoben, November 2018

Affidavit

I declare in lieu of oath that I wrote this thesis and performed the associated research myself using only literature cited in this volume.

Eidesstattliche Erklärung

Ich erkläre an Eides statt, dass ich diese Arbeit selbständig verfasst, andere als die angegebenen Quellen und Hilfsmittel nicht benutzt und mich auch sonst keiner unerlaubten Hilfsmittel bedient habe.

Name, 20 November 2018

Manuela Kurz

Master Thesis 2018 supervised by
Dipl.-Ing. Gerald Hollinger
Dipl.-Ing. Anton Lettner
Univ.-Prof. Dipl.-Ing. Dr.mont. Gerhard Thonhauser

Relief Well Profile Analysis and Evaluation of a Passive Seismic Method for Relief Well Placement in the Shallow Wisting Discovery

dpe DEPARTMENT PETROLEUM ENGINEERING

MONTAN UNIVERSITÄT

To my family, Anita, Friedrich, and Susanne,
who created my chance to write a thesis.

Abstract

A blowout is one of the most catastrophic events that can happen in the oil and gas industry, requiring operators to have relief well strategies in place for intersecting the out-of-control well in the worst-case scenario. The Wisting discovery imposes a unique challenge on the relief well trajectory: It is exceptionally shallow, thereby providing too little depth for the industry standard S-shaped design. Therefore, the operator has devised three J-shaped designs for potential relief wells, all of which are difficult to drill because they require either extremely high inclinations or a very high build rate. Further, the intersection process of the blowing well is complicated by the J-shaped design, leading to a longer estimated time for successful intersection and thus to an increased amount of damage in the case of a blowout.

To provide a criterion for identifying the best compromise between high build rate and high inclination, the thesis introduces a relationship between the two parameters that allows to derive a most effective build rate and corresponding inclination. The goal is to help the operator decide if one parameter should be reduced on the expense of the other, resulting in an optimized trajectory within the technical limitations of the drilling tools. Further, it provides the operator with comparable, quantitative results to justify the need for the development of higher capability directional drilling tools. To enhance the intersection process with a J-shaped relief well, it is necessary to improve the wellbore positioning accuracy. For this purpose, a seismic event positioning system that has been field tested in Wisting is evaluated for its suitability in reducing the uncertainty in the wellbore position derived from survey measurements. The objective of this evaluation is to assess if further investigation of this seismic method is likely to bring an improvement to the positioning accuracy of directional wells.

Zusammenfassung

Ein Öl- oder Gasausbruch aus einer Bohrung ist einer der katastrophalsten Zwischenfälle, die sich in der Öl- und Gasindustrie ereignen können. Die für die Bohrung verantwortlichen Unternehmen sind daher verpflichtet bereits vorab Erleichterungsbohrungen zu planen, die die außer Kontrolle geratene Bohrung im Ernstfall anbohren können. Die Lagerstätte Wisting erschwert die Planung geeigneter Bohrpfade auf spezielle Weise: Sie ist außergewöhnlich seicht und lässt es daher nicht zu, die Bohrung nach Industriestandard S-förmig zu planen. Die alternativen, J-förmig geplanten Bohrpfade sind schwierig zu bohren, da sie entweder eine extrem hohe Neigung oder eine sehr hohe Neigungsaufbaurate benötigen. Außerdem erschwert das J-förmige Design das sichere Treffen der Zielbohrung, wodurch mehr Zeit für die Erleichterungsbohrung eingeplant werden muss, während dieser der Schaden durch den Ausbruch zunimmt.

Um ein Kriterium für den besten Kompromiss zwischen hoher Neigungsaufbaurate und hoher Neigung abzuleiten, wird ein Zusammenhang zwischen den beiden Parametern hergestellt. Darauf basierend wird die effektivste Neigungsaufbaurate bei möglichst geringer Neigung bestimmt. Dadurch kann im Planungsprozess die Sinnhaftigkeit einer Erhöhung des einen Parameters auf Kosten des anderen evaluiert werden, wodurch der Bohrpfad im Rahmen des technisch Umsetzbaren optimiert wird. Außerdem stattet es den Bohrungsverantwortlichen mit belegbaren Argumenten aus, um die Weiterentwicklung geeigneter Bohrgeräte mit höherer Neigungsaufbauratenkapazität zu fordern. Um das gezielte Treffen mit einer J-förmigen Bohrung zu verbessern muss die Bestimmungsgenauigkeit der Bohrlochposition verbessert werden. Zu diesem Zweck wird ein auf seismischen Signalen beruhendes Positionierungssystem hinsichtlich seiner Eignung für die Positionsbestimmung von Bohrungen im Vergleich zu Bohrlochmessungen evaluiert, das in Wisting getestet wurde. Aufgrund dieser Evaluierung kann eine Aussage darüber getroffen werden, ob die weitere Erforschung seismischer Positionsbestimmung aus Sicht der Bohrtechnik eine Verbesserung für abgelenkte Bohrungen bringen wird.

Acknowledgements

I would like to thank Gerald Hollinger, who had the original idea for my thesis topic and supported me throughout the thesis with his technical expertise, information, and advice.

I would also like to thank Anton Lettner for his fast and excellent support that shaped this thesis.

Univ.-Prof. Dipl.-Ing. Dr.mont. Gerhard Thonhauser and the Department Petroleum Engineering, office managers Patrizia Haberl, Irene Jauk, and Bettina Matzer, create the helpful and productive environment that made it possible to follow through the process of this thesis, for which I am very grateful.

I am grateful for the opportunity to write this thesis as part of the IPA scholarship programme that was granted to me by OMV. Specifically I would like to thank Dag Breivik and the Well Engineering department for welcoming me to their office and offering their continuous support. Helene Veire at OMV (Norge) has guided me through the geophysical parts of my research and provided expert feedback.

Further, John Even Lindgård at Octio has been available for a critical discussion where he provided many helpful inputs that complemented the information provided to OMV through his company. I would therefore like to thank him and Octio.

On a professional and personal level I want to thank my mentors, Neal Whatson and Antony Martin.

Neal has encouraged and supported me during my entire time as a scholarship student and created the opportunities that eventually lead up to this thesis.

Antony has been and continues to be my friend and mentor, for which I am eternally grateful. Cheers Ant!

Contents

Chapter 1 Introduction 1

Chapter 2 The Wisting Discovery in the Barents Sea 3

2.1 Geographic Location 3

2.2 Lithology Encountered by Wisting Central 4

2.3 Horizontal Appraisal Well Wisting Central II 7

Chapter 3 Relief Well Planning 13

3.1 Spud Location 15

3.2 Relief Well Trajectory Designs 17

3.2.1 S-Shape 22

3.2.2 J-Shape 29

3.2.3 Effective Trajectory Under Constraints at Wisting 33

3.3 Directional Control 38

3.3.1 Positive Displacement Motors 38

3.3.2 Rotary Steerable Systems 40

3.3.3 DLS Prediction 45

3.4 Surveying 48

Chapter 4 Evaluation of a Passive Seismic Drill Bit Positioning Method 53

4.1 Subsurface Wave Propagation 53

4.2 Octio's DrillWatch Project on Wisting Central III 56

4.3 Application of Seismic Event Positioning Method in Relief Well Placement 61

Chapter 5 Conclusion 63

Chapter 6 Discussion 65

Appendix A 67

A.1 Relationship between lower and upper sail angle limit 67

A.2 Minimum DLS 68

A.3 Relationship between dogleg and sail angle 69

A.4 Derivative of dogleg with respect to sail angle 70

Chapter 1 Introduction

Oil and natural gas are often found trapped in reservoir rocks in the subsurface. To access these valuable resources, wells are drilled that open a pathway for the hydrocarbons to flow from the reservoir to the surface. While hydrocarbon production from the reservoir is the ultimate goal of oilwell drilling, unintentional flow of hydrocarbons during well construction is one of the greatest hazards in the process. To mitigate this and keep the well under control, primary and secondary barriers are in place and the well is constantly monitored for fluid or gas influx. Despite these safety measures, in rare instances control over a well is lost. Hydrocarbons are then violently expelled to the surface in a blowout and the outcome is catastrophic. Loss of life, damage to the environment, loss of assets, and damage to the oil industry's reputation are some of the consequences resulting from a blowout and they become more and more severe the longer the well is out of control. Therefore, it is of utmost importance to regain control of the well as fast as possible.

Because the blowing well is expelling fluids or gasses at a high rate, the well site can often not be accessed from the surface. The very last option to stop the flow is then to drill a second well that intersects the flowing well and pump heavy fluid through it until the blowout stops. This so-called relief well is spudded from a minimum safety distance of 500 m to the incident site and deviates towards the blowing well. There are two well profiles that are suitable for this purpose: the J-shaped profile and the S-shaped profile. The J-shaped well drills towards the target and intersects it directly at a high incident angle while the S-shaped profile aligns with the target wellbore before it intersects at a low incident angle.

While the goal of the well is quite simple, namely intersect the target wellbore to stop the flow, this is challenging to achieve. One major factor making intentional intersection difficult is the positional uncertainty of wellbores in the subsurface. To determine the well's position during the drilling phase, surveys are taken in discrete intervals with measurement while drilling (MWD) and sometimes gyro while drilling (GWD) tools. The tools measure the inclination and direction of the wellbore at survey stations. Every survey measurement is likely to be slightly erroneous due to limited measurement accuracy, eccentricity of the tool in the wellbore and other influences. These can be corrected for to a certain degree of accuracy. The wellbore's position is then calculated by assuming the most likely trajectory the drill bit has taken to result in the change of measured parameters between one survey station and the next. Along with the accumulating error at each subsequent survey measurement, assuming the trajectory between discrete points causes the uncertainty of the wellbore's position to increase along its measured depth. This uncertainty ranges from several metres for the vertical position to tenths of metres for the lateral position at the end of the wellbore. In addition, the position of the target wellbore is not accurately known for the same reasons.

It is therefore extremely unlikely for a J-shaped well to hit a wellbore, which measures less than half a metre across, directly upon the first attempt. Since the relief well targets

the blowing well's lowermost casing joints, there is not enough space to correct the trajectory course and attempt an intersection at a deeper point. It must be kept in mind that the reason for drilling a J-shaped trajectory that is less ideal for intersection is precisely because there is not enough vertical depth available to build an S-shaped trajectory. Thus, every time the target is missed, the relief well must be plugged back and sidetracked. This is a very time consuming process, leading to increased damage caused by the blowout.

The S-shaped profile is preferable for relief wells because it does not rely on the absolute positions of the wellbores at the critical phase of intersection. The purpose of aligning the relief well near parallel with the target well is to bring the MWD tool or dedicated ranging tools as close to the target well casing as possible while the drill bit is still in a position to intersect. By interpreting the casing interference detected on the MWD tool, the relative positions of the two wellbores is estimated. This process is repeated as the drill bit is slowly steered towards the target wellbore until it comes close enough to drill into it. This requires sufficient vertical depth for the S-shape to cover in its drop section.

The relief well plans devised by OMV (Norge) AS for the wells on the Wisting discovery in the Norwegian Barents Sea showed that aligning the bores in this way would not be possible while maintaining sufficient safety distance at surface because Wisting is a very shallow reservoir. There is not enough vertical depth to construct the drop section of an S-shaped well. A blowing well would have to be intersected directly by a J-shaped profile, resulting in an estimated time of 75 days until a blowout could be stopped. In addition, due to the shallow depth, the devised J-shaped profiles require either a high build rate or a very high final inclination, leading to severe difficulties in drilling such a profile. Therefore, relief well drilling and the positional uncertainty of wellbores remain a major concern in Wisting.

The objective of this work is to analyse the S-shaped and J-shaped well profile under the constraints imposed by the Wisting discovery and review them with the knowledge gained from one representative horizontal well on the discovery. The analysis aims to provide an optimized trajectory design within the technical limitations of market available directional drilling tools. This can help in designing directional profiles within the narrow constraints at Wisting so that they become more likely to be drillable.

Furthermore, a reservoir monitoring system that records passive seismic signals was deployed during the construction of a vertical well at Wisting. To tackle the problem of positional uncertainty in relief well drilling at Wisting, a subsurface event positioning method based on the system is evaluated for its use in drill bit positioning. If this method has the potential to reduce the positional uncertainty derived from standard survey tools, it can save critical time in relief well drilling by placing the planned profile with more accuracy. The use of this evaluation is to determine if seismic event positioning has an application in directional drilling, or if it is better to focus on further improving wellbore surveying and thus make relief well drilling as fast and efficient as possible in the worst-case scenario.

Chapter 2 The Wisting Discovery in the Barents Sea

Wisting's geographical location along with its shallow reservoir formations imposes specific challenges on relief well drilling. Therefore, its location and the lithology that overlies and comprises the targeted reservoir are introduced. The horizontal well that has been drilled is discussed within this geological frame as a base of reference. It is of particular interest because it provides the first practical experience for building inclination in the shallow lithology.

2.1 Geographic Location

The Wisting Discovery is located in production licence 537 in the Norwegian Barents Sea and operated by OMV (Norge) AS. As the map in Figure 1 shows, its location between the 73rd and 74th latitude is very remote.

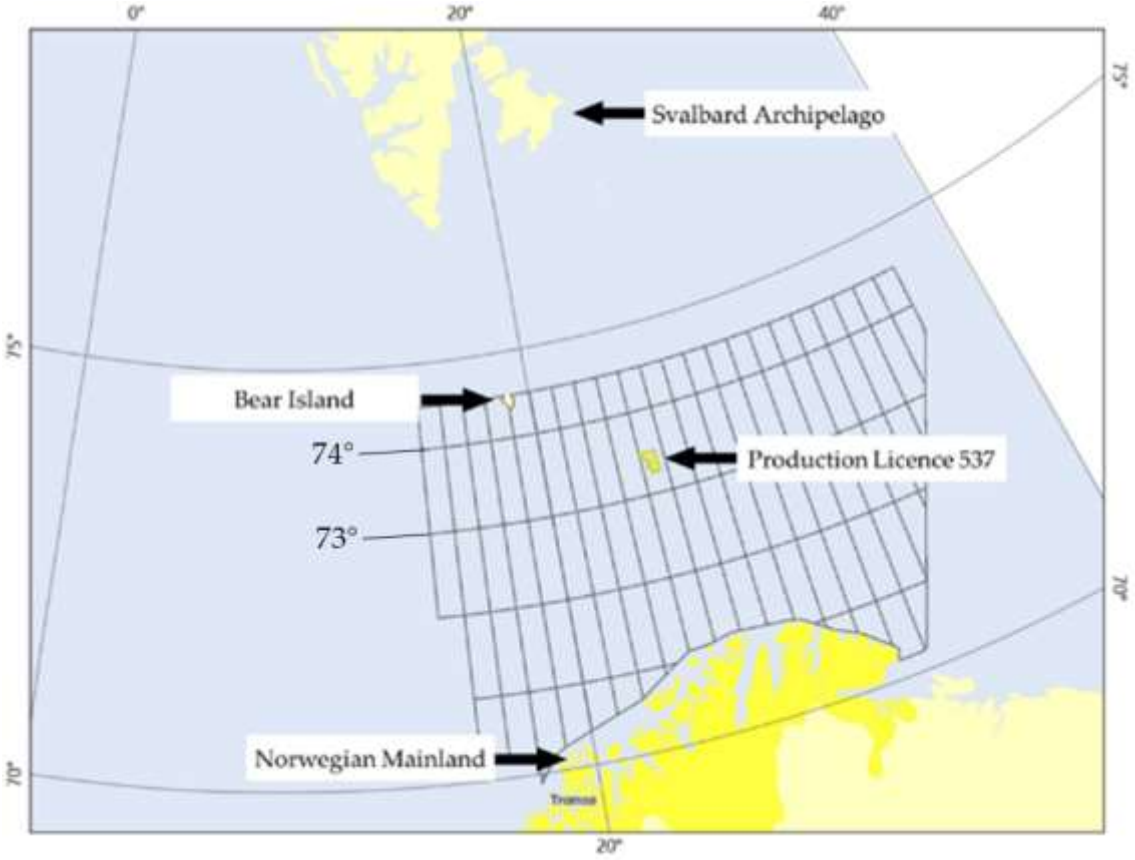

Figure 1: Production Licence 537 in the Norwegian Barents Sea. (Modified after Norwegian Petroleum Directorate n.d.).

The considerable distance to the Norwegian mainland and Svalbard adds a logistic challenge to fast emergency response in case of a blowout. This includes mobilization of

specialized equipment and personnel for relief well drilling (Petroleum Safety Authority Norway 2014), (Nedrum 2015).

The relative proximity of the environmentally sensitive Bear Island has lead OMV (Norge) AS to contribute in a study for developing a dedicated oil spill response plan for the area (Pedersen, et al. 2016). The study shows that the type of oil spill response and its expected success depends strongly on the season. Due to the northern location, the operating conditions become increasingly difficult during winter, which also affects relief well operations. Suitable drilling rigs, equipment, and materials that can be mobilized in time, must be capable of operating in harsh winter conditions. These include cold weather, drift ice, and darkness. Even if a well is spudded during summer, relief well operations are difficult and can therefore span into the winter season (Petroleum Safety Authority Norway 2014).

Another factor related to the northern location affects the magnetic-based azimuthal measurement of MWD tools. Frequent disruptions to the Earth's magnetic field are caused by solar storms and electric currents present in the ionosphere. These increase the uncertainty of survey measurements and negatively affect the accuracy of wellbore positioning in northern latitudes (Petroleum Safety Authority Norway 2014).

While the placement of vertical wells is not severely affected by interferences to the Earth's magnetic field, the uncertainty in lateral position of directional wells is greatly compromised. This makes steering directional wells more difficult with increasing latitude due to increased disturbance of MWD tools.

Wisting adds an additional challenge to drilling directional wells: As the reservoir formations are located in a shallow depth, the wells require a high build rate to land out horizontally in the reservoir. The same holds true for relief wells. The most likely scenario for a blowout to occur is right after the reservoir is penetrated. For this reason, the wells' casing schemes are designed to set the surface casing just above the reservoir. The surface casing shoe is the target point for the relief well, which would therefore have to build at a similarly high rate or fall back on a contingency solution that requires drilling to a very high inclination. Before the constraints on constructing a directional well in Wisting are discussed on the example of Wisting Central II, the following section provides an overview of the drilling environment based on the vertical exploration well Wisting Central.

2.2 Lithology Encountered by Wisting Central

Wisting Central is the first well that was drilled on the Wisting discovery in 2013. Its schematic is illustrated in Figure 2, along with the formations it has penetrated. The corresponding depths of the formation tops are measured depths along the well. However, since the wells maximum inclination is reported to be 1,6°, it provides a good picture of the formations' succession and their thickness.

The water depth at the well's spud location is 398 m. This is quite typical for Wisting, with reported water depths of 402 m and 394,5 m for the other two wells that have been drilled on the discovery to date, Wisting Central II and Wisting Central III.

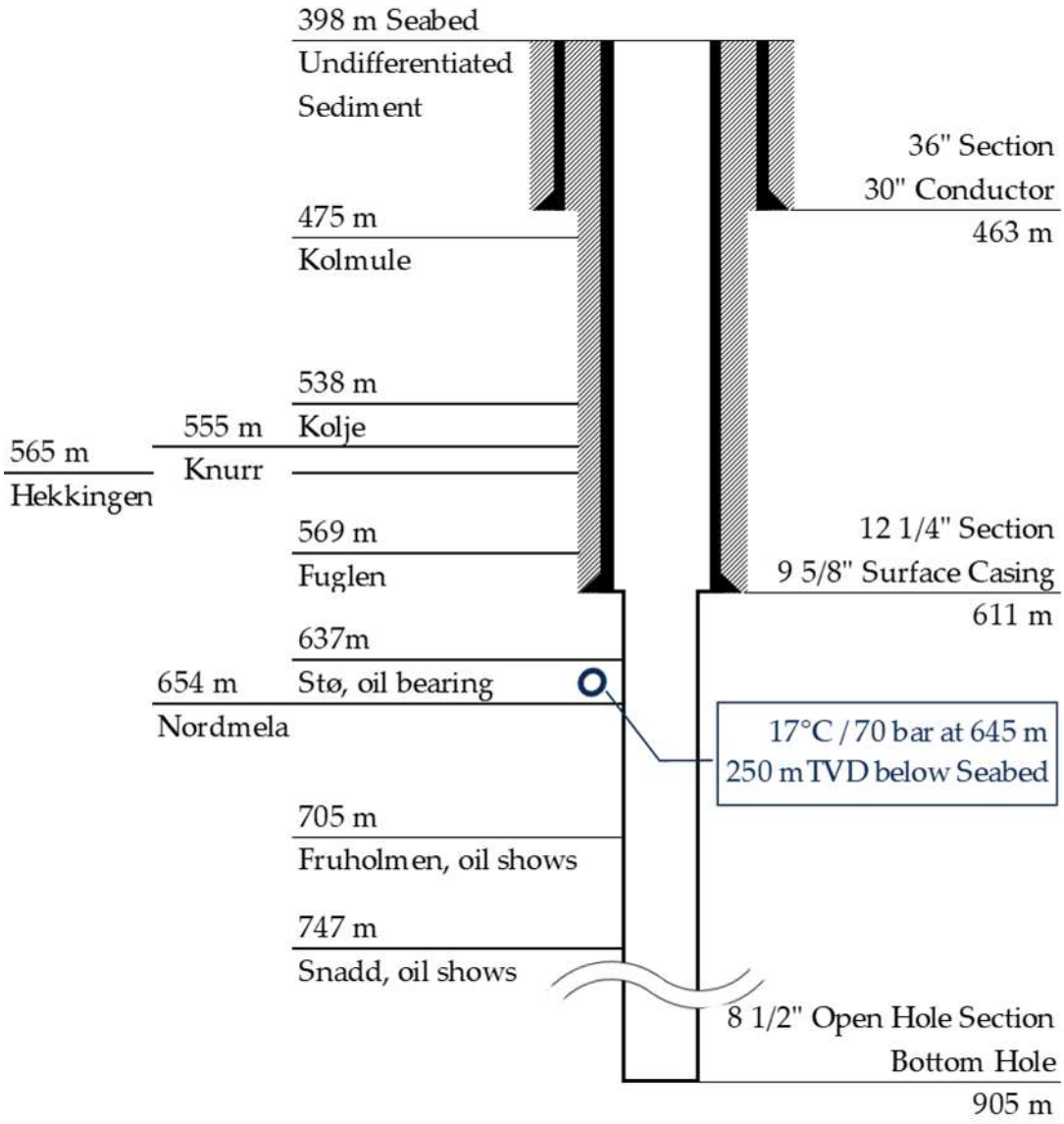

Figure 2: Schematic of Wisting Central. After Norwegian Petroleum Directorate (2015).

Wisting Central's conductor is set in the yet undifferentiated sediment, which is referred to as Nordland group. Below roughly 77 m of sediment, the formations Kolmule, Kolje, Knurr, Hekkingen, and Fuglen make up the Adventalen group. These formations are described as shales, claystones, and mudstones with interbeddings of limestone, dolomite, sandstone, and siltstone (Smelror, et al. 1998), (Bugge, et al. 2002), (Norwegian Petroleum Directorate 2014). Between the formations Knurr and Hekkingen there is a relatively thin layer of marls and limestone that constitutes the formation Klippfisk (Smelror, et al. 1998). In this vertical well, it is negligible. The Hekkingen formation also constitutes a source rock (Norwegian Petroleum Directorate 2014) which makes Kolje and Knurr a possible secondary play in Wisting (Veire 2017). Hekkingen and Fuglen form the cap rock for the underlying reservoir.

The well's surface casing is set in the silty shales of the Fuglen formation. Setting a casing in the Fuglen formation is a recurring feature in the Wisting casing design, as Fuglen is the last formation that separates the overburden from the reservoir. In a blowout

scenario, it would most likely be the last cased-off formation and the target formation into which a relief well would drill.

Stø, Nordmela, Fruhlolmen, and Snadd make up the Kapp-Toscana group. This group is further divided into the Realgrunnen subgroup, which consists of Stø, Nordmela, and Fruholmen and the Storfjorden subgroup, which is the Snadd formation. The formations of the Kapp-Toscana group are described as sandstones and shales, with mudstones and conglomerate, siltstone and interbedded coals (Norwegian Petroleum Directorate 2014). The Snadd formation is a possible secondary play in Wisting.

The Realgrunnen subgroup is the main play in Wisting. It was encountered oil bearing. The reservoir temperature and pressure are relatively low at 17° and 70 bar in the Stø formation, likely owing to the formations' shallowness and Wisting's location above the 73rd latitude. Due to the low pressure, the likelihood of a blowout is not as high as it would be in a highly pressured formation. It must be noted though that the well was intentionally located at the downdip of a flank. It is suspected that the Stø formation might have a gas cap further up in the structure, which would negatively impact a well kill scenario in case of a blowout (Norwegian Petroleum Directorate 2015).

The well reached its total depth in the Snadd formation and was later plugged and abandoned.

Even though the formations in Wisting lie in a shallow depth, they are relatively competent. The Barents Sea went through a period of substantial uplift and erosion, with some parts being lifted several hundred metres (Veire 2017). Wisting is further located close to a geologic structure called the Hoop fault complex. Figure 3 displays a high-resolution seismic cross section in Wisting. It shows that the area is strongly influenced by the fault complex, which causes the reservoir to be compartmentalized and heavily faulted (Veire 2017), (Hollinger, et al. 2017).

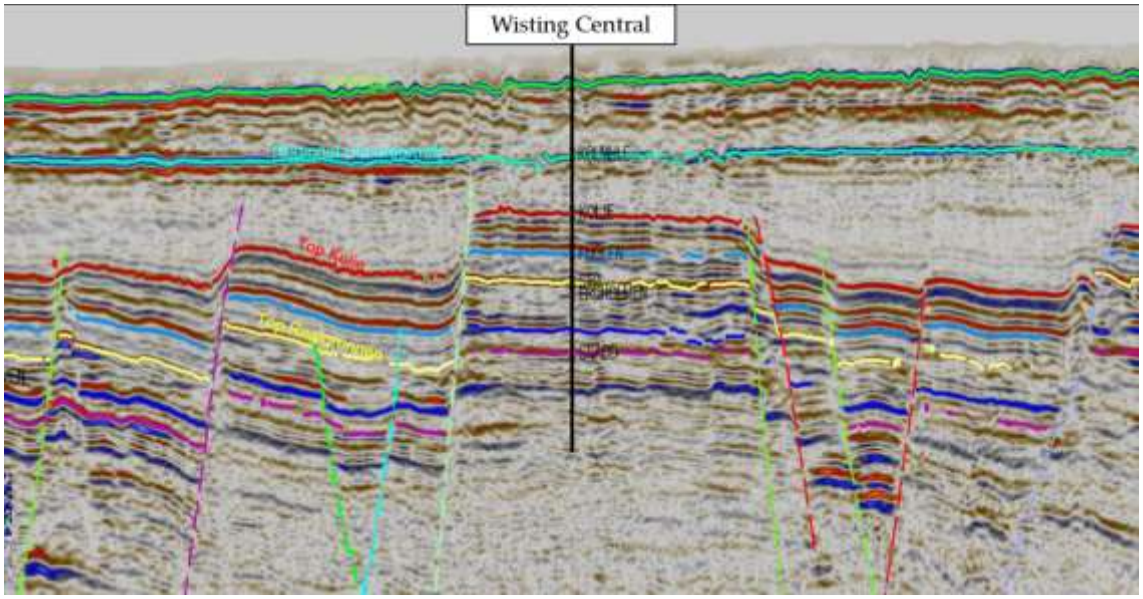

Figure 3: High-resolution seismic cross section in Wisting. From Veire (2007).

Wisting Central II, the subsequent well that was drilled on the discovery in 2016, is a horizontal appraisal well. It advanced laterally through the Realgrunnen subgroup on

its north-eastern path. The wellpath crossed several faults and re-entered the reservoir formations horizontally by penetrating an uplifted fault-block (Hollinger, et al. 2017).

The primary motivation for drilling a horizontal appraisal well was to conduct inflow tests in the reservoir formations and to prove the feasibility of drilling horizontally in such a shallow depth (Hollinger, et al. 2017). The feasibility of constructing horizontal wells is a deciding factor for the economic development of Wisting and had to be determined early on (Veire 2017). Conveniently, the well also provides valuable experience that is useful for relief well drilling in Wisting. It is therefore discussed in the following section.

2.3 Horizontal Appraisal Well Wisting Central II

Based on wellbore surveys, the final trajectory of Wisting Central II is introduced in Figure 4. Key elements are the shallow KOP and the high build rate to be able to land horizontally in the shallow reservoir. The build rate required a high average DLS of 9°/30m. No rotary steerable system (RSS) capable of achieving this rate in larger hole sizes was identified for Wisting Central II, therefore a positive displacement motor (PDM) set to a high bend angle setting had to be used (Hollinger, et al. 2017). Drilling with a PDM can have several negative impacts on the drilling performance, compared to a RSS. As the drilling performance is an important parameter in fast and reliable relief well drilling, directional BHAs are reviewed later in this thesis (3.3 Directional Control).

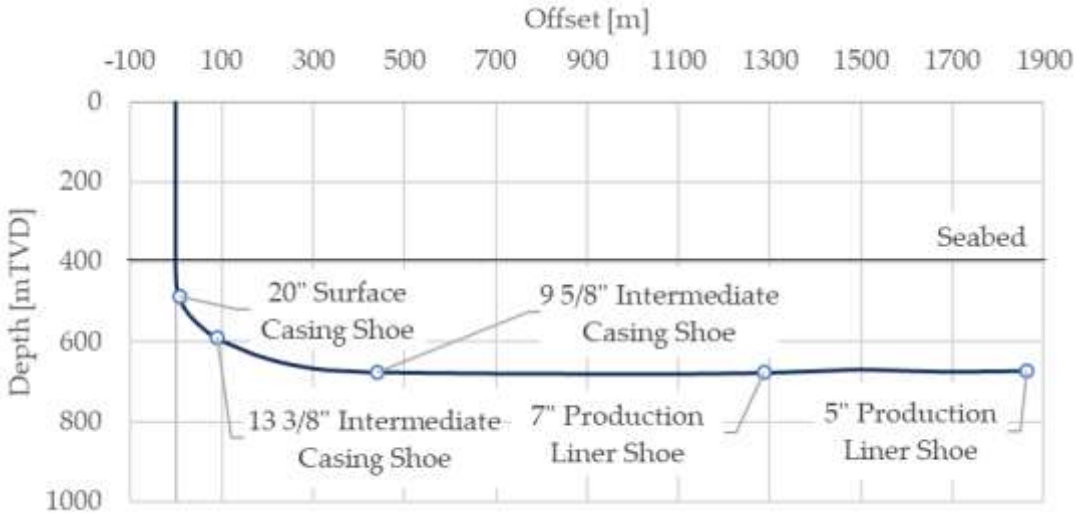

Figure 4: Wisting Central II trajectory profile

In the planning stage of Wisting Central II, fatigue analysis of the BHA showed that due to the high bend angle setting, the stress would be too high to rotate the string in the 17 1/2" section from the 20" casing shoe to the 13 3/8" casing shoe planned total depth (TD). Therefore, this section was drilled as a 12 1/4" pilot hole and underreamed to 17 1/2" in a dedicated run with a two-stage hole opener (Trauner 2016).

While feasible, the simulated stress state in the rotating hole-opening BHA was high, limiting its application to hole diameters which are similar in size. It is believed that drilling a smaller pilot hole and opening it to 17 1/2" would exceed the fatigue limit of the underreaming BHA and further result in a poor hole condition (Gerald Hollinger, personal communication, 5.10.2018).

Because of the high bend angle setting, the 12 1/4" directional BHA could be rotated with only limited revolutions per minute (RPM), resulting in poor hole cleaning, especially in highly inclined sections of the hole (Hollinger, et al. 2017). Inefficient hole cleaning as a consequence of cuttings not being carried out of the hole effectively can lead to a decreased ROP and an increased risk of getting stuck. The limited RPM further makes it difficult to ream out of the hole, but reaming can become necessary if there is significant overpull seen during tripping out on elevators.

To achieve the necessary build rate, a sufficiently high mud weight is required to keep the hole stable and ensure proper contact between the borehole and the directional BHA. Since the downhole temperature in Wisting is relatively low due to its geographic location and shallow overburden, the required mud density results in a relatively high viscosity. This is problematic because Wisting is also heavily faulted and the equivalent circulation density (ECD) is therefore restricted. To prevent losses due to exceeding the ECD limit, the mud flow rate has to be limited which in turn makes hole cleaning even more difficult. Further, all tools whose operational capacities depend on the mud flow rate must be matched to the low flow rate (Hollinger, et al. 2017).

Despite the difficulties that need to be overcome to drill a directional well in the discovery, Wisting Central II proved that it is possible. The inclination and azimuthal measurements taken by the survey tools are displayed in Figure 5.

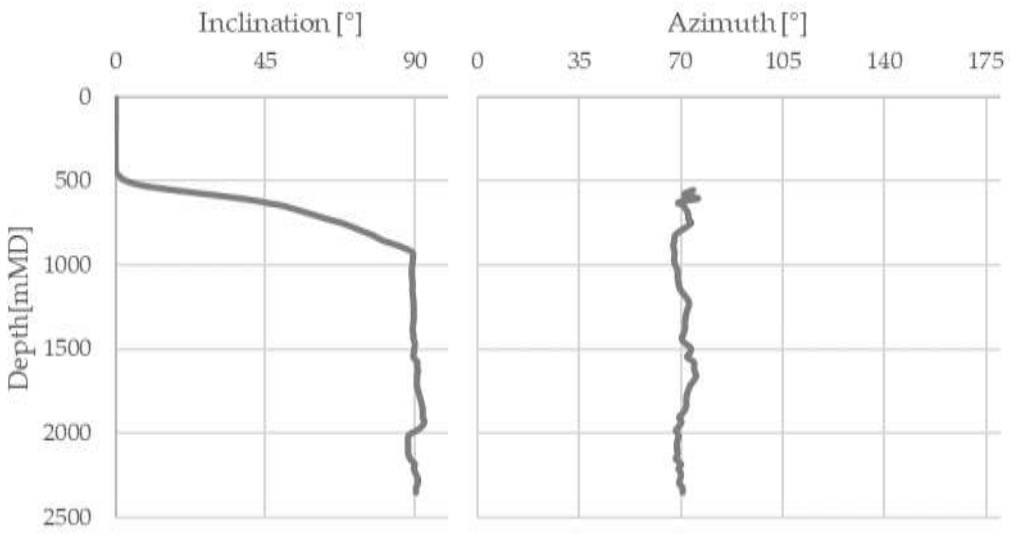

Figure 5: Inclination and azimuth survey data from Wisting Central II

They show that the inclination builds up at a relatively constant rate over the entire build section. Based on the data points, there is a short section at the top when it is comparatively low. Then the well builds at a high rate until the inclination reaches 45°.

Thereafter, it builds to horizontal at a lower constant rate. In the horizontal section, the well is geosteered through the reservoir. The azimuthal measurements stabilize quickly as the well builds inclination and stay relatively constant around 70° over the entire well trajectory.

To be able to kick off as shallow as required, Wisting Central II used a Conductor Anchor Element (CAE) to stabilize the 30" conductor (Hollinger, et al. 2017). The conductor contained in the well schematic in Figure 6 is cemented into the CAE.

A CAE as described by Sivertsen and Strand (2011) and Mathis, Strand and Hollinger (2017), acts as the primary load bearing element of the well. The conductor can be significantly shortened since the CAE bears the bending moments and axial loads that the conductor would normally have to support on the sediment. (Sivertsen and Strand 2011). The CAE and conductor were installed at the well site prior to rig arrival (Mathis, Strand and Hollinger 2017).

Out of this conductor, the 26" section was drilled into the undifferentiated sediment with a bent housing of the motor set to 1,2° bend angle. In this way, the well could kick off towards 70° azimuth and build to 4,15° inclination within its first 65 m (Trauner 2016).

The next section drilled out of the 20" surface casing as a 12 1/4" pilot hole. It experienced first mud losses at the beginning of the section that could be cured by lowering the section mud weight from 1,2 SG to 1,1 SG. Prior to drilling Wisting Central II, on which several leak off tests (LOT) and formation integrity tests (FIT) were performed, there was little geomechanical offset data available that covered the Wisting discovery. Only one FIT was conducted in Fuglen on Wisting Central (Norwegian Petroleum Directorate 2015).

The pilot assembly was set to a bend angle of 1,83°. In this configuration, it drilled almost 100 m of build section through the Kolmule and into the Kolje formation. The PDM achieved an average dogleg severity (DLS) output of 12,5°/30 m. At this rate, the well would have landed high, above the reservoir. At 564 mMD / 560 mTVD and roughly 40° inclination, the BHA was pulled from the Kolje formation and the bend angle was reduced to 1,56°. The well continued to build at a lower rate through Knurr and Klippfisk into Hekkingen. This reduction in build rate, due to reducing the bend angle setting at around 45° inclination, is also visible on the inclination measurements as pointed out in Figure 5. After opening the pilot hole to 17 1/2", the 13 3/8" intermediate casing was set in the cap rock Hekkingen, slightly higher than planned.

Out of this casing, the directional work continued with a 12 1/4" assembly, with the PDM set to a bend angle of 1°. It drilled through the Fuglen formation and into the reservoir formations of the Realgrunnen subgroup where it landed the well horizontally in the Nordmela formation. The reduced build rate in this section reflects in the inclination data in Figure 5. The section was cased with a 9 5/8" casing. In addition to the cement, an annular barrier elastomer element (ABE) was placed in the casing-casing annulus to provide an additional seal against hydrocarbon migration from the reservoir formations.

The ABE, in comparison with a conventional liner hanger system, has a much higher DLS tolerance. This needs to be taken into consideration when hanging off a liner in a high DLS bore and is relevant for the next well section (Hollinger, et al. 2017).

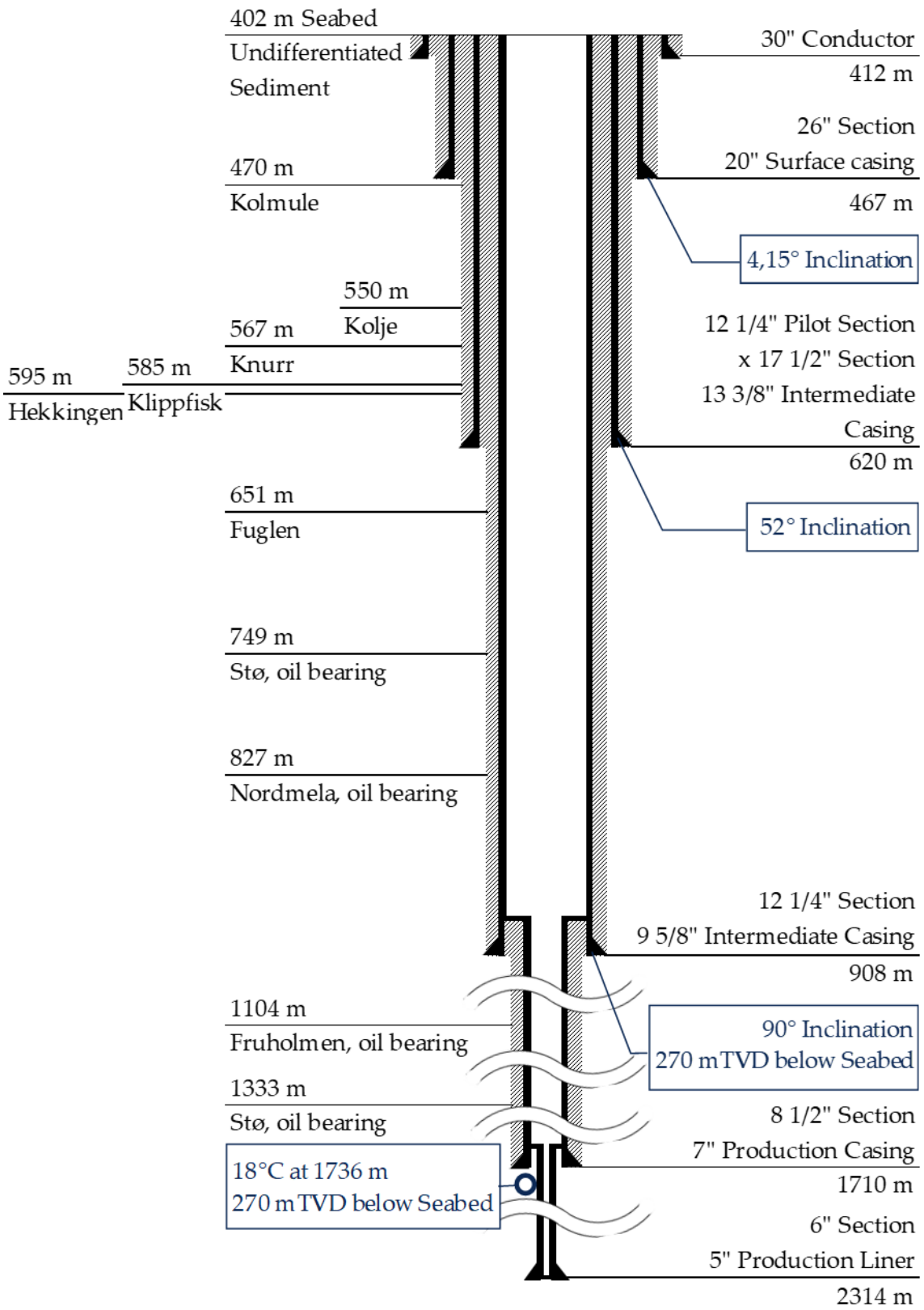

Figure 6: Schematic of Wisting Central II. After Norwegian Petroleum Directorate (2016).

This 8 1/2″ section was geosteered with a RSS. Due to the many faults that were encountered, the section had to be cased off prematurely to stop the mud losses. The 7″ liner was hung off on an ABE and cemented.

The hole continued with a 6″ contingency section that was cased for the subsequent well tests, but not cemented (Trauner 2016).

The directional experience gathered on Wisting Central II showed that the shallow formations support the BHA well. It is now believed that a DLS of 9°/30 m that is needed to build 90° inclination within a vertical depth of approximately 250 m can be achieved with a motor bend setting of 1,56° and drilling in full sliding mode (Gerald Hollinger, personal communication, 13.06.2018). If the required build rate could not have been achieved, the well trajectory would have fallen back on a contingency solution. This trajectory entails drilling through and below the reservoir in a longer radius curve, depending on the achievable DLS and building to more than 90° to re-enter the reservoir from below (Trauner 2016). Such a low DLS contingency profile was planned for drilling a relief well for Wisting Central and Wisting Central II, prior to the experience on build rate capability becoming available from drilling Wisting Central II (Trauner 2017). The following chapter examines relief well planning under the conditions at Wisting.

Chapter 3 Relief Well Planning

The Norwegian Petroleum Directorate (NPD) requires a relief well plan for every well that is drilled. Ideally, offshore wells should be designed in such a way that they can be killed with one relief well in case of a blowout. If one relief well would be insufficient to kill the blowing well, it must be demonstrated that drilling two relief wells is feasible. An offshore well design that would require more than two relief wells to bring the well back under control in case of a blowout is not accepted by the NPD (NORSOK 2013). In general, even if the well is deemed to be within the killing capacities of one relief well, additional relief wells are planned and a second relief well may be spudded as a contingency in case the first relief well fails to get the well back under control (Oskarsen, et al. 2016).

A blowout contingency plan that models a blowout in Wisting shows that a blowing well could be killed with one relief well and an intersection hole size of 8 1/2" (Nedrum 2015). Since Wisting Central II enters the reservoir with this section size, it provides a good example of a possible relief well schematic (Nedrum 2015). In the common S-shaped relief well, the last casing string should be set and cemented immediately before the point of planned intersection. This ensures that the formations above the intersection point do not fracture when the target well is killed through the relief well. During the killing procedure, mud is pumped through the relief at a high rate into the blowing well. The kill mud is often pumped through the drill string-casing annulus of the relief well. During the killing procedure, the drillstring is pulled back into the last relief well casing and kept static to monitor the downhole pressure while pumping through the annulus This is advisable, because the dynamic pressure resulting from bullheading the kill fluid into the blowing well creates a significant overbalanced pressure in the relief well. Pulling back into the casing is intended to prevent the drill string from getting differentially stuck on the open formation in the process (Goobie, et al. 2015). The killing procedure is started right after the connection is established with the blowing well, therefore it is beneficial if the last casing is spaced less than one pipe stand from the intersection point. In this way, the drill bit can be retracted fully into the casing without breaking a connection (Goobie, et al. 2015). However, in a J-shaped relief well, the likely chance that the target will be missed and sidetracking becomes necessary needs to be taken into consideration. Sufficient spacing between the last casing setting point and the target relief well must therefore be factored into the planned casing schematic so that the relief well can be sidetracked. From the last casing shoe it must be possible to reach the all every position in the area where the target well could be.

To achieve this optimal spacing of the last relief well casing from the intersection point for the killing procedure, it is necessary to have precise knowledge of the relative wellbore positions. This becomes even more important when it comes to avoiding unintentional intersection of the blowing well. Intersection at a depth shallower than planned presents a serious hazard to the relief well. In such an instance, aside from the formations exposed by the relief well not being protected by a casing, the well might carry too little hydrostatic pressure. The reason for this can be insufficient fluid weight in the well at the time or insufficient hydrostatic head due to the shallow intersection. If

this is the case, the relief well will not be capable of stopping the blowout solely with the dynamic pressure it creates. The vertical depth of the planned intersection point and the intersection hole size are therefore governing design criteria for a relief well.

The S-shaped trajectory is designed to bring the relief well as close to the target wellbore as possible before the intersection so that the relative wellbore positions can be estimated with ranging tools. The well is then steered based on the relative wellbore positions in this intersection phase. The J-shaped trajectory steers towards the target directly based on the position of the blowing wellbore and its own position. By the time it is close enough to the target wellbore to estimate the relative positions, its course has likely missed the blowing well already. Thus, knowing the subsurface positions of the wellbores with high accuracy is even more important for the success of J-shaped relief well designs. However, both trajectories are at risk of intersecting too early when the relief well is not prepared for the killing procedure. This hazard might be greater in S-shaped trajectories as they come intentionally close to the target in a depth shallower than the planned intersection point.

The deepest possible intersection point in Wisting is expected to be in the cap rock above the reservoir. In all three Wisting well designs so far, a 13 3/8″ casing was set into either the Hekkingen or Fuglen formation. The 13 3/8″ casing shoe is the planned target for a relief well and was therefore pre-magnetized to facilitate detecting the wellbore from a distance and increase the chances of direct intersection once the well has been detected (Wolf 2016).

In the casing schematic of the relief well plan devised for Wisting Central II, the 13 3/8″ casing shoe is planned to be intersected by a 8 1/2″ hole. In the planned trajectory, the 12 1/4″ section dives below the reservoir and drills upwards towards the target point. Therefore, a 9 5/8″ casing would be cemented into a 12 1/4″ section to case off the reservoir formations prior to the intersection. Like in Wisting Central II, a 13 3/8″ relief well casing is set in the cap rock above the reservoir. Further, there is a 20″ surface casing. A 30″ conductor is planned to be set roughly 100 m into the undifferentiated sediment, presumably close to top Kolmule (Nedrum 2015).

In this solution, the DLS is lower than if the relief well built to a final inclination of 90° and landed out horizontally in the cap rock. If it is possible to build at the required rate to reach the target without penetrating the reservoir formations, the relief well casing schematic could potentially be modified to forego the 13 3/8″ casing string and set a 9 5/8″ casing in the cap rock instead. Thereby, valuable time could be saved and the risk of a further influx from the reservoir formations into the relief well is mitigated. However, this would need thorough analysis of geomechanical conditions and well barriers, which is out of the scope of this work.

To facilitate landing out horizontally in the cap rock, a high DLS relief well would benefit from kicking off shallow and building as much inclination as possible in the surface section. Contrary to the relatively deep setting depth of the 30″ conductor at 100 m in the relief well plan devised for Wisting Central II, this might require a CAE to allow for a shortened conductor. The applicability of a CAE depends on the soil condition (Sivertsen and Strand 2011) at the relief well's spud location and is therefore a further criterion for selecting a suitable location for the well.

3.1 Spud Location

The NPD requires that a minimum of two well surface locations be identified for the relief well. If the well design requires two relief wells to kill the blowing well, a minimum of three relief well surface locations are to be identified.

To ensure the surface locations for the relief well are suitable for drilling, site surveys with sonar tools and visual inspections must be conducted for the relief well locations, along with the site survey of the location for the main well. The site surveys assess the presence of shallow hazards, such as shallow gas (Flores, et al. 2014), as these would pose a well control hazard to the relief well itself. Furthermore, the site surveys assess the water depth since the water depth is a criterion for the drilling rigs that can be made available to drill the potential relief well The seabed condition at and around the potential well site must be checked. There might be hazards and obstacles present, such as pipelines or cables. The soil around the location must be suitable for anchoring, if a floater is used, or the soil at the well site must be able to support a jack-up rig, if a jack up rig would be used for the relief well (NORSOK 2013).

The surface facilities of the relief well operation must be placed at a safe distance to the blowout (Flores, et al. 2014). To identify potential relief well surface locations, the wind and current conditions around the well need to be assessed. The NPD recommends that the relief well locations be placed up-wind and up-current of the wind and current directions that dominate at the site of the main well (NORSOK 2013). In the event of a blowout, formation fluids are likely to migrate through the water column to the sea surface, where they pose hazards to drilling rigs, vessels, and helicopters. Such areas around the well need to be identified by modelling the migration path of discharged formation fluids for the blowout scenario prior to drilling the main well. These areas are excluded as potential surface locations for relief wells (Flores, et al. 2014).

The direction of the potential relief well surface locations relative to the main wellbore will govern the azimuth of the relief well. Above certain wellbore inclinations, the azimuthal direction can compromise the accuracy of the magnetic surveys to determine the well path azimuth (see 3.4 Surveying). As an example, Figure 7 illustrates the planned surface locations relative to the surface location of Wisting Central III. Two relief well surface locations were identified for Wisting Central III. The relief well would have been drilled from an azimuth of either approximately 255° or 147° (Trauner 2017). In this example, the relief well surface locations are at an offset of approximately 700m and 788m from the main well.

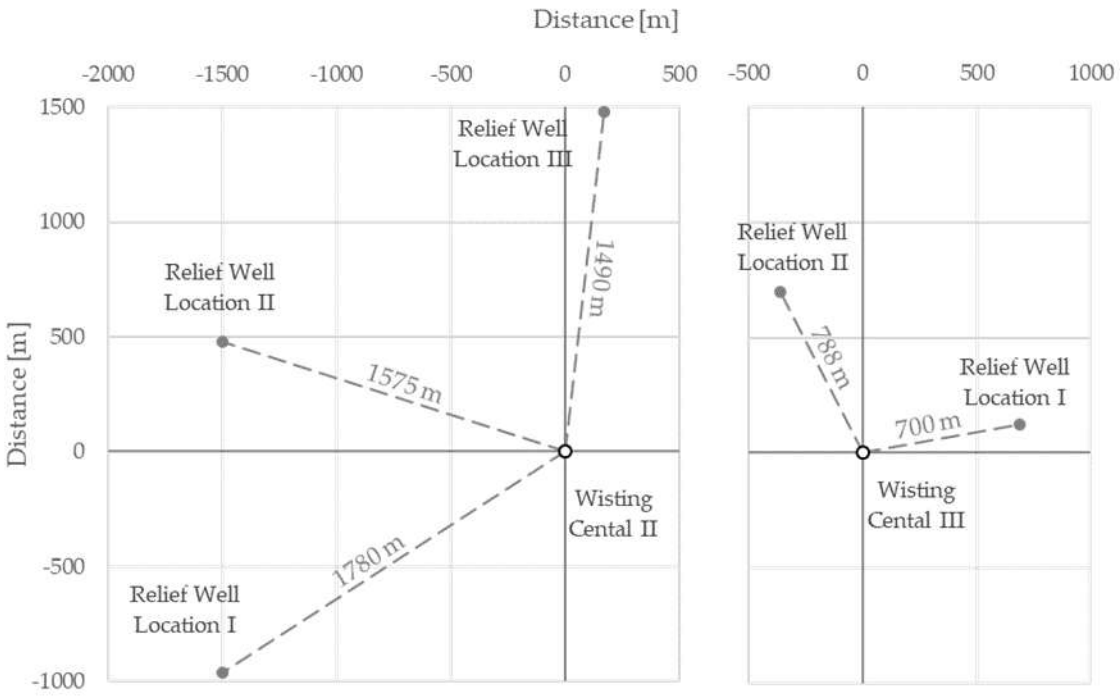

Figure 7: Planned relief well surface locations for Wisting Cental II and Wisting Central III. After Nendrum (2015) and Trauner (2017).

Further, to keep a safe distance to the blowing wellbore, the expected DLS capability can be a criterion for selecting a relief well surface location. Consider Figure 8. In this example, the depths and offset distances are chosen arbitrarily. The high DLS profile (blue line) builds at a continuous DLS until it intersects the target (grey line) at the point EOB (end of build). In case the planned DLS to build to this point cannot be achieved and the actual DLS is lower, the relief well would miss the target, as illustrated by the dashed green line. In order for a well building at a low DLS (relative to the higher DLS), this well would have to be spudded from a distance further away from the target wellbore, as illustrated by the solid green line.

Since it was not proven prior to drilling Wisting Central II that the wellbore inclination can be built at an average rate of 9°/30m in Wisting, such a contingency solution was devised for a potential relief well (Wolf 2016). In the case of Wisting Central II, the contingency solution entails missing a part of the horizontal section in the reservoir. Since the intersection point would be missed if the contingency relief well trajectory would be spudded from the same surface location as the non-contingency relief well trajectory, the DLS capability needs to be taken into account for identifying suitable spud locations. According to Wolf (2016), the minimum distance to the target wellbore is 500m for high and medium DLS under the conditions at Wisting. The surface location for the contingency profile that builds at lower DLS needs to be at greater distance from the target well to be able to intersect the target.

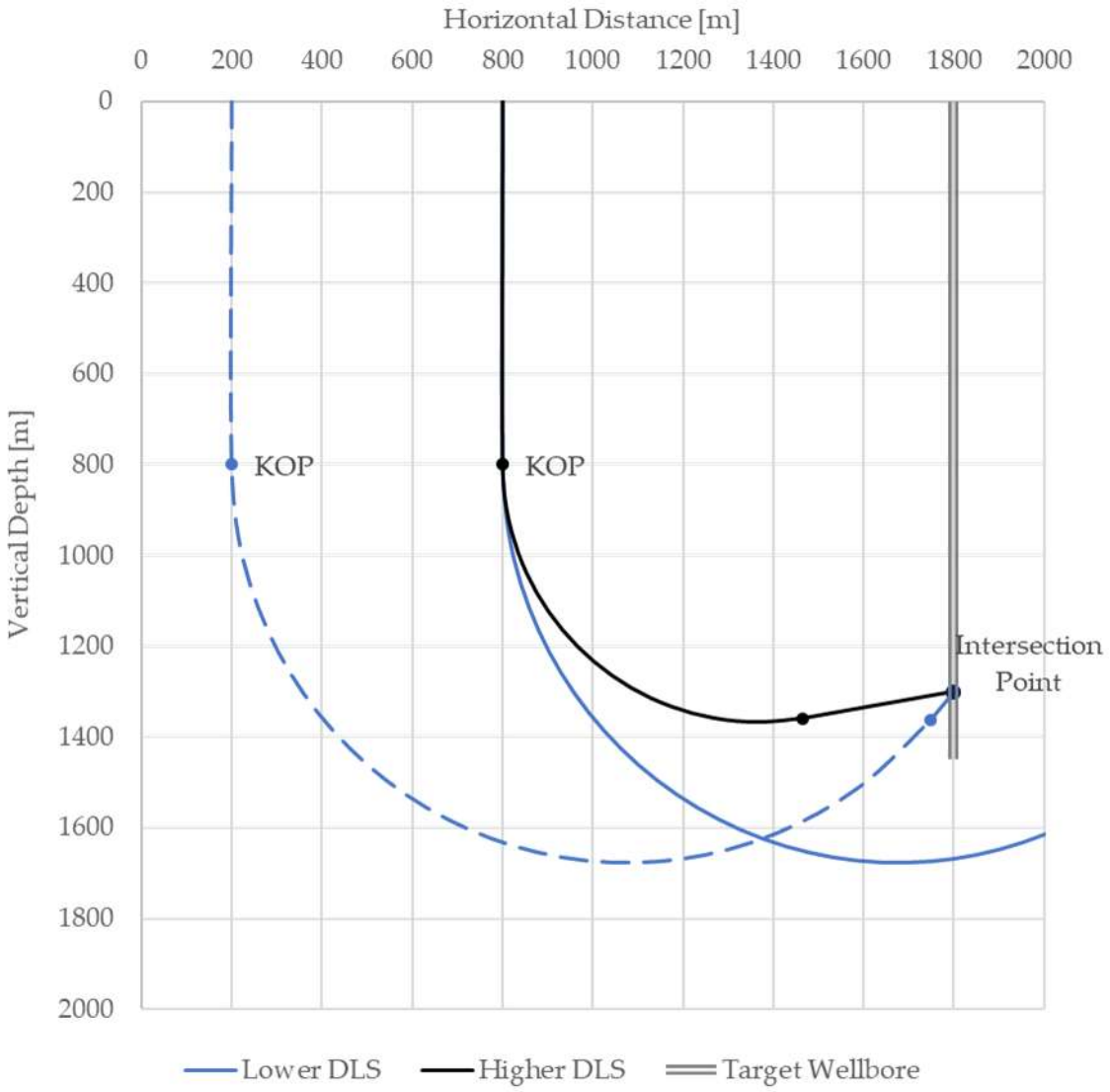

Figure 8: Schematic of J-shaped relief well profile and contingency solution. After Wolf (2016)

In conclusion, the distance of the relief well spud location to the target, along with the target depth, governs the relief well trajectory. The following section analyses possible relief well trajectories within the constraints of distance and depth between relief well KOP and target wellbore intersection point.

3.2 Relief Well Trajectory Designs

The Norwegian Petroleum Authority requires simplified relief well trajectories to be submitted as part of the relief well plans (NORSOK 2013). There are two basic relief well profiles that are suitable for purposely intersecting another wellbore: The S-shaped well profile and the J-shaped well profile. If there are no further restrictions, the S-shaped profile is the preferred relief well profile as it has a better chance of intersecting the target well upon the first attempt (Flores, et al. 2014). Figure 9 shows both trajectory types intersecting a target well.

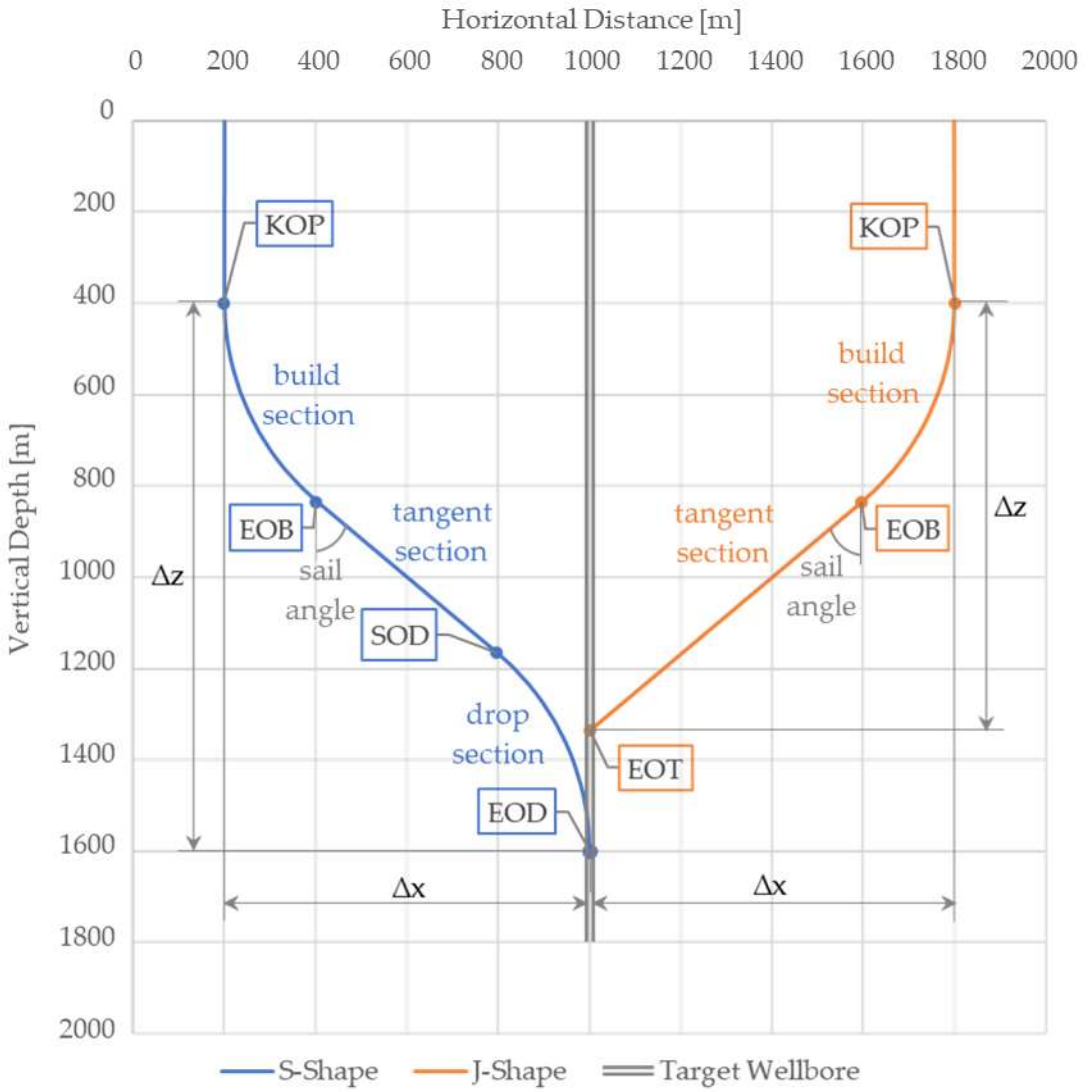

Figure 9: Schematic of S-shaped and J-shaped relief well trajectory

The parameters in the example are chosen arbitrarily, but the KOP, the horizontal offset (Δx) from the target, the DLS in the build section, and the sail angle are the same in both profiles. This illustrates that under the same conditions, the J-shaped profile needs less vertical depth (Δz) to reach the target. It is therefore considered to be more suitable for the Wisting discovery where there is only a shallow vertical depth available to build the profile.

In general, the relief well trajectory should be kept as simple as possible (Flores, et al. 2014). Arguably, the simplest trajectory is a vertical well, as it has no DLS and no inclination. A vertical trajectory can only reach a target that lies directly below its spud location. The relief well is spudded in a safe distance from the target. It is assumed here that the target is a vertical wellbore and therefore lies at the same horizontal offset from the relief well spud location as the blowing well's surface location. To cross the distance between its spud location and the target wellbore, the relief well has to build to an inclination, referred to as the sail angle.

Bringing the well up to the inclination requires an appropriate DLS in the build section, as well as the drop section in an S-shaped profile. To keep the well simple and easy to drill, both the DLS and the sail angle should be kept as low as possible. It is found that this is hardly possible under the narrow constraints in the Wisting discovery, but the required DLS is lower when the well is designed as a J-shaped profile. However, the J-shaped profile makes the intersection of the blowing well more difficult. Thus, a trade-off must be made between drilling a J-shaped profile that might take longer to intersect and an S-shaped profile that might not be feasible to construct under the conditions.

For the Wisting discovery, OMV devised three J-shaped trajectories as relief well strategy for the worst case scenario of a blowout (Wolf 2016). The trajectories' parameters are summarized in Table 1 and visualised in Figure 10.

	High DLS	**Medium**	**Low DLS**
Δx [m]	500	500	1118
Δz [m]	175	175	175
φ [°]	89°	121,2	149,67
DLS [°/30m]	10	6,3	3

Table 1: Relief well parameters for high, medium, and low DLS strategy. After Wolf (2016).

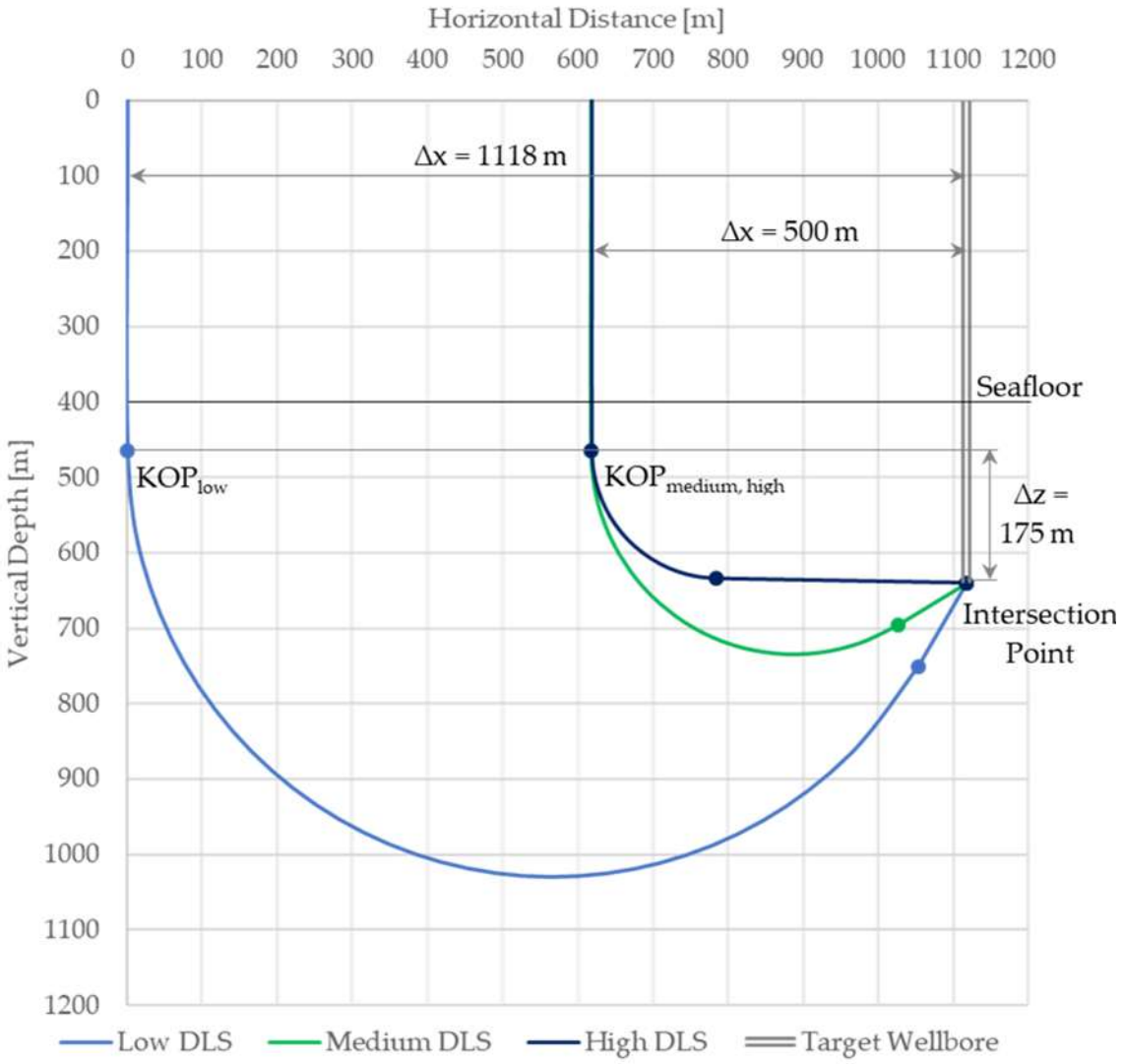

Figure 10: Relief well trajectories for high, medium, and low DLS strategy. After Wolf (2016).

Prior to drilling the horizontal well Wisting Central II, it was not clear what the achievable DLS in the overburden would be. The low DLS profile that builds at 3°/30m would have to build to a very high sail angle of almost 150°. The high inclination makes this profile extremely difficult to drill, but the relatively low DLS is not expected to limit the directional tools. The medium DLS strategy builds at 6,3°/30m to a sail angle of slightly over 120°. This angle is also very high and the profile will therefore be difficult to drill, but it is expected to be more feasible than an inclination of 150°. However, greater DLS results in a limitation of directional drilling tools that are capable of drilling the curve and has a greater impact on the fatigue life of the components. The high DLS trajectory builds at 10°/30m to an inclination of almost 90° and steers towards the target horizontally. As mentioned in the review of Wisting Central II, the high DLS leads to difficulties in the drilling performance because the drillstring RPM is limited severely for concern of the drillstring components fatigue life.

The potential relief well for Wisting Central II was planned at a DLS of roughly 6,5°/30m, therefore corresponding to the medium DLS strategy. However, it was demonstrated in the well that 10°/30m and even higher DLS curves can be built in Wisting without tool failure in the 12 1/4" section. Therefore, the high DLS strategy can be considered a feasible solution. This raises the question whether it makes sense to increase the build rate further for the sake of reducing the inclination and, if this is within the technical limitations, whether there is a limit where it is better to accept a certain amount of inclination for the sake of a reduced DLS. In other words, is there an optimum trade-off between DLS and inclination in J-shaped and S-shaped profiles? Further, what are the minimum DLS and sail angle requirements to build an S-shaped profile in Wisting and thereby increase the chances of fast intersection.

To analyse the trajectories in this respect, a relationship between the DLS and the sail angle is established as a function of the horizontal distance and the vertical depth, Δx and Δz. The symmetry of the S-shaped trajectory makes it easier to derive the relationship between DLS and sail angle. It will therefore be used to establish and discuss the relationship. Since the J-shaped profile is contained in the symmetry of the S-shaped profile, the findings can then be modified to result in the relationship between DLS and sail angle for this trajectory.

To simplify, some limitations are applied to the profile analysis:

First, it is assumed that the profiles kick off from vertical and, in the case of the S-shaped trajectory, drops back to vertical. In reality, when sufficiently close to the target wellbore, the S-shaped profile is planned to drop back to an inclination of 3-6° incident angle with the target wellbore (Flores, et al. 2014). Further, the wellbore can already have an inclination before it kicks off, either unintentionally or intentionally, as the example of Wisting Central II shows.

Second, the S-shaped trajectory is analysed between KOP and EOD, where the EOD is considered to be the intersection point. In reality, the S-shaped profile drills deeper after the EOD during the intersection phase (Flores, et al. 2014). This neglect is partly compensated for by building the trajectory back to vertical, as stated in the first limitation.

Third, the build and drop sections in the S-shaped profile are chosen to build at the same DLS, resulting in a symmetrical profile. This might not be the case when the well is drilled, as the achievable build rate is influenced by several factors, one of them being the inclination of the wellbore.

Fourth, the build and drop sections are assumed to build and drop continuously and at a constant DLS. This is not necessarily true and can be dependent on the directional BHA, the wellbore inclination and the formation properties. These influences on the achievable build rate are addressed in the next section of this chapter (3.3 Directional Control).

Finally, the profiles are assumed to build in a flat plane and no change of azimuth is factored into the DLS.

3.2.1 S-Shape

The motivation for analysing the trajectories is the exceptionally shallow vertical depth of the Wisting discovery. The S-shaped trajectory consists of a build and drop section, for which the defining parameter is the DLS, and a tangent section, whose defining parameter is the sail angle. The point of interest is how the KOP can be connected to the EOD with an S-shaped profile and how the horizontal distance and the vertical depth between KOP and EOD impact the trajectories' parameters, the DLS and the sail angle. Figure 11 illustrates this on the example of three fictitious S-shaped trajectories.

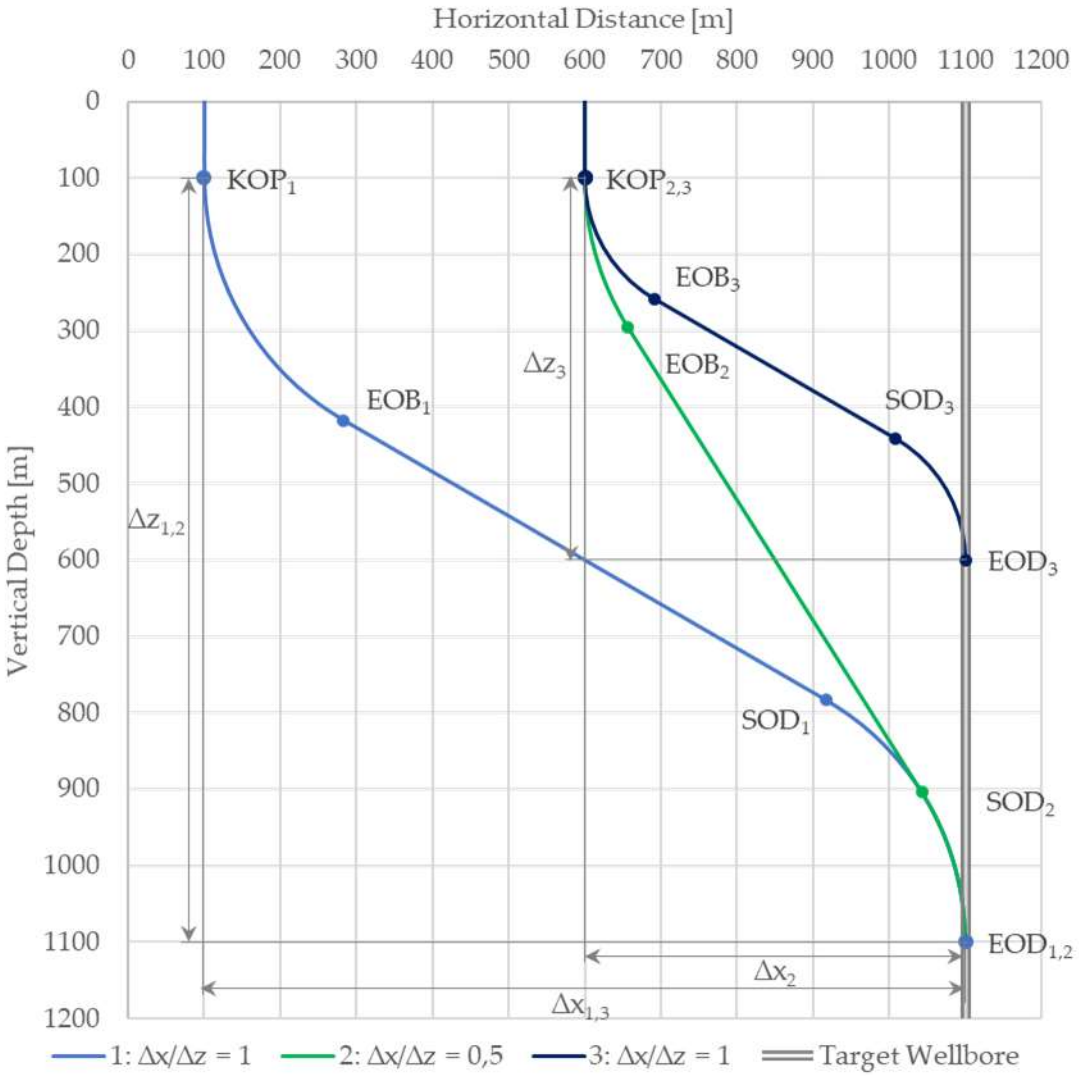

Figure 11: S-shaped profiles at different Δx/Δz intersecting a vertical target wellbore

Trajectory 1 (blue) and trajectory 2 (green) build at the same rate, so their DLS is equal. Trajectory 1 and trajectory 3 (dark blue) have the same sail angle. The DLS in trajectory 3 is higher than in the other two trajectories.

This shows that the sail angle is controlled by the ratio between the horizontal offset and the vertical depth (Δx/Δz). The DLS is controlled by the sail angle, and thus by the ratio Δx/Δz, but also by the magnitude of either the horizontal offset or the vertical depth. As

the limiting factor in Wisting is the vertical depth of the intersection point, the magnitude of Δz is considered as the controlling factor here.

Horizontal offset and vertical depth, Δx and Δz, have now been identified as the governing factors that influence the trajectory parameters, DLS and sail angle. However, the sail angles in the previous examples in Figure 11 could be altered, resulting in a different DLS, but still yielding a valid trajectory. This is illustrated in Figure 12 for Δx/Δz = 1 and a vertical depth Δz of 1000 m, but the concept applies to any confining offset and depth condition.

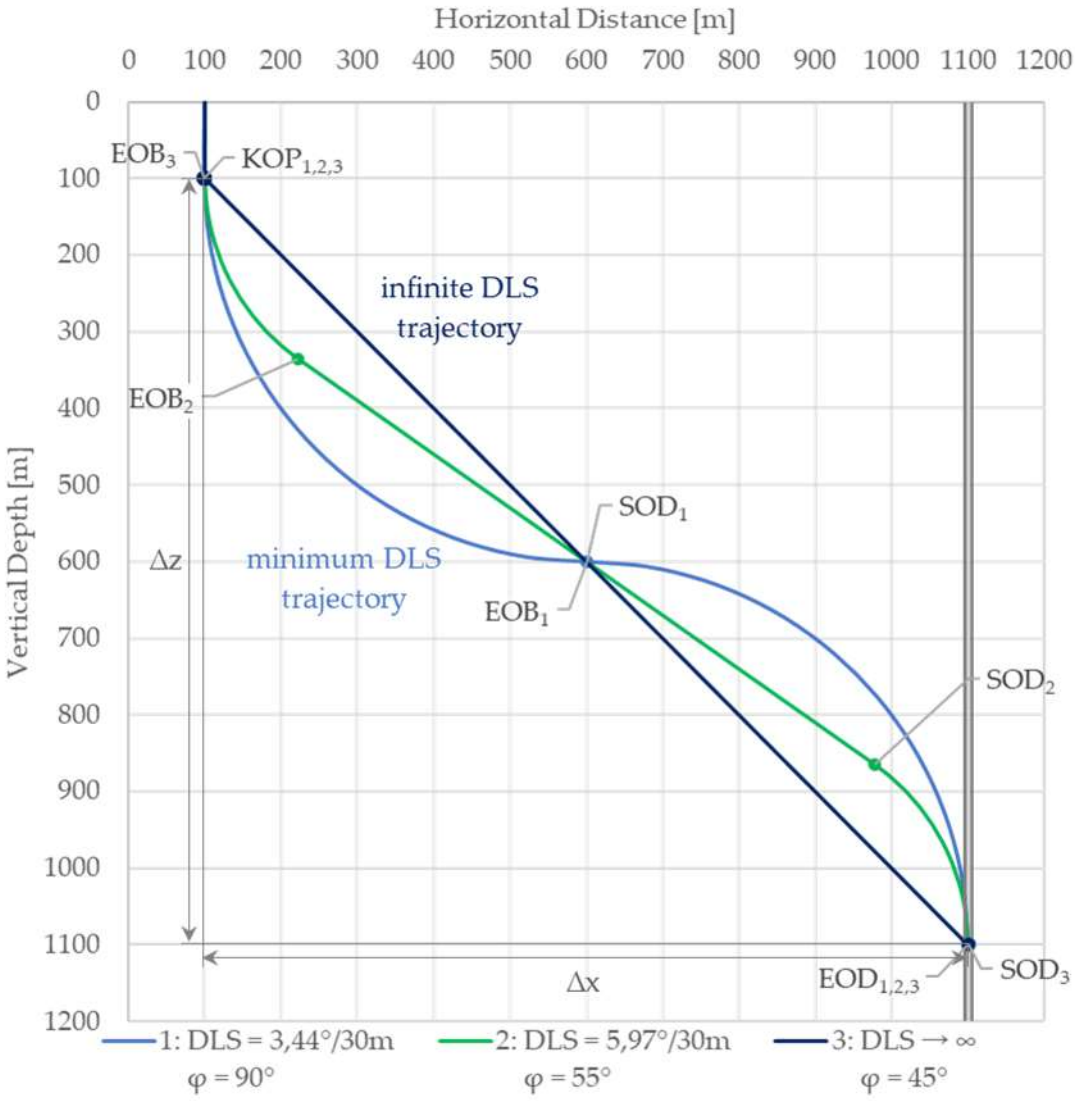

Figure 12: Possible trajectory parameters at fixed Δx/Δz.

Trajectory 1 (blue) builds at the smallest possible DLS. If the DLS were any smaller, the trajectory would miss the planned intersection point. In this limiting case, the profile consists only of build and drop section, the tangent section vanishes completely. The DLS in this limiting case will be called "minimum DLS" and denoted as DLS_{min}. The corresponding sail angle of the tangent in the turning point (EOB/SOD) is referred to as the "minimum sail angle", denoted as φ_{min}. Even though φ_{min} is the upper limit for the

sail angle inclination, the denotation "min" ties the minimum DLS and corresponding sail angle together.

The opposite limiting case is illustrated in trajectory 3 (dark blue). The profile builds at an infinitely high DLS to the corresponding sail angle, denoted as DLS_{inf} and φ_{inf}. Thus, the build and drop sections vanish and the profile consists only of the tangent section. While this trajectory cannot be realistically constructed, it provides a theoretical lower limit for the sail angle inclination.

Together, the minimum DLS trajectory and the infinite DLS trajectory provide the boundaries for all possible trajectories. Trajectories outside these boundaries, that is, trajectories whose DLS fall below DLS_{min} or whose φ fall below φ_{inf} or exceed φ_{min}, do not yield a valid trajectory.

Trajectory 2 (green) lies within the boundary values. Its parameters are chosen arbitrarily, but the comparison of its build and drop sections DLS with the minimum DLS of trajectory 1 shows that the profile reacts very sensitively to change in DLS in this range. Even though the DLS has hardly been doubled, the sail angle is closer to the upper limit sail angle (45°) than the lower limit sail angle (90°). Yet this also means that a further increase in the DLS will result in less reduction of the sail angle. Vice versa, an increase in the sail angle towards the upper limit (90°) will not bring a significant reduction in DLS.

These observations lead to two main considerations that require further investigation: First, what are the boundaries DLS_{min}, φ_{min}, and φ_{inf} for other horizontal offsets and vertical depths. This will allow to immediately determine the parameter boundaries under the constraints of any offset and depth. Second, how do the parameters DLS and sail angle influence one another within these boundaries. If the relationship between the parameters is known, the behaviour of DLS and sail angle can be analysed and used to select a DLS within the technical tool limitations that is most efficient in keeping the inclination low.

Figure 13 displays a sheave model that mimics the S-shaped trajectory. The model consists of two sheaves of radius r that are connected by a string. Where the string curves around the sheaves, it represents the build and drop section of the profile, in between the sheaves it represents the tangent section. The DLS of the build and drop section is represented by the curvature radius r and the opening angle φ.

The DLS is a measure of curvature of the well trajectory defined as degrees of change in the well trajectory per 30m of trajectory length. Since there is no change in azimuth in the S-shape and J-shape trajectories considered here, the DLS is the change in inclination per 30m trajectory length (Carden and Grace 2007, 3-1). This is expressed as

$$DLS = \frac{\delta}{30} \tag{1}$$

Where the dogleg δ is the change of inclination in degrees.

The curvature radius is given as (Carden and Grace 2007, 2-7)

$$r = \frac{180}{\pi\, DLS} = \frac{5400}{\pi\, \delta} \tag{2}$$

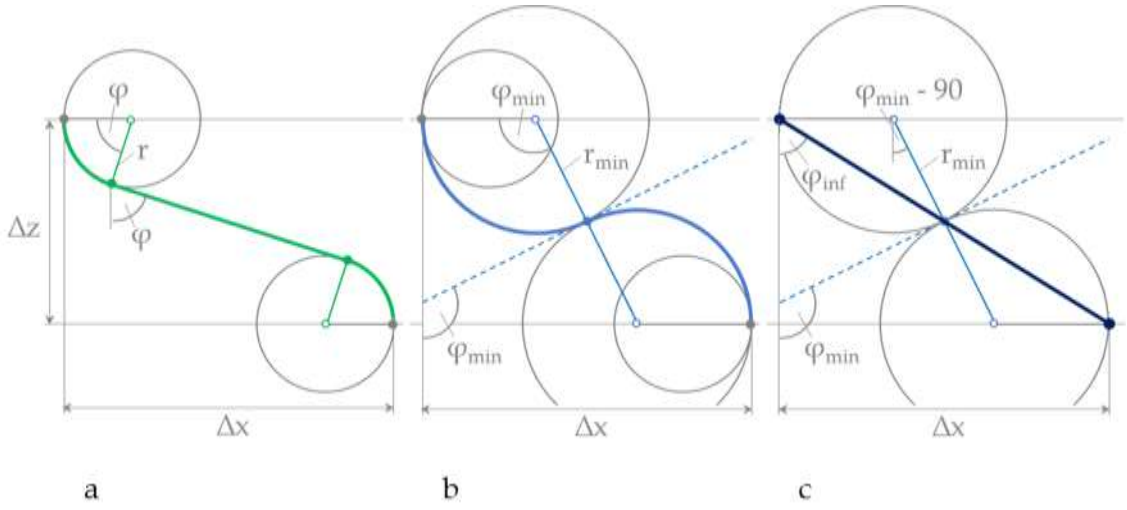

Figure 13: Sheave model for S-shaped trajectory

Thus, the larger the curvature radius, the smaller is the DLS. Figure 13a depicts the S-shaped trajectory for arbitrarily chosen parameters r and φ that lie within the boundary values of the offset and depth constraints. Figure 13b shows the sheaves enlarged so that they touch at exactly half the offset distance. This follows from the symmetry of the S-shaped profile. The sail angle φ is equal to the opening angle of the build and drop sections. This provides a link between the DLS and the sail angle, as well as the key to defining the upper limit for the sail angle.

Figure 13c depicts the curvature radius reduced to 0, so that the DLS in the build and drop section has to become infinitely large. The tangent that connects the KOP to the EOD builds at the smallest possible sail angle, φ_{inf} that can connect the two points. This lower limit is given as

$$\varphi_{inf} = arctan\left(\frac{\Delta x}{\Delta z}\right)\frac{180}{\pi} \tag{3}$$

As this tangent passes through the point where the sheaves touch at half the offset distance and half the vertical depth, the sail angle φ_{min}, that represents the upper limit is given as (Figure 13c – Appendix A.1)

$$\varphi_{min} = 2\,\varphi_{inf} \tag{4}$$

$$\varphi_{min} = 2\,arctan\left(\frac{\Delta x}{\Delta z}\right)\frac{180}{\pi} \tag{5}$$

As pointed out above, the sail angle is a depends on the ratio between the horizontal offset and the vertical depth. This reflects in the relationships for the lower and upper limits of possible sail angles. Figure 14 plots these limits over a range of Δx/Δz. As these ratio increases, φ_{inf} and φ_{min} approach 90° and 180° respectively. The sail angle inclination of an S-shaped profile must lie in between those boundaries, sail angles outside of the boundaries are not possible. Further, the lower boundary φ_{inf} is only a theoretical boundary that cannot be reached. Realistically, sail angles have to be larger than the lower limit, yet the boundary still provides a quick assessment of the range of possible sail angles.

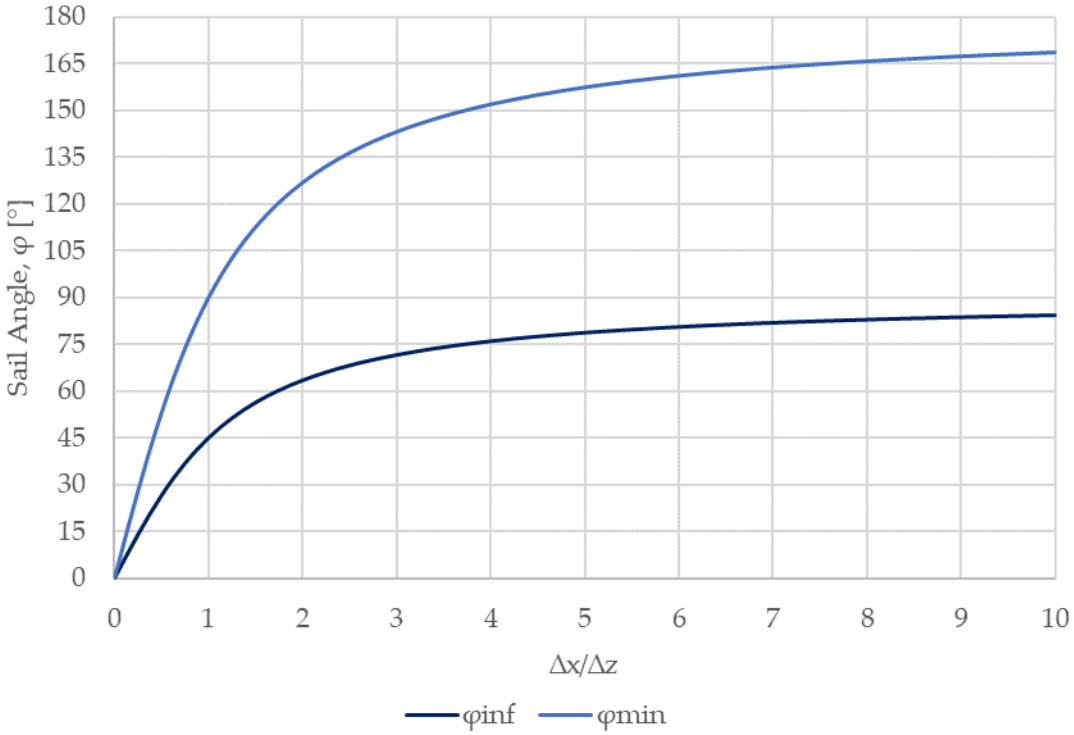

Figure 14: Upper and lower limit for sail angle as function of Δx/Δz.

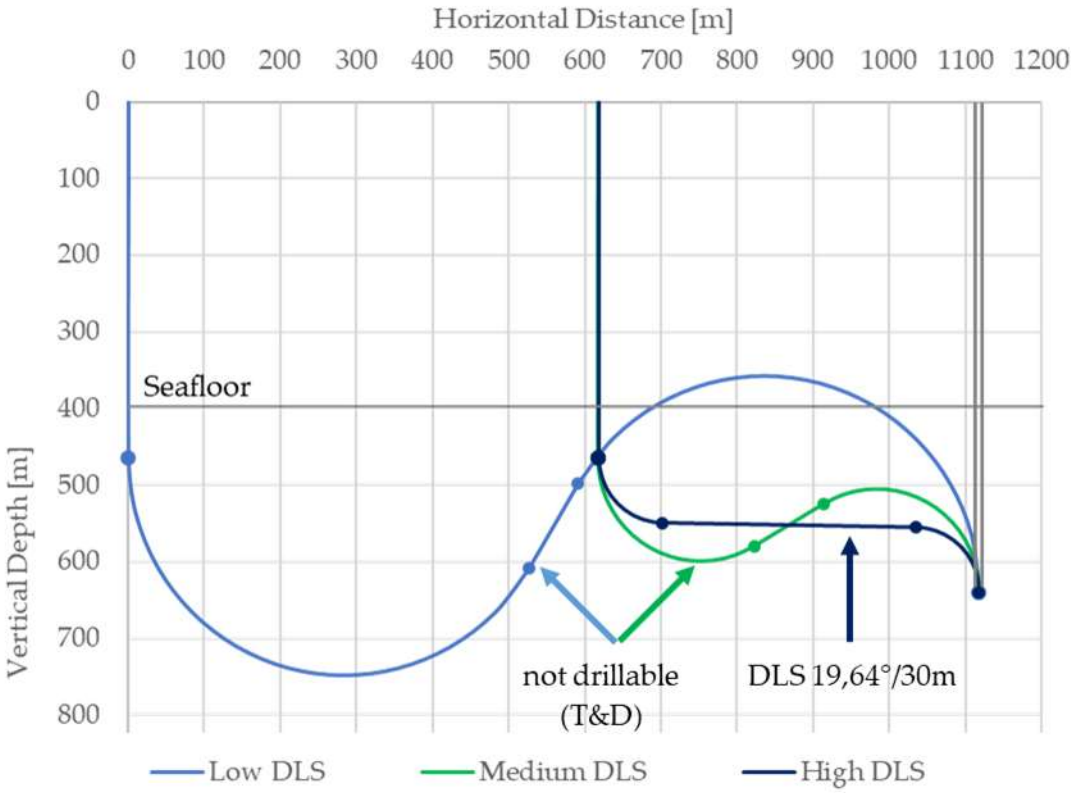

Figure 15: Low, medium, and high relief well strategy visualised as S-shape trajectories.

A further constraint that needs to be taken into account for S-shaped trajectories is that not only are high inclinations in excess of 90°difficult to drill, but above certain inclinations the trajectory will have to build above its own KOP to yield a solution. This is depicted in Figure 15, which shows the low, medium, and high DLS relief well strategies that were devised for the Wisting discovery as S-shaped trajectories. Even if the inclination could be drilled, such a profile would not make sense. Realistically, S-shapes exceeding 90° cannot be drilled due to the high torque and drag in such a profile. This consideration renders the upper sail angle limit an invalid zone at higher inclinations and narrows the range of possible sail angles down further.

However, based on the upper limit φ_{min} a relationship for the minimum DLS can be defined as a function of the horizontal offset and vertical depth. Again, use is made of the symmetry of the S-shaped trajectory as depicted in Figure 13b. In combination with the relationship between DLS and curvature radius (equation (2)) the minimum DLS is given as (Appendix A.2)

$$\delta_{min} = \frac{10800 \sin(\varphi_{min})}{\Delta z \, \pi} \tag{6}$$

Replacing φ_{min} (equation (5)) yields

$$\delta_{min} = \frac{10800 \sin(2 \, arctan\left(\frac{\Delta x}{\Delta z}\right) \frac{180}{\pi})}{\Delta z \, \pi} \tag{7}$$

The relationship shows that the shallower the depth (Δz) that is available for building the profile, the higher is the minimum requirement for the DLS. The relationship is plotted in Figure 16 for a vertical depth of 175 m, which is the depth that was assumed to be available for constructing the trajectory on the Wisting discovery (Table 1) and Δz = 500 m for comparison.

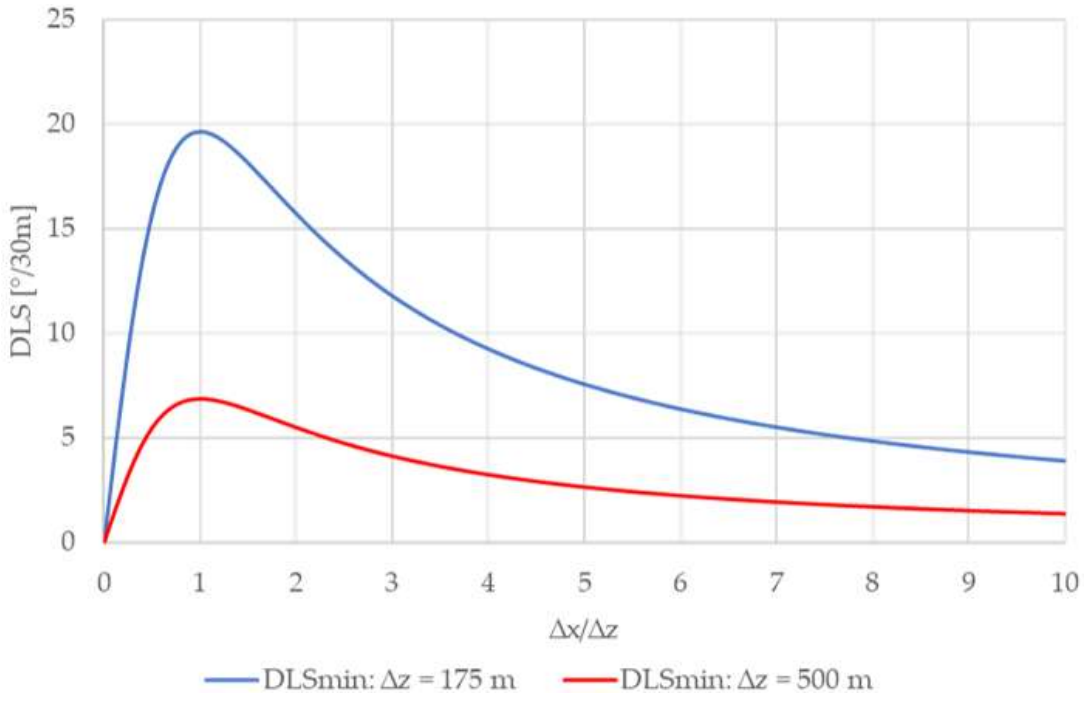

Figure 16: Minimum DLS in S-shape for vertical depth of Δz = 175 m and Δz = 500 m.

The DLS in the trajectory can only assume values above the minimum DLS. Since it peaks at Δx/Δz = 1, this DLS will yield a solution for all offsets at the particular depth. If the spud location is located further from the target than the vertical depth between KOP and target, at this DLS the resulting profile will have a horizontal tangent section, like the high DLS trajectory in Figure 15.

For an increasing Δx/Δz, the minimum DLS approaches 0. However, the graphs need to be combined with the upper boundary of the sail angle. As the inclination becomes increasingly high, the profiles become unrealistic, as shown in Figure 15, and this applies equally for the decreasing minimum DLS.

Equation (7) provides a relationship between the DLS and the sail angle for the limiting case of the minimum DLS and the corresponding upper sail angle limit. To generalize this relationship for any DLS and sail angle within the limiting boundaries, the link between sail angle and opening angle as indicated in the trajectory in Figure 13a and the symmetry of the trajectory is used to yield (Appendix A.3)

$$\delta = \frac{10800\ (1 + \sin(\varphi - 90) - \cos(\varphi - 90)\tan\varphi)}{\pi\ (\Delta x - \Delta z \tan\varphi)} \tag{8}$$

In this general case, the DLS is a function of the horizontal distance and vertical depth, Δx and Δz, between KOP and target and the sail angle φ, which can assume values between φ_{inf} and φ_{min}. The confining factors on the relief well trajectory are the horizontal distance and the vertical depth, as they are fixed by the relief well's spud location and the setting depth of the last casing in the blowing well. To study the relationship of the parameters that can be adjusted, DLS and sail angle, under the given constraints, Figure 17 plots equation (8) for the horizontal offset and vertical depth of the Wising medium and high DLS strategy (Table 1).

As suspected for the trajectories displayed in the example in Figure 12, the behaviour of the DLS vs sail angle changes between the limit boundaries. The more the DLS is increased above a certain point, the less effect the increase has on reducing the inclination. Below a certain point, further reduction of the DLS by increasing the sail angle becomes less and less effective. Where the slope of the curve assumes an inclination of -45°, both the DLS and the inclination are kept as low as possible in the most effective way. In other words, in the point indicated in Figure 17 as DLS_{eff} and $\varphi_{eff,}$, one gets the most out of the invested DLS in terms of a low sail angle. To find this point, equation (8) is differentiated with respect to the sail angle φ, resulting in (Appendix A.4)

$$\delta' = \frac{10800}{\pi}\left[\frac{(\sin(\varphi - 90) * \tan\varphi - \cos(\varphi - 90) * \cos^{-2}\varphi + \cos(\varphi - 90))}{(\Delta x - \Delta z \tan\varphi)} + \frac{\Delta z \cos^{-2}\varphi\ (1 + \sin(\varphi - 90) - \cos(\varphi - 90)\tan\varphi}{(\Delta x - \Delta z \tan\varphi)^2}\right] \tag{9}$$

The derivative δ'(φ) is solved for -30 by altering the sail angle φ.

In the presented case, however, the DLS_{eff} is larger than the achievable build rate. Therefore, the build rate has to be lowered to a realistically achievable DLS by increasing the sail angle. The minimum DLS under the conditions is 12,25°/30m and would require a sail angle of more than 140°.

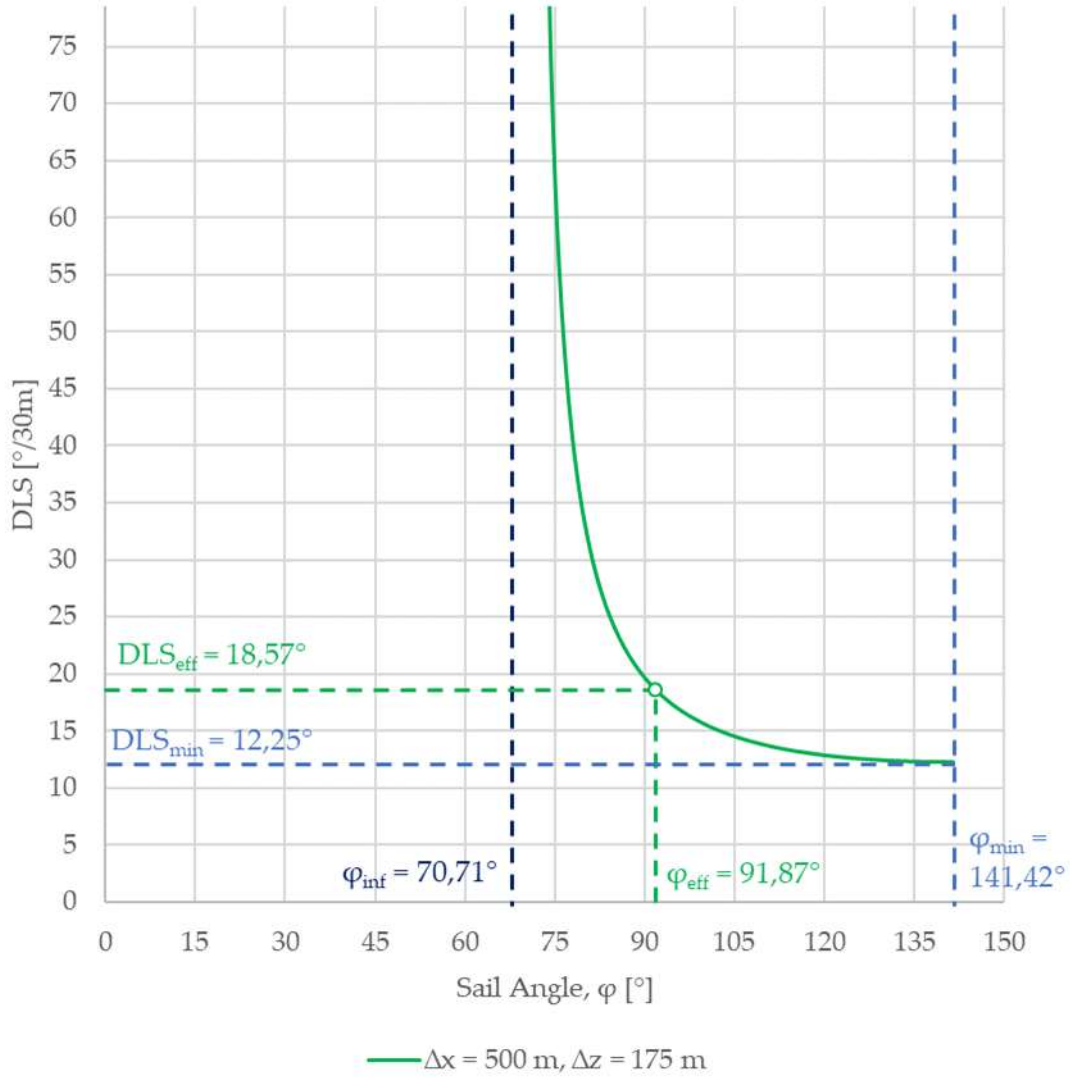

Figure 17: DLS vs sail angle behaviour and most effective DLS in S-shaped trajectory under conditions in Wisting.

In conclusion, it is not possible to construct an S-shaped trajectory under the given conditions. A similar relationship and analysis must be established and conducted for the J-shaped profile to compare it to the S-shaped trajectory.

3.2.2 J-Shape

The relationships obtained for the S-shaped trajectory can be modified for the J-shaped trajectory by thinking of the J-shaped trajectory as being contained in the first half of the symmetric S-shaped trajectory. Figure 18 illustrates this on the sheave model.

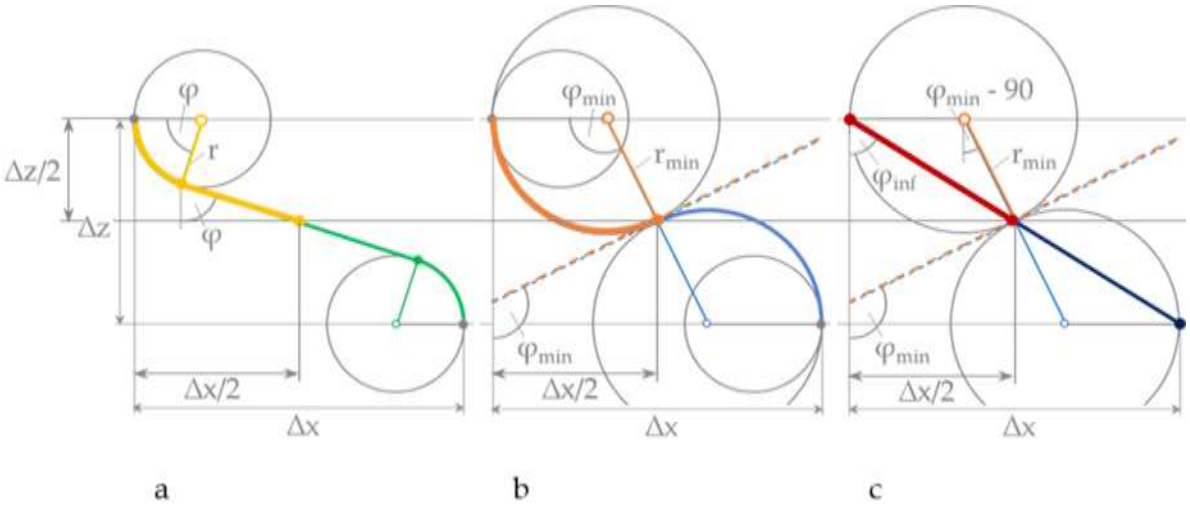

Figure 18: Sheave model for J-shaped trajectory

By replacing Δx and Δz in the relationships derived for the S-shaped trajectory by Δx/2 and Δz/2, as indicated in Figure 18, the relationships can be easily modified for the J-shaped trajectory:

$$\varphi_{\inf J-shape} = arctan\left(\frac{\Delta x}{\Delta z}\right)\frac{180}{\pi} \tag{10}$$

$$\varphi_{\min J-shape} = 2\ arctan\left(\frac{\Delta x}{\Delta z}\right)\frac{180}{\pi} \tag{11}$$

$$\delta_{\min J-shape} = \frac{5400\sin(\varphi_{min})}{\Delta z\ \pi} \tag{12}$$

$$\delta_{J-shape} = \frac{5400\ (1+\sin(\varphi-90)-\cos(\varphi-90)\tan\varphi)}{\pi\ (\Delta x-\Delta z\tan\varphi)} \tag{13}$$

$$\delta'_{J-shape} = \frac{5400}{\pi}\left[\frac{(\sin(\varphi-90)*\tan\varphi-\cos(\varphi-90)*\cos^{-2}\varphi+\cos(\varphi-90))}{(\Delta x-\Delta z\tan\varphi)} + \frac{\Delta z\cos^{-2}\varphi\ (1+\sin(\varphi-90)-\cos(\varphi-90)\tan\varphi}{(\Delta x-\Delta z\tan\varphi)^2}\right] \tag{14}$$

The upper and lower limit for the sail angle are identical in J-shape and S-shape trajectories. Therefore, these relationships can be used universally for assessing the range of possible sail angles at a glance.

The relationships concerning the DLS are identical to the relationships for the S-shaped trajectories multiplied by a factor 1/2. Therefore, at identical sail angles, the J-shaped profile requires exactly half the DLS that would be required in an S-shaped profile.

The concept of the minimum DLS and the most efficient DLS have already been introduced in the discussion of the S-shaped trajectory. To take this one step further, Figure 19 provides a link between the minimum DLS and the concept of the most effective DLS. The most effective DLS, as described for the S-shaped trajectory, is found by subjecting the derivative DLS'(φ) to a value of -30 (= slope inclination of -45°). Subjecting the derivative DLS'(φ) to 0 (= slope is horizontal) yields exactly the minimum DLS. This is expected, because the concept of the minimum DLS means that the sail angle is entirely sacrificed for the DLS.

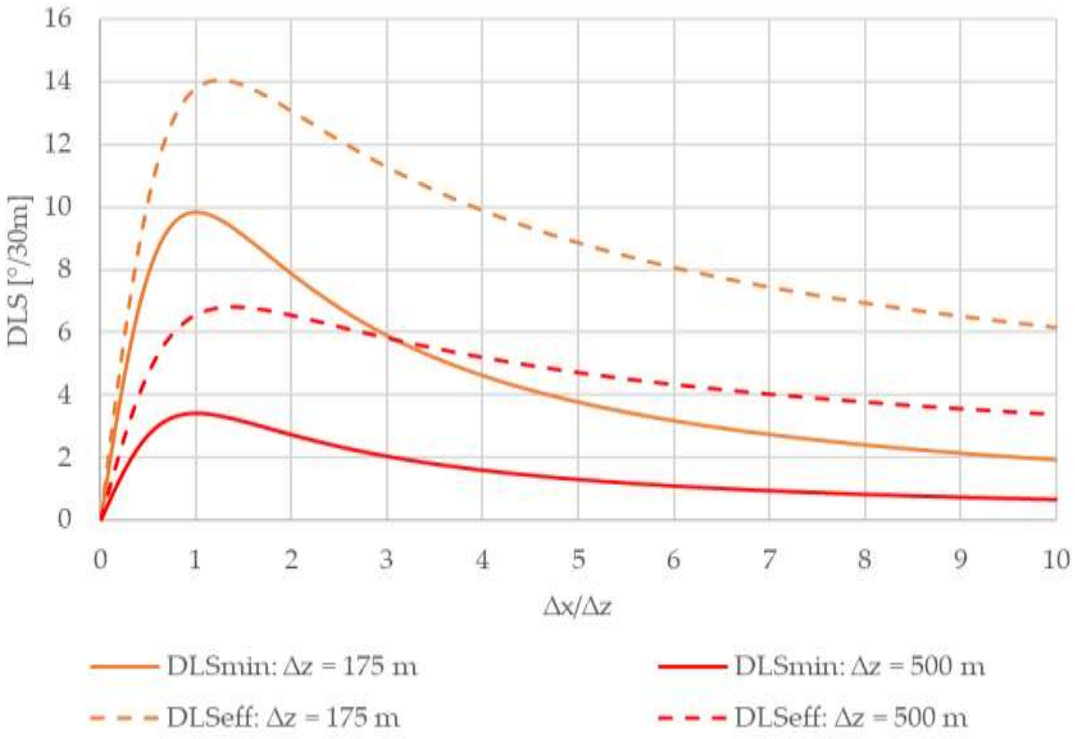

Figure 19: Minimum DLS and most effective DLS in J-shape for vertical depth of Δz = 175 m and Δz = 500 m.

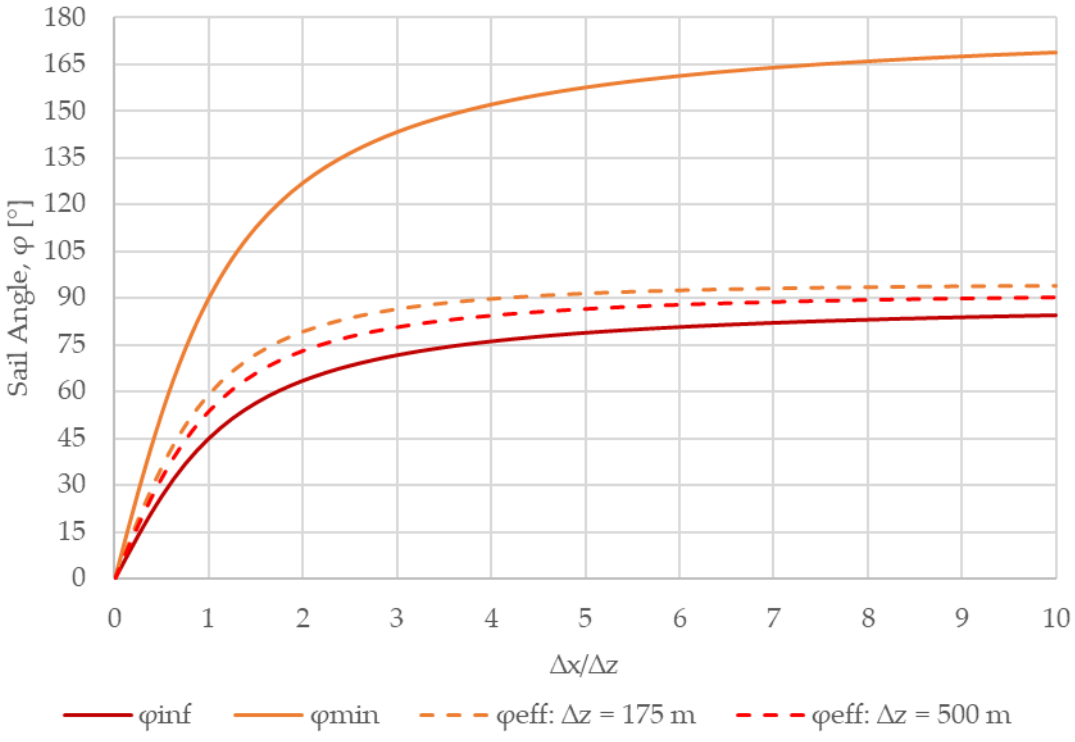

Figure 20: Upper and lower limit for sail angle and most effective sail angle in J-shape for vertical depth of Δz = 175 m and Δz = 500 m as function of Δx/Δz.

Figure 20 applies this concept to the corresponding sail angles. While the φ_{inf} and φ_{min} are universal for identical rations of horizontal offset and vertical depth, the most effective sail angle depends on the available vertical depth (Δz) between KOP and target.

Lastly, Figure 21 plots the relationship between DLS and sail angle for a J-shaped trajectory. As the experience gained from constructing the horizontal well Wisting Central II shows, the most effective DLS of 11,5°/30m is realistically achievable and such a profile could be constructed.

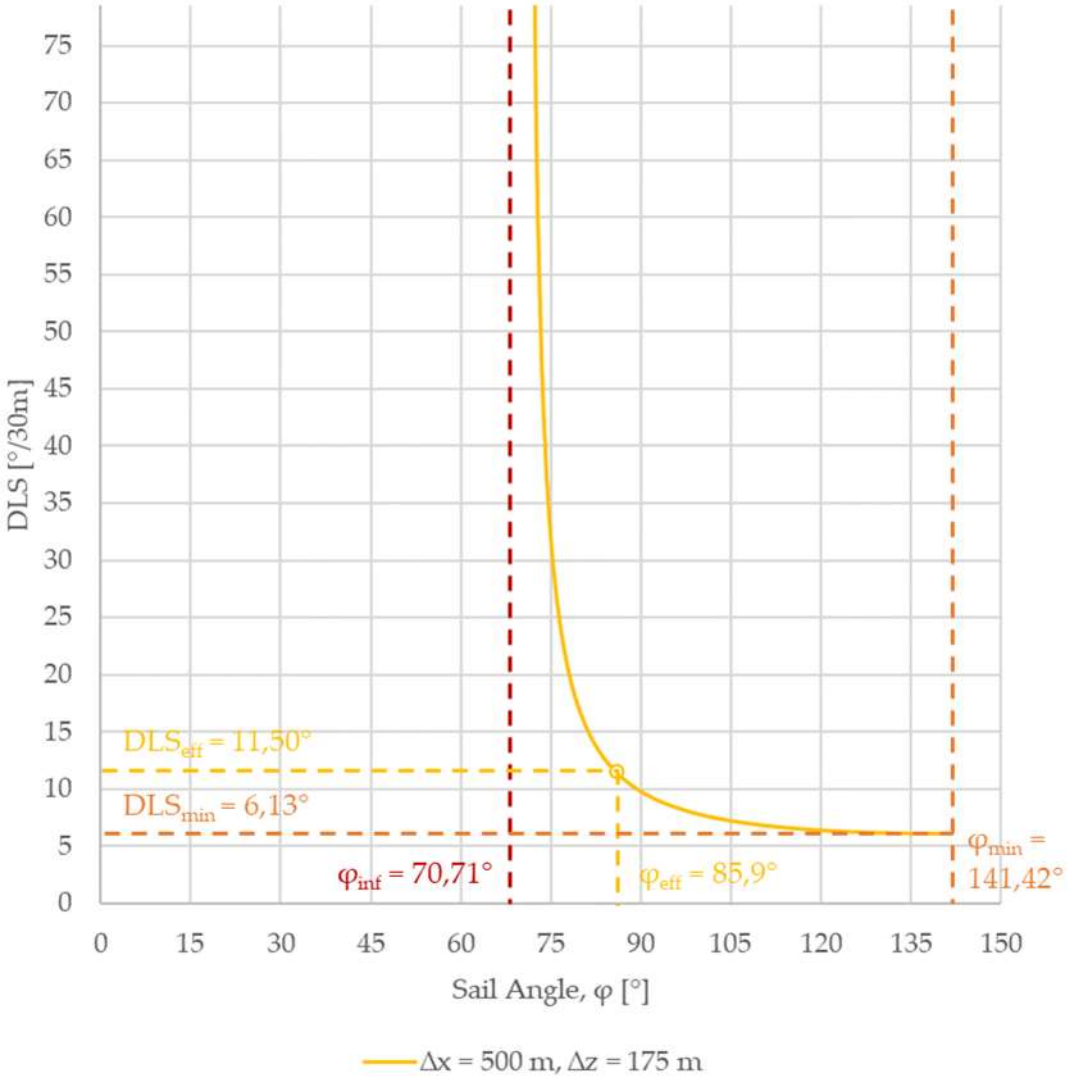

Figure 21: DLS vs sail angle behaviour and most effective DLS in J-shaped trajectory under conditions in Wisting.

In conclusion, under the given conditions the J-shaped trajectory is preferable to the S-shaped trajectory. In the following section, these findings are applied to the low, medium and high relief well strategy designs that were devised for Wisting. Furthermore, optimised designs for the most efficient DLS will be suggested for the relief well locations that were identified for the wells Wisting Central II and III (Figure 7).

3.2.3 Effective Trajectory Under Constraints at Wisting

The following graphs in Figure 22 are generated based on the relationship between DLS and sail angle for J-shaped trajectories (equation (13)) that was derived from the sheave model. The horizontal offset and vertical depth, Δx and Δz, are the KOP and intersection point of the low, medium, and high DLS relief well strategies that were devised for Wisting (Table 1). The DLS and sail angle of those three trajectories (Figure 10) are also plotted into the Figure.

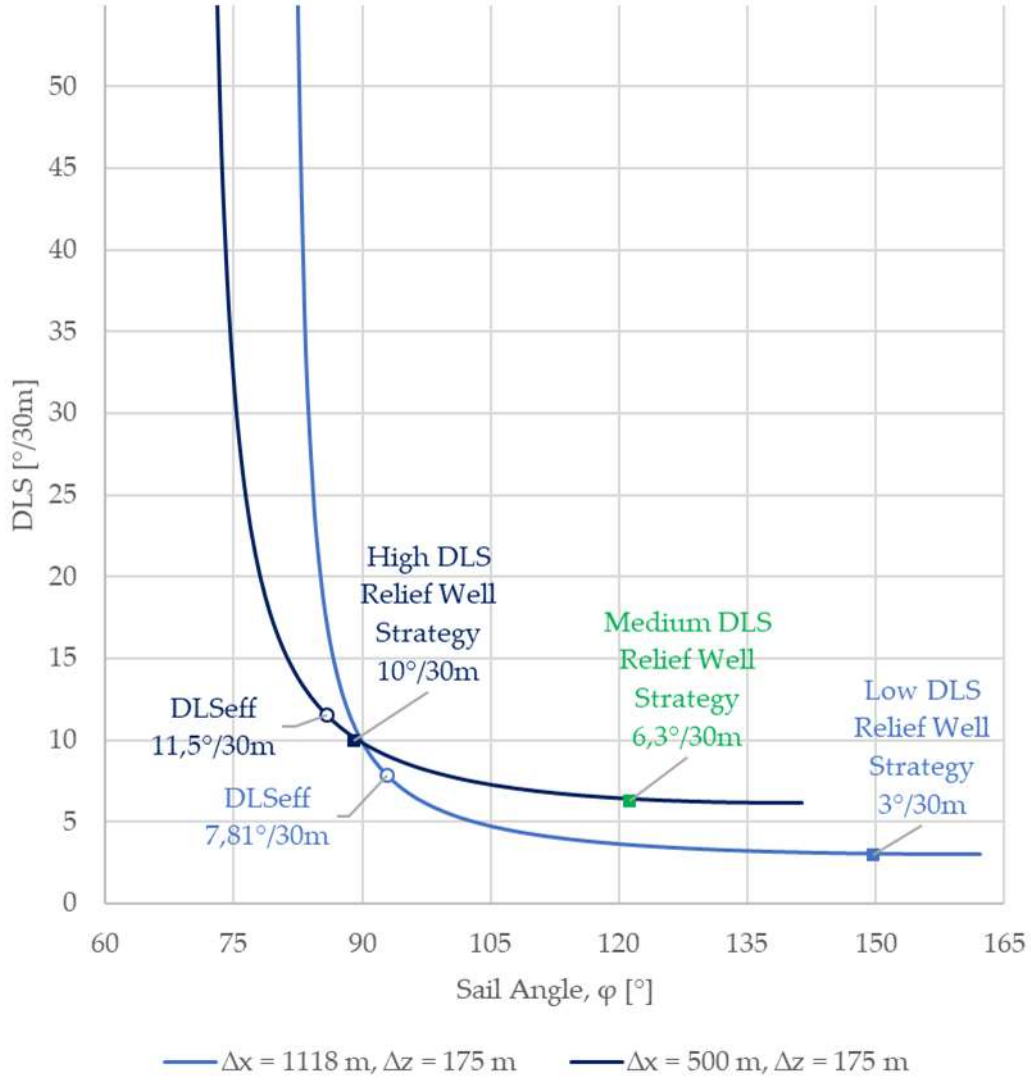

Figure 22: DLS vs sail angle for J-shaped trajectories for low, medium, and high DLS relief well startegy

The DLS and sail angles of the relief wells that were planned as J-shaped trajectories in a commercial software match the DLS/sail angle behaviour derived from the sheave model quite well. At the same inclinations, the sheave model results in DLS of 10,16 / 6,38 / 3,04 for the high, medium, and low DLS design. This confirms the validity of the sheave model.

The relief well strategies were devised based on three different scenarios for the DLS capability in the Wisting overburden, which was not known at the time. Through experience gained on Wisting Central II, it can now be assumed that DLS in the range of 10-12,5°/30m are possible. However, a relief well that is spudded from a distance of 500 m from the target, does not profit from a further increase in DLS beyond 11,5°/30m.

The medium DLS scenario was applied to the potential relief well for Wisting Central II. Under the presented conditions, the trajectory would profit from an increase in the DLS. The same applies to the low DLS scenario. Even a slight increase in the DLS would cause a tremendous improvement in the trajectories sail angle. Therefore, in scenarios where build rates in this range are to be expected (medium and low DLS) it is recommended to put efforts into increasing the DLS capability. Even a slight increase in the range of 0,5 – 1°/30m additional DLS will lower the sail angle significantly.

Based on the DLS vs sail angle behaviour depicted in Figure 22 and the DLS capability that was proven on Wisting Central II, relief well trajectory plans for future wells should aim for the high DLS strategy, as this design is the most efficient under the conditions.

In the following, the concept of the most efficient DLS is applied to the relief well spud locations that were identified for two most recent wells on the discovery (Figure 7). It is assumed that the water depth at the locations is 400 m and that the trajectories can kick off at 411 m by the use of a CAE, similar to Wisting Central II.

Table 2 summarizes the conditions that confine the relief well trajectory for Wisting Central II and Wisting Central III. Based on these confining conditions, the relief well trajectories are constructed for each well.

	Wisting Central II	**Wisting Central III**
Intersection casing setting depth	594m	610m
Offset distance to spud locations	1490m / 1575m / 1780m	700m / 788m
Azimuth from spud locations	187° / 108° / 57°	255° / 147°
Δx [m]	1490 / 1575 / 1780	700 / 788
Δz [m]	183	199
$\Delta x/\Delta z$	8,1 / 8,6 / 9,7	3,5 / 4,0

Table 2: Wisting relief well trajectory confining conditions. After Nedrum (2015) and Trauner (2017).

The most effective sail angle as a function of the ratio between offset and vertical depth is plotted in Figure 23 within the limiting boundaries. Since the last casing is set at similar depths in both wells, the curves almost overlap each other. For each location that was identified as a possible relief well spud location for the two wells, the most effective sail angle is indicated.

Figure 24 plots the most effective DLS over the minimum DLS for both wells. Since the minimum DLS for a horizontal relief well is below 10°/30m for Wisting Central it might be better in this case to exceed the most effective DLS to reduce the sail angle inclination

to 90°. The behaviour between DLS and sail angle is analysed individually for each well in Figure 25 and Figure 27.

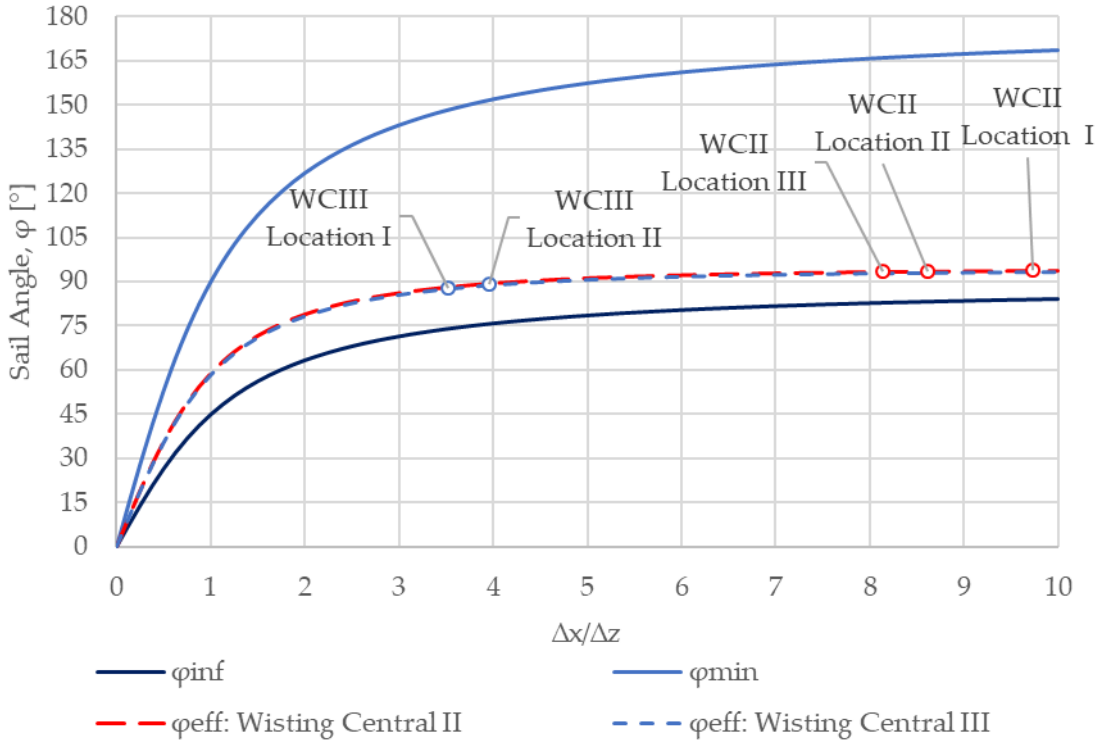

Figure 23: Most effective sail angle and upper and lower limit sail angle for Wisting Central II and III.

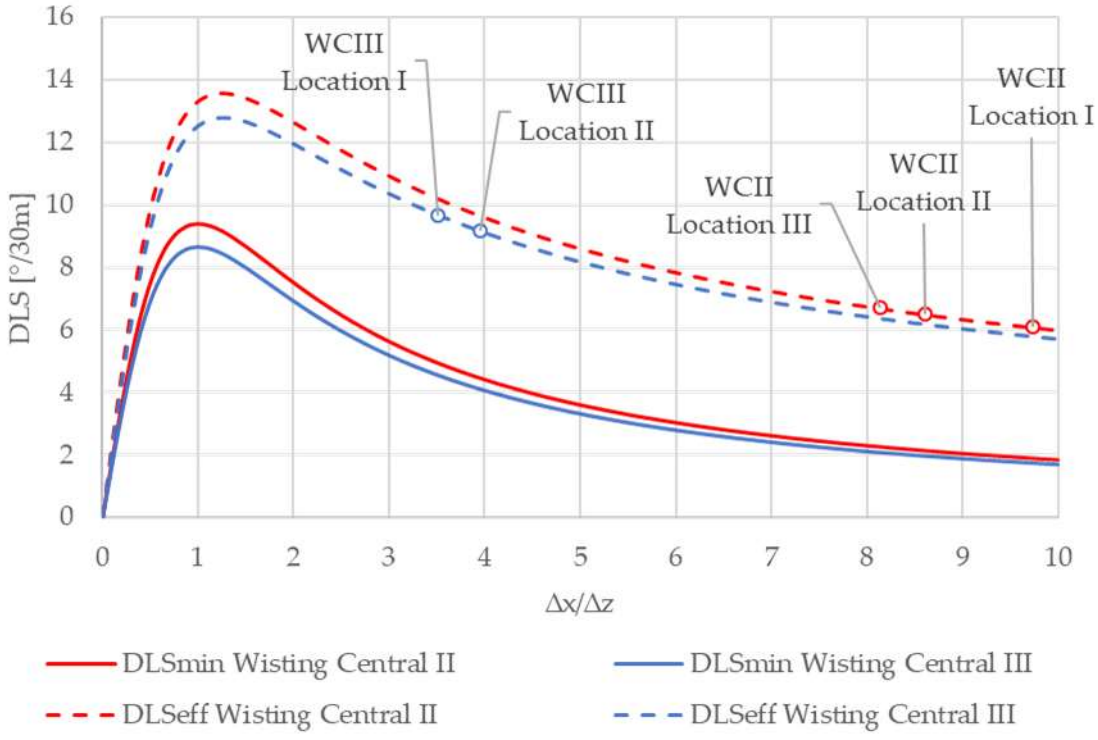

Figure 24: Most effective DLS and minimum DLS for Wisting Central II and III.

Figure 25 shows the DLS vs sail angle behaviour for the three spud locations that were identified for Wisting Central II. The curves lie closely together, because the ratio $\Delta x/\Delta z$ are similar for the locations. Thus the most effective DLS and sail angle are also similar. The profile would build to more than 90° inclination in this most effective design, but as the curve shows, increasing the DLS to 10°/30m would reduce the sail angle to horizontal. However, a further reduction of the sail angle below 90° is not recommended as this would require a disproportional increase in DLS.

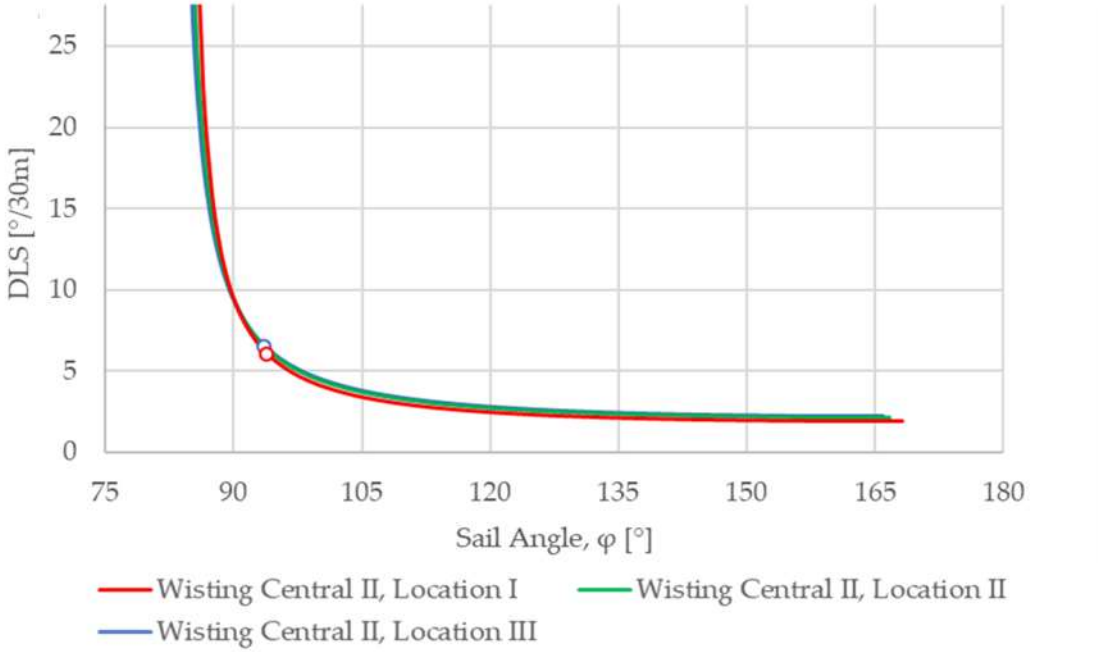

Figure 25: DLS vs sail angle for Wisting Central II potential relief well spud locations.

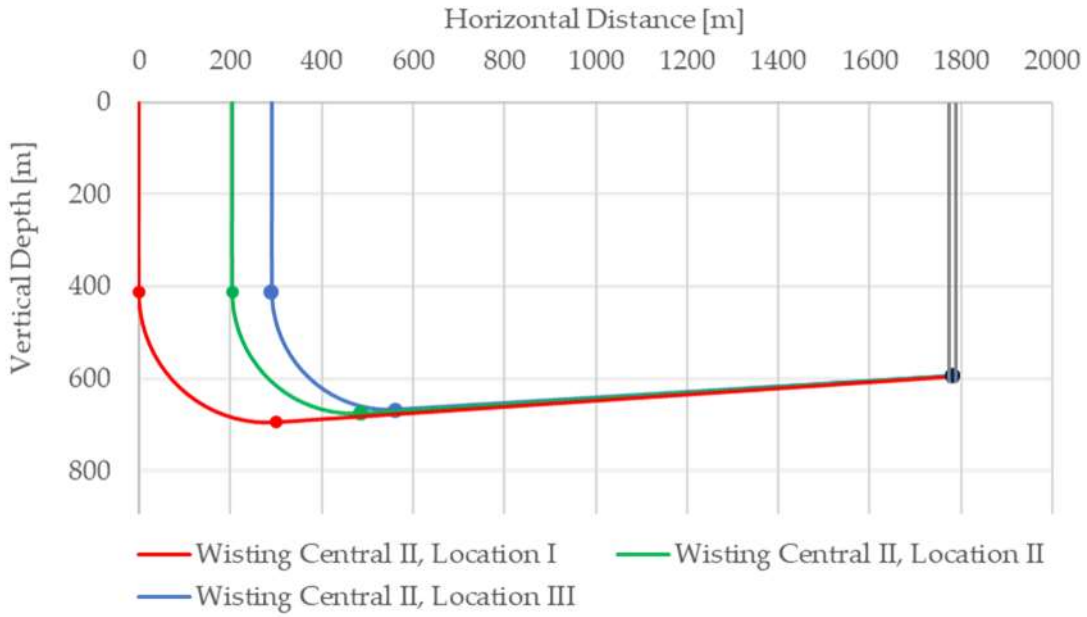

Figure 26: Most effective J-shaped relief well trajectories for Wisting Central II.

Figure 26 visualizes the J-shaped trajectories in the most effective point. Due to the long tangent section a reduction in sail angle to 90° on expense of the DLS might be preferable.

Wisting Central III presents a similar picture. From both spud locations, the most effective DLS and sail angle assume similar values, as shown in Figure 27. The ratio $\Delta x/\Delta z$ is much lower in comparison to Wisting Central II, thereby shifting the sail angles to lower values. The most effective trajectory builds at a DLS of slightly below 10°/30m and to slightly below horizontal.

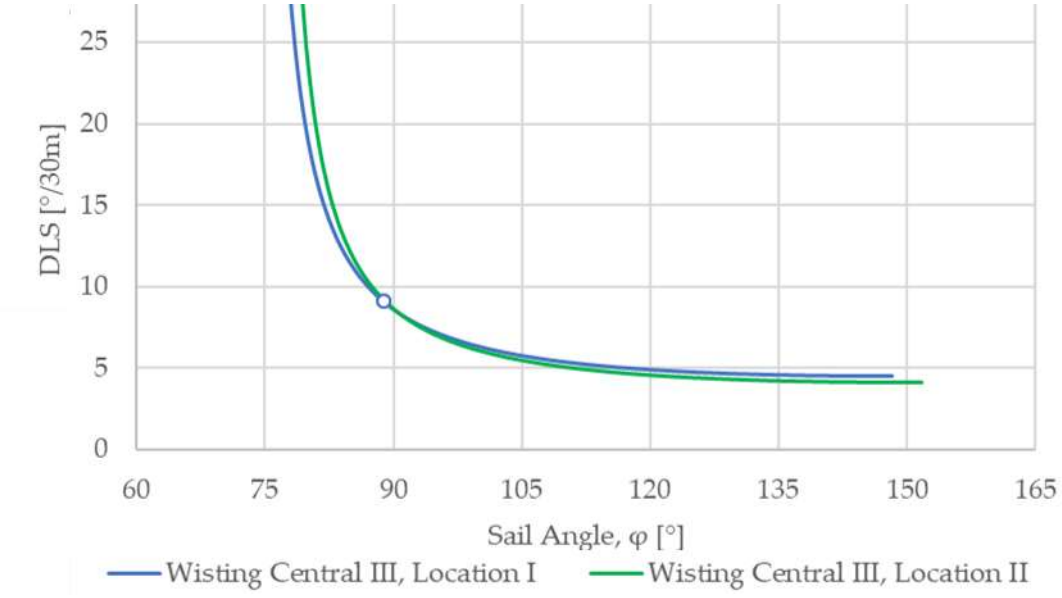

Figure 27: DLS vs sail angle for Wisting Central III potential relief well spud locations.

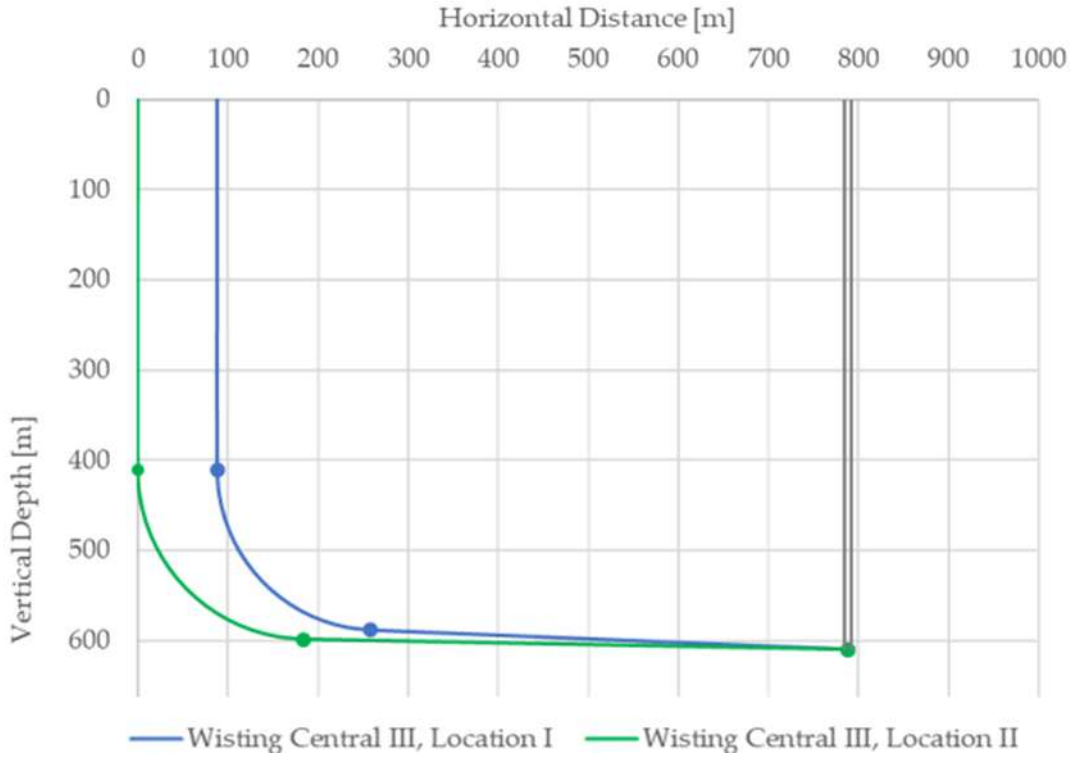

Figure 28: Most effective J-shaped relief well trajectories for Wisting Central II.

Figure 28 visualizes the J-shaped trajectories that build at the most effective DLS for the spud locations that were identified for Wisting Central III. The parameters of the presented trajectories are summarized in Table 3, including the DLS requirement for horizontal wells.

	Wisting Central II	**Wisting Central III**
Δx [m]	1490 / 1575 / 1780	700 / 788
Δz [m]	183	199
φ_{eff} [°]	93,5 / 93,6 / 93,8	87,7 / 88,9
DLS_{eff} [°/30m]	6,7 / 6,5 / 6,1	9,7 / 9,2
$DLS_{\varphi = 90°}$ [°/30m]	9,4	8,6

Table 3: Most effective DLS and sail angles for J-shaped trajectory; DLS to build to 90°.

To conclude, the recommended design for relief wells in the shallow discovery is a high DLS J-shape design, as it results in the most efficient combination of DLS and sail angle. A further increase of the DLS would not yield an efficient reduction of the sail angle. The required build rate is thus in the range of 10°/30m. For a hole size of 12 1/4", this presents limitations in the selection of directional drilling tools and drilling performance. The following section reviews available directional tools with regards to their application for the required hole size and DLS capability.

3.3 Directional Control

On Wisting Central II, the required DLS in the build section was achieved with positive displacement motors (PDM). After the wellbore had reached almost 90° inclination, the horizontal section was drilled with rotary steerable systems (RSS). Bryan, et al. (2009) state that well sections that require a high DLS are drilled with PDMs because they can reliably and consistently build at rates > 10°/30m, whereas such high DLS are considered too aggressive for RSS (Malcore and Murray 2010). This subsection examines commercially available directional drilling tools and discusses their influence on the planned trajectory.

3.3.1 Positive Displacement Motors

PDMs are installed in the BHA, usually directly above the drill bit. They either have a bent housing or are combined with a bent sub between motor and drill bit. The bent housing or bent sub can be set on surface to introduce a bend of up to a few degrees into the BHA. This bend is referred to as the bend angle. Above the bend, the PDM incorporates a power section that consists of a rotor-stator configuration. The stator is the housing and contains the stator elastomer while the rotor rotates the drill bit via a drive shaft. The rotor in turn is driven by the mud that is circulated through the drillstring. The rotation speed of the rotor, and therefore the rotation speed with which the PDM rotates the drill bit, depends on the rotor/stator lobe ratio and the flow rate of the drilling mud. At the same flow rate, a lower lobe ratio will result in more rotor RPM than a higher lobe ratio. The pump pressure, which generates the flow rate of the drilling

mud, controls the motor torque output when the bit is on bottom. There is a pressure drop across the motor when the drilling mud is pumped through it. The longer the motor and the more stages it incorporates, the higher the pressure drop will be and the higher the resulting torque available to drill (Schlumberger 2004). The stator is elastomer lined, therefore the deformable elastomer will absorb some of the energy generated by the pump. High efficiency PDMs have a thin even-wall-thickness elastomer lining to increase their torque output efficiency (Malcore and Murray 2010).

To steer the wellbore with a PDM, the bend angle is set to the desired value on surface and the offset between it and the MWD orientation is measured, before the assembly is run into the hole. The orientation of the bend is referred to as toolface. In the hole, the toolface is oriented from surface by small increments of pipe rotation, so that it will point into the desired direction of wellbore deflection when drilling with the selected WOB. Toolface orientation is influenced by the WOB because of the resulting reactive torque between drill bit and formation. In this sliding mode, the drill bit rotation only stems from the rotor being driven by the circulating drilling mud. The drillstring, including the BHA, does not rotate and therefore slides into the borehole. The wellbore is deviated into the direction of the toolface when drilling in sliding mode.

When drilling in rotating mode, the resulting drill bit RPM is the combination of the drillstring RPM and the RPM generated by the PDM. As the drillstring is rotated, the toolface rotates with it and creates a hole along the axis of the BHA.

When changing between rotating and sliding, the drill bit has to be picked up off bottom and the toolface needs to be oriented before sliding. In applications where the drilling mode is often altered between rotating and sliding, this can add a considerable amount of time during which the drill bit is not on bottom and therefore not making hole (Bryan, et al. 2009). Since the motor bend setting is adjusted on surface prior to running in hole, changing the bend angle requires a round trip. In the case of Wisting Central II the bend angle was reduced to 1,56° because the build rate that was achieved with a bend angle setting of 1,83° was too high.

Steering a wellbore with a PDM by alternating between rotating and sliding intervals comes with several limitations, due to the working principle of PDM. Alternating between steering and rotary drilling causes the DLS in slide sections to be higher than the planned average DLS in the overall section while no build rate is achieved in the rotated sections. This can lead to a higher tortuosity of the wellbore (Bryan, et al. 2009), (Malcore and Murray 2010) and in turn to high local doglegs. Alrushud, et al. 2018 define tortuosity as the deviation of the actual wellpath from the planned wellpath with the implication that the actual wellpath will result in higher DLS than the planned wellpath, due to the corrections that are made continuously to follow the planned trajectory.

High DLS in general decreases the fatigue life time of drillstring components that are run into, and rotated through these doglegs. Further, a tortuous wellbore increases the torque and drag in the borehole (Janwadkar, et al. 2011).

When drilling in sliding mode, the drag of the drillstring is greatly increased because it is not rotated. This drag counteracts the transfer of weight to the drill bit and can also cause a reduced rate of penetration to the point where extended horizontal sections

cannot be steered with PDM because of excessive drag (Malcore and Murray 2010), (Warren 2006).

Another result of not rotating the string is that cuttings are not transported out of inclined sections of the hole as efficiently as they could be if the string rotation would sweep them into the drilling mud stream. This compromised hole cleaning can reduce the rate of penetration (ROP) if cuttings beds form. Furthermore, a cuttings bed can put the BHA at risk of getting stuck when pulled out of the hole (Bryan, et al. 2009). Not rotating the string further increases the risk of becoming differentially stuck when the BHA lies against the borehole wall during sliding intervals in overbalanced borehole conditions (Tribe, et al. 2003), (Tipu, et al. 2015).

When drilling in rotating mode, a high bend setting can lead to an increased stress state of the BHA. Depending on the flexibility of the BHA (string stabiliser number and placement, tool OD, etc.) and the strength of the formation it drills in, the bit is forced into the centre of the hole by the confining rock while the string is rotated, forcing the BHA to flex with the rotation. This can significantly limit the RPM at which the string can be rotated or render rotating unfeasible altogether even when rotating off bottom (Janwadkar, et al. 2011), (Malcore and Murray 2010). In weaker formations, on the other hand, the bend angle of the assembly is more likely to cause the hole to be slightly overgauge and spiralled (Moody and Boonen 2005), (Gharib and Kirkhope 2017). Poor hole quality can affect the dogleg capability of the motor when the well is being steered again in sliding mode after rotating (Schlumberger 2004). Further, the quality of some borehole logs can be compromised if the sensors lose contact with the borehole wall (Moody and Boonen 2005). A higher bend angle, on the other hand, can enable the BHA to achieve a higher DLS.

On Wisting Central II, the build section was drilled entirely in sliding mode to achieve the required build rate. This caused severe hole cleaning concerns. The build section was drilled as a pilot hole and subsequently underreamed to the required hole size because the resulting stress state of the 17 1/2" section BHA was deemed too high to drill or back ream when set to the required bend angle to drill the curve.

3.3.2 Rotary Steerable Systems

Due to the operating principle of RSS, they have several advantages over PDMs, one of the most prominent in the literature being their ability to rotate while steering (Bryan, et al. 2009), (Malcore and Murray 2010), (Warren 2006).

Generally, RSS are categorized into point-the-bit and push-the-bit systems, based on their steering principle. Sugiura (2008) argues that the systems' steering principles cannot be strictly separated into point and push principle, as both rely on stabilization points in the BHA which allow the bit to be pushed against the side of the borehole it is steered into. To achieve this, the lower part of the BHA must be deflected off the centre axis of the BHA above it, therefore pointing the drill bit into this direction. The RSS schematics presented in Sugiura's paper suggest that the distinguishing factor between point- and push-the-bit principle is the relative position of deflection force and pivoting point.

RSS that are categorized as point-the-bit, rely on a deflection mechanism that introduces a bend into the BHA, similar to the bend angle of a PDM. However for most commercially available point-the-bit RSS the bend angle can be adjusted downhole while drilling (Gyrodata n.d.), (Halliburton 2018), (Weatherford 2018). Only one RSS that is marketed as point-the-bit system was identified that does not have downhole adjustable bend angle setting. This system has a fixed toolface deflection, which is oriented by counter-rotating an internal deflecting sheave in reference to the drillstring rotation. The deflecting sheave has an eccentric hole which the shaft connecting to the drill bit is lead through, thus achieving a fixed deformation of the shaft. In this way, if the tool drills straight ahead, it has the potential to drill an overgauged and spiralled hole, similar to, but not as severe as, a PDM (Schlumberger 2018).

The other systems marketed as point-the-bit also have an internal deflection mechanism, which acts on a shaft that connects to the drill bit. To make the shaft deflection adjustable, the mechanism incorporates hydraulically actuated swellable pads (Gyrodata n.d.) or spring loaded pins (Weatherford 2018) which are distributed around the circumference of the shaft inside the tool housing or two eccentric rings whereas the shaft is lead through a hole in the inner ring (Halliburton 2018).

The shaft is pivoted between the deflecting mechanism and the drill bit and fixed behind the deflection mechanism. The deflection mechanism, whether adjustable or fixed, acts on the shaft and deforms it to pivot it's axis over the pivoting point. Thus, the drill bit is deflected into the opposite direction of the deflecting force acting on the shaft. To orient the toolface, the point-the-bit RSS with adjustable bend angle rely on a non-rotating outer housing to as a reference. This outer housing must rotate at a limited RPM and should ideally not rotate at all in order for the deflection mechanism to keep the toolface stable. The point-the-bit RSS that has a fixed bend angle fully rotates with the drillstring. Once oriented, it keeps the orientation by the eccentric ring counter-rotating with the drillstring RPM.

Sugiura (2008) describes a point-the-bit system with an external deflection mechanism. It has external mounted pads, similar to push-the-bit mechanisms. As opposed to push-the-bit mechanisms, the pads are mounted behind a near bit stabiliser, which is positioned between the external pads and the drill bit. Thus, the near bit stabiliser becomes the pivoting point and the drill bit is deflected by the external pads pushing against the borehole wall and bending the BHA axis over the near bit stabiliser. This system setup best allows comparison between point-the-bit and push-the-bit RSS.

In push-the-bit RSS, external pads are mounted around the outer circumference of the RSS. As opposed to the point-the-bit system described by Sugiura (2008), the pads are placed directly behind the drill bit. Behind the pads, an upper stabiliser is usually included in the BHA. This stabiliser is assumed to be in contact with the borehole wall. The pads push against the borehole wall and thus tilt the drill bit over the upper stabiliser as pivoting point. Contrary to the point-the-bit principle, the drill bit is forced into the direction the pads push it.

In push-the-bit systems, the toolface is oriented either by referencing it to a non-rotating housing which the pads are mounted on or fully rotating the string and orienting the toolface with a geostationary valve (Sugiura 2008).

One commercially available RSS is marketed as a hybrid system between point-the-bit and push-the-bit. It consists of a fixed shaft, which extends into a steering sleeve. The shaft is not intended to be deflected, its axis stays aligned with the centre axis of the BHA. The drill bit is connected to the steering sleeve. The steering sleeve is pivoted on the shaft that extends into it. Over this pivot point, the entire steering sleeve is deflected off the centre axis of the BHA. The deflection force is applied behind the pivot point on the shaft. The shaft is deflected by pads, which are distributed around the outer circumference of the shaft. They push against the inner diameter of the steering sleeve and thus point the bit into the opposite direction the pads push. As in a fully rotating push-the-bit system, the pads are controlled via a geostationary valve to orient the toolface, therefore the tool can fully rotate (Schlumberger 2018). Like most other point-the-bit systems, the hybrid system can control the bend angle of the steering sleeve. This is achieved by distributing the pads' deflection force equally around the steering sleeves inner diameter, similar to drilling straight ahead with a push-the-bit system (Schlumberger 2011).

As mentioned above, RSS drill by rotating the entire drillstring with the possible exception of a non-rotating housing. Since RSS are driven only by the drillstring rotation, they achieve fewer RPM at the drill bit than a rotating PDM. Where applicable, this can be compensated by running a straight PDM above the RSS in the BHA (motor driven RSS). While the drillstring rotates and drives the drill bit, the RSS behind the bit deflects the drill bit into the desired direction. RSS incorporate a control unit, which receives commands from the surface, often transferred through mud pulses, and controls the deflection mechanism so that the drill bit holds the selected toolface. Furthermore, for most RSS, with one point-the-bit exception, the amount of deflection can be controlled. In this way, the RSS can steer without changing between rotate and slide mode. The toolface and deflection setting can be changed during drilling and without picking the BHA up off bottom. It is argued that this causes the hole to be less tortuous for all RSS as the DLS can be adjusted within the capabilities of the tool in the environment it drills in rather than altering the length of the slide and rotate section to result in the overall planned build rate (Malcore and Murray 2010), (Bryan, et al. 2009). As pointed out for PDMs, a lower DLS is beneficial for the fatigue life of the drillstring components that are rotated in the dogleg. While RSS, which can adjust their bend setting to become completely straight, should not be limited in their rotation speed because of their own bend angle, doglegs in the wellbore still have to be taken into account. The RSS is rather stiff and most service providers define a maximum DLS the RSS can be run through and rotated in, without causing damage to the tool.

The primary benefit of RSS over PDMs that is emphasized in the literature is the RSS' ability to rotate the drillstring while steering. This has several implications in terms of drilling mechanics. As mentioned for PDMs, rotating the drillstring makes hole cleaning more efficient in highly inclined sections of the hole. Further, rotating the string reduces the friction between the drillstring and the borehole wall. In combination with a less tortuous borehole, the RSS' ability to rotate while steering gives it the potential to transfer weight to the drill bit more easily. This, in combination with more efficient hole cleaning, can improve the ROP. Lastly, efficient hole cleaning in highly inclined sections reduces the risk of getting stuck due to a cuttings bed formation.

While drilling with an RSS is advantageous to drilling, as it allows mitigation of some of the issues faced in drilling the build section on Wisting Central II, namely challenges related to hole cleaning, they are limited in their application due to their build and working principle.

The reviewed literature that compares PDM to RSS generally advocates the use of RSS for their improved drilling performance. For simple well profiles that can be drilled either with RSS or PDM, PDMs are attributed an economical advantage over RSS, as RSS are more expensive (Malcore and Murray 2010). The profiles in which PDMs are economically beneficial are described as not complex in a way so that drilling with a PDM instead of an RSS does not have too much of a negative impact on the drilling performance and overall condition of the well. Furthermore, PDMs are classed as more reliable than RSS as their steering mechanism is purely mechanical while RSS incorporate electronic parts, which are often battery powered to receive commands and orient the toolface. Their deflection mechanism requires a more complex mechanical system, making them more prone to failure (Bryan, et al. 2009).

While RSS, due to their steering principle, are attributed with drilling a smoother, more in-gauge hole, their steering principle makes them more susceptible to the formation properties of the formation they drill in. Push- and point-the-bit RSS which, rely on a non-rotating housing to orient the toolface axially, stabilize the non-rotating housing with fins, blades, or similar parts on the outside of the housing that cut into the formation. If the formation is too soft to support the shear stress required to keep the housing from rotating with the string, or if the hole is too over gauge for the parts to cut into the formation deep enough, it might only be reduced to a somewhat lower RPM than the drillstring RPM. If the non-rotating housing is spinning too fast the RSS cannot orient the toolface fast enough and it becomes impossible to steer. For fully rotating and non-rotating push-the-bit RSS, their deflection capability is dependent on the pads contacting the borehole wall to push the BHA off the borehole centre axis. If the formation is too soft to support the pads areal and they sink into the formation, or if the hole is too over gauge for the pads to push the bit against the borehole with sufficient force, the RSS will not be able to achieve the planned build rate.

Fully rotating point-the-bit systems as well as the fully rotating hybrid system are thought of as more reliable in terms of their DLS output (Bryan, et al. 2009). They introduce a bend into the BHA and orient the toolface without relying on contact with and sufficient support of the formation. Therefore, they behave similar to a PDM and this makes their DLS capability less prone to be influenced by the environment compared to other RSS. However, while a PDM can theoretically be set to a very high bend angle to achieve a high build rate, the bend angle of a RSS is limited by the capabilities of the RSS' deflection mechanism and the RSS' build.

Figure 29 displays the maximum DLS capability for different RSS as per the service providers' product sheets. To generate Figure 29, available product sheets of RSS from different service providers were collected and categorized based on their deflection mechanism (point-the-bit, push-the-bit, or hybrid) and their method of referencing the toolface (fully rotating housing containing a geostationary valve or non-rotating housing). Note that some service providers offer a range of RSS, which operate on the

same principle and have the same maximum DLS capability, but are distinguished by other features. These are grouped together as one RSS in Figure 29. Where different types overlie each other in the same point, the overlaid types are called out. Some RSS are marketed as high dogleg rotary steerable systems (HRSS). These are indicated by a superscript H.

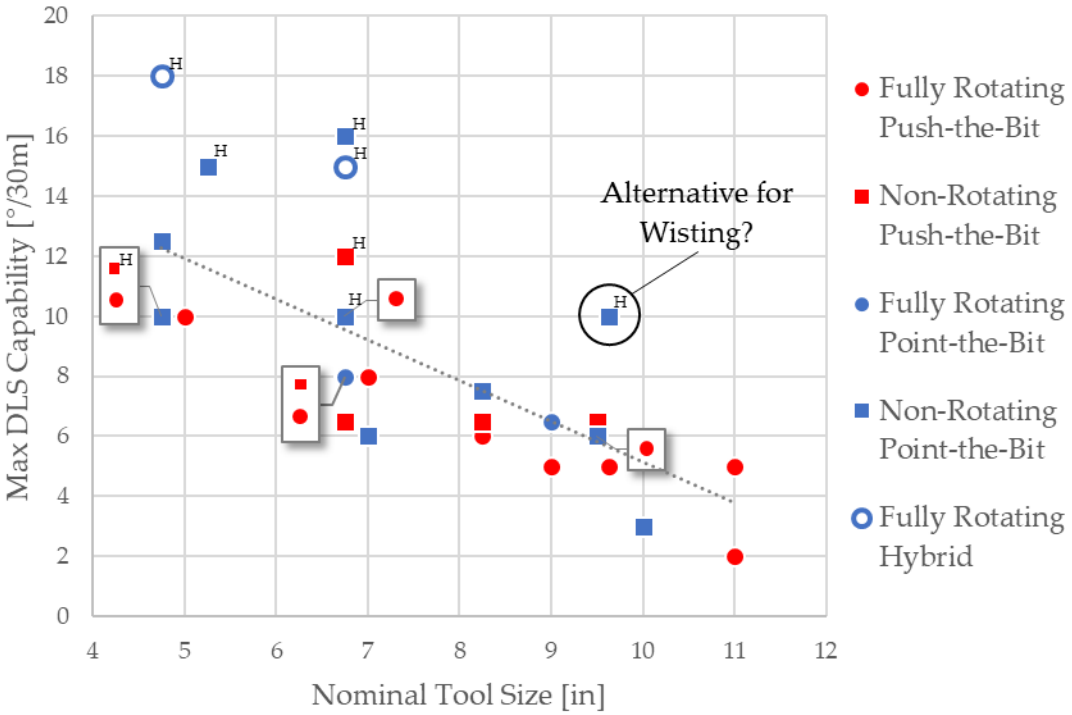

Figure 29: Maximum DLS capability as per tool specifications of various service providers' RSS

Figure 29 indicates that the maximum DLS capability decreases with increasing tool size. While this is not immediately explicable by the RSS' achievable bend angle, as a larger tool might be expected to provide more inner space to house a deflection mechanism that can achieve more deflection, it can be speculated that the maximum DLS capability might be limited by the RSS' stress state. One indication for the stress state being a major concern is that the service provider of the hybrid RSS, which is advertised for its high DLS capability, offers a fatigue life monitoring system to be employed together with the tool (Schlumberger 2018). It can be assumed that tools become stiffer with increasing diameter as their second moment of inertia increases. This assumption is supported by the simulated stress state of the PDMs, which were analysed for drilling the build section on Wisting Central II. While the stress state was deemed too high to rotate a 17 1/2" BHA PDM in a dogleg of 9°/30m, a 12 1/4" BHA PDM allowed limited rotation. The formations in Wisting are relatively competent due to their burial history (Veire 2017) so that the BHA would have to flex cyclically in the hole during rotation, subjecting it to reverse bending stresses. A stiffer BHA would suffer more damage and be severely limited in its fatigue life. This might force a limitation on the maximum DLS capability with increasing size, as the trend in Figure 29 shows.

A case study published by Janwadkar, et al. (2011) addresses the concern of fatigue failure when rotating a PDM set to a high bend angle. The study evaluates non-rotating push-the-bit HRSS for building at a rate of 10°/30m to 14°/30 m in a 8 1/2“ hole section. The study concludes that the HRSS is preferable for this application.

It can further be noted in Figure 29 that fully rotating push-the-bit systems and non-rotating point-the-bit systems cover a large range of tool sizes. Therefore, they seem to be the most established types of RSS. Fully rotating push-the-bit RSS follow a relatively linear trend of decreasing maximum DLS capability with increasing tool size. Along this trend, point-the-bit systems, both fully rotating and non-rotating, and non-rotating push-the-bit systems, with the exception of those marketed as HRSS largely have similar maximum DLS capabilities. Therefore, it seems that no system can be identified as naturally more suitable for higher DLS capabilities, than other systems.

With the exception of a 9 5/8” non-rotating point-the-bit RSS, RSS capable of building 10°/30m and more are limited to sizes below 7”. This might be due to a lack of demand in building high rates in hole sections larger than 8 1/2" or it might be an integral issue of the build and working principle of RSS. While this is not addressed in the reviewed literature, PDMs might have the advantage of sliding in build sections. Their fixed bend angle causes additional deformation when rotating in a dogleg. However, as discussed above, PDMs can be built to be less stiff because they are mechanically simpler. Further, if a PDM set to a high bend angle can be tripped on elevators or washed out of the hole without rotating it, it might not be necessary to subject it to reverse bending stresses. Only when it needs to be backreamed is it necessary to subject the PDM to alternating stress cycles at the rotating RPM. While most RSS have the advantage of a downhole adjustable bend angle for backreaming, they must be rotated to enable them to drill. This is beneficial for hole cleaning as pointed out by several authors, but it subjects the RSS to continuous reverse bending stresses when it drills a high build rate curve. As discussed above, it is likely that the tools’ tolerance for reverse bending stresses decreases with increasing stiffness, which correlates with the tools’ size.

For the 9 5/8” point-the-bit HRSS capable of achieving 10°/30m it further needs to be considered that the maximum DLS capacities displayed in Figure 29 are the result of numerically modelling the BHA under ideal assumed conditions by the service provider. The actual DLS output of the directional drilling tool is dependent on the BHA configuration the tool is run in, drilling parameters, and formation tendencies to which RSS are more susceptible than PDM (Bryan, et al. 2009). Actual build rates experienced in the field are therefore a more reliable predictor of a BHA’s DLS capability (Schlumberger 2004). As the maximum achievable DLS of the 9 5/8” HRSS is equal to the required build rate that must be achieved to drill the high dogleg scenario relief well profile, the risk of failing to achieve the build rate under the conditions at Wisting and missing the target is high.

3.3.3 DLS Prediction

While numerical modelling provides a thorough assessment of the BHA behaviour and its stress state, it is not practical for a quick on site assessment since it is more complicated and can take a considerable amount of calculation time to run (Gharib and

Kirkhope 2017). To estimate the DLS output of a given BHA, simpler models exist that take the contact points between the BHA and the borehole wall, drilling parameters, and the condition of the borehole into account. While this Three-Point Geometry concept of modelling the BHA behaviour was introduced a considerable time ago, it is still the industry standard for assessing BHA behaviour (Marchand and Kalantari 2013). Recent publications revisit and modify the Three-Point Geometry method and compare the derived DLS prediction models to the actual DLS output obtained from field experience. The comparison between the model and the field observation allows assessment of the factors that influence the directional tools' DLS performance.

The Three-Point Geometry method assumes that the bent or deflected part of the BHA has three contact points with the borehole wall. In case of PDM, these are the drill bit, the motor bend, and the upper stabiliser. Point-the-bit RSS have a geometry similar to a PDM as they steer by introducing a bend into the BHA. Their contact points are considered to be the drill bit, the near bit stabiliser, and the upper stabiliser (Bryan, et al. 2009). In push-the-bit RSS, the contact points are considered to be the drill bit, the pads that push the bit, and the upper stabiliser. The hybrid RSS has two stabilisers, one near bit stabiliser on the steering sleeve and one further back on the tool body (Schlumberger 2011).

For PDMs, a shorter distance between the drill bit and the bend results in a higher DLS output (Marchand and Kalantari 2013). Similarly, a shorter distance between the drill bit and the near bit stabiliser increased the DLS output (Sugiura 2008). For push-the-bit RSS, decreasing the distance between the pads and the upper stabiliser is found to increase the DLS output of the tool (Sugiura 2008).

Further, the position of the upper stabiliser is a factor for the DLS capability of a given PDM and bend angle setting (Schlumberger 2004). This likely also applies to point-the-bit RSS and hybrid RSS, as their geometry is similar to that of a PDM. If no upper stabiliser is run with any of the systems, that is, if they are run as a slick assembly, the position of this contact point along the BHA is not clearly defined (Bryan, et al. 2009). In this case it is found that the missing stabilization point and resulting greater flexibility of the BHA leads to a greater influence of the WOB applied and the hole inclination the BHA is in (Gharib and Kirkhope 2017).

The applied WOB is considered to additionally deform the BHA in the hole, leading to a more pronounced bend angle with increasing WOB and thus resulting in an increased build rate (Gharib and Kirkhope 2017).

The borehole inclination is thought to influence the build rate as the gravity effect will pull the BHA towards the low side of the hole and thus bend it towards the low side between the contact points. This effect should become more pronounced with increasing inclination. For a point-the-bit RSS the build rate was found to increase with increasing inclination (Wu and Chen 2006). Gharib and Kirkhope (2017) point out that the severity of this effect is reduced by the buoyant force resulting from the drilling mud density. If the well profile is to be dropped, the drop rate is thought to decrease with increasing inclination as the gravity force counteracts the bend introduced by the directional drilling tool. Again, buoyancy would reduce this effect.

Due to their similar geometry, the influence of WOB and inclination on the DLS output should apply to point-the-bit RSS and PDM alike. It is of interest to note that the build rate of a push-the-bit RSS and a point-the-bit RSS whose deflection is achieved by external pads behind a near bit stabiliser is not influenced by the borehole inclination (Sugiura 2008).

Push-the-bit RSS are considered to be affected more by borehole enlargement as they rely on more on the contact with the borehole wall to be able to steer. PDM, point-the-bit, and hybrid RSS introduce the bend angle into the BHA independently of the contact with the borehole wall. Point-the-bit RSS with a non-rotating housing do not rely on contact with the borehole wall to achieve bit deflection, but the non-rotating housing needs sufficient contact with the borehole wall to axially stabilise and enable the RSS to orient the toolface. Thus, only point-the-bit RSS that are fully rotating can be considered to be less sensitive to borehole enlargement (Bryan, et al. 2009). While PDM, hybrid RSS and fully rotating point-the-bit RSS might still be able to steer in an over gauge hole, their DLS output is affected by the borehole enlargement, because it alters their contact points with the borehole wall (Gharib and Kirkhope 2017).

To summarize, the DLS capability of all directional drilling BHA's depends on the borehole condition and thus on the formations it drills in. The formations in Wisting are relatively competent due to its burial history. As the experience on Wisting Central II showed, a PDM could achieve a high build rate. It might therefore be possible that a RSS could achieve a similarly high DLS with the benefits of improved drilling performance, but there is only one tool in the required size that is theoretically capable of building at the necessary rate. This tool has not been field tested in Wisting yet.

Stabilized BHA's show a tendency to build inclination. This might facilitate achieving a high DLS in the build section of a profile with increasing inclination. If this is true, then the kick off in a J-shaped profile is the most critical part in terms of building to inclination. In deeper reservoirs, where the well trajectory requires a tangent and drop section to be drilled, a BHA's building tendency would not be beneficial. Drilling a tangent section with a PDM would likely result in a greater tortuosity as corrections to the inclination would require sliding intervals. An RSS would be more suitable since it can correct for the assemblies build tendency while drilling.

In the last section that focussed on analysing S-shaped and J-shaped profiles it was assumed that the DLS in the build and drop section of an S-shaped profile is equal. During this review of directional drilling tools it has become evident that this assumption is wrong.

Finally, since many unknown factors influence the behaviour of the BHA assembly when it is drilling, it is not possible to precisely predict the path the drill bit is taking subsurface. This makes it necessary to survey the wellpath as it is being drilled, and compare it to the planned wellpath. Based on the information gained from the surveys, drilling parameters and directional drilling tools are manipulated to steer the drill bit so that it follows the planned wellpath.

3.4 Surveying

The DLS of the wellbore is derived from the survey measurements taken in the wellbore. The industry standard method for calculating the wellpath between survey stations is the minimum curvature method (Heisig, et al. 2004). The minimum curvature assumes that the well builds a smooth circular segment between one survey station to the next at a curvature that results in the change in inclination and azimuth measured at two subsequent survey stations. Typically, surveys are spaced roughly 30 m along the measured depth of the well, as they require the drill string to be static for taking a valid survey. Therefore, they are commonly taken in between stands of drillpipe when the drill bit has to be picked up off bottom to add a new stand of pipe (Menand, Mills and Suarez 2016).

This relatively low frequency of surveying can introduce a considerable amount of uncertainty into the wellbore position, even if all survey measurements were correct. Because one continuous DLS is assumed between the survey stations, the second survey station might be positioned at a different location to where it would be if the section had a high DLS in one part and a lower DLS in another part, which in total resulted in the same change in inclination and azimuth. Such can be the case when changing between slide and rotary mode when drilling with a PDM (Menand, Mills and Suarez 2016), when there are changes in the drilling parameters (Lubinski and Woods 1953), (Gharib and Kirkhope 2017), or when the drilling environment changes. Figure 30 illustrates this in an example between two survey stations.

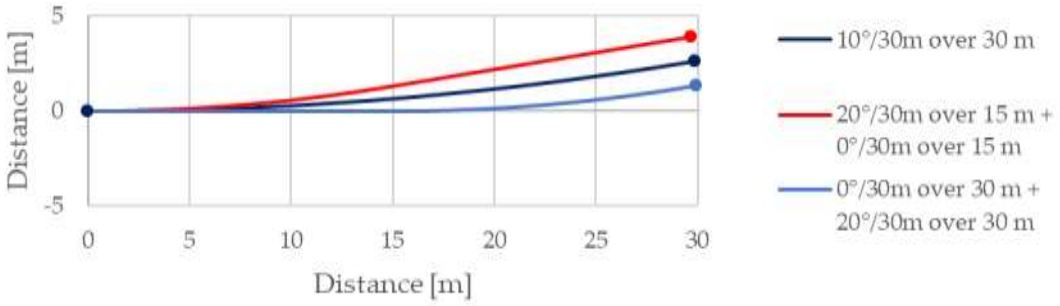

Figure 30: Effect of well trajectory between subsequent survey stations

All three sections in the example build 10°/30m between the two survey stations. Therefore, they result in the same measurement at the second survey station, yet their true position is different. The dark blue path builds at a continuous curvature as assumed by the minimum curvature calculation. The red path builds 10° over the first 15 m of the interval, and then holds that inclination. The light blue path holds the original inclination over the first 15 m, and then builds the 10° of inclination over the last 15 m.

If there is only one survey station erroneously positioned in this way, it will shift the entire subsequent wellpath to a different position. Aside from the survey stations in the wellbore, this also applies to the relief well's spud location. Its position needs to be determined with high accuracy as it influences the position of the entire wellbore through the survey stations that are tied on to it (Goobie, et al. 2015).

Since it is known that uncertainties accumulate by modelling the wellpath from survey station to survey station, the uncertainty in the wellbore position grows along the measured depth of the well. To reduce the uncertainty introduced by constructing the wellpath from discreet survey stations, it is suggested to survey the wellbore continuously (Menand, Mills and Suarez 2016).

Additional errors are introduced into the survey measurements and, thereby into the wellbore position, by imperfections of the surveying tools and external influences. The standard measurement while drilling (MWD) tools that are placed in the drillstring, contain triaxial accelerometers that measure the Earth's gravity field (Buchanan, et al. 2013). This measurement determines the wellbore's inclination. They further contain triaxial magnetometers that measure the Earth's magnetic field to determine the direction of an inclined wellbore section (Amundsen, et al. 2008). These are also needed to determine the toolface orientation of the directional BHA.

The Earth's magnetic north pole has a time varying offset from the Earth's true North Pole, to which the azimuth is referenced. Therefore, a grid convergence needs to be applied to the magnetic survey measurement (Kabirzadeh, et al. 2017). However, the magnetic field that is measured by the survey tools is subject to several external influences. These cause the resulting measured magnetic field vector to be altered. The azimuthal difference between magnetic north and the measured field vector is referred to as magnetic declination, the dip between the horizontal plane and the field vector is called magnetic inclination (Kabirzadeh, et al. 2017).

Disturbances on the main magnetic field that alter it originate from crustal anomalies at the area of the well site which are often attributable to base rocks at depths of 10 000 m to 30 000 m, but can also be caused by magnetic sediments in shallower depths (Esketh and Weston 2010). Further, the time varying influence of solar activity that induces electric currents in the Earth's ionosphere and thereby alters its magnetic field locally, increases with increasing latitude (Edvardsen, et al. 2014), (Arsentiev, Hathaway and Lessard 2013). To reduce the azimuthal error and thereby the lateral uncertainty in the wellbore position, in field referencing (IFR) is applied to the gathered magnetic measurements. As Wisting is located at a high latitude, this is of special concern.

Furthermore, the presence of the drillstring components close to the MWD tools disturb the magnetic field. By gathering redundant magnetic surveys during drilling, multi station analysis (MSA) seeks to account for the drillstring's alteration of the magnetic field (Buchanan, et al. 2013).

While IFR and MSA are the recurring recommendation in the literature for combating errors in the magnetic measurement caused by disturbances to the magnetic field, Almundsen et al (2008) address the issue of magnetic shielding by the drilling mud. Magnetic particles that are present in the mud, either because of additives, minerals contained in the drilled formation, or pipe wear, dampen the magnetic field and lead to errors of 1-2% in the azimuthal measurement. However, this error can be significantly larger in severe cases. Almundsen et al (2008) therefore recommend taking surveys immediately after the mud circulation is stopped.

Despite these measures to improve the accuracy of magnetic measurements in the borehole, the uncertainty in azimuth can be quite large. Esketh and Weston (2010) show

in a mathematical model that the magnetic azimuthal error increases with latitude, vertical depth, and increasing inclination. Further, it is more severe when drilling at an azimuth close to or along the east-western direction. While Wisting is shallow, and unfavourable azimuthal directions at high inclinations can be excluded when selecting the relief well spud location, the survey program in case of a relief well recommends running a gyro while drilling (GWD) tool in addition to the MWD tool when drilling in the east-west direction. The GWD measures the azimuth of the well's inclination by seeking geographic north. It provides an additional azimuthal measurement, independent of the magnetic field and can therefore be used in combination with the magnetic measurement to reduce the overall gross error in azimuth and lateral uncertainty (Monterrosa, et al. 2016).

A further source of error that affects all sensors in the survey tools alike is the position of the tool in the borehole. The survey tools are usually located behind the PDM or the steering mechanism of the RSS and therefore several metres behind the drill bit. If the tool's axis is deflected off the centre of the borehole axis, which is commonly the case when the BHA lies on the low side of the hole in an inclined borehole, the sensors measure the magnetic field and gravity field in reference to the tool axis. This introduces an error into the TVD derived from the measurement. To reduce the uncertainty in TVD, the position of the BHA with respect to the borehole axis is modelled with SAG correction (Ulaeto, et al. 2018).

The various error sources combine into a growing ellipse of uncertainty (EOU) along the length of the wellpath. The uncertainty in the TVD of the well is less severe than the uncertainty in the wells lateral position. The uncertainty in lateral position, which affects both the relief well and the target wellbore, makes it relatively unlikely that the wells will happen to intersect upon the first try. Furthermore, projecting the drill bits position based on the uncertain position of the survey tools several metres behind it and the predicted DLS behaviour of the BHA decreases the chances of intersection (Buchanan, et al. 2013).

Many RSS incorporate at-bit-inclination or near bit inclination, often in combination with gamma ray sensors for geosteering. This gravity field measurement provides an additional input to reduce the statistical gross error on the derived inclination. Further, it helps in steering the wellbore because information on the wellbore's inclination and thus its approximate position becomes available earlier. This is critical in direct intersection of a wellbore, as the information from the survey tool is available only once the survey tool passes through the point in the wellbore. Therefore, if the drill bit misses the target, even if the positions of both the relief well and the blowing well were known with absolute accuracy, this information is only gathered when the survey tools pass by the blowing well. The last part of the relief well then needs to be plugged back to steer the drill bit into the target well based on the new information, but the path the drill bit is taking can still only be estimated by projecting ahead from the position of the survey tools.

In an S-shaped relief well, the near-parallel alignment of relief wellbore and target wellbore cause the MWD tools in the borehole to come close to the casing of the blowing well. From the magnetic interference the MWD picks up from this casing, the relative

distance between the two wellbores is estimated by triangulating and projected ahead to the drill bit. Usually at this stage ranging runs are made on wireline to get an estimate of the relative positions closer to bottom hole. This process is repeated until the wells intersect. Magnetic interference from premagnetized casing joints in the formation can usually be detected from a distance of 20 m (de Wart, et al. 2013). This interference can be detected in the relief well when the magnetic survey or ranging tools are close enough to the casing. Therefore, if the directly intersecting relief well misses the target by more than ~20 m, the blowing well will not be detected and the next sidetrack cannot be planned with high precision towards the target. Thus the J-shaped design has to rely strongly on the accuracy of the known wellbore position.

For these reasons, improving the direct intersection of a blowing well would require reducing the positional uncertainty along the measured depth of the wellpath and obtaining measurements closer to the position of the drill bit. The growing uncertainty is found to be a combination of accumulating measurement errors and the assumed trajectory between the survey stations. While a certain error is inherent to any form of measurement, the accumulation of this error could be mitigated by measuring the position of the wellpath in absolute terms rather than tying measurements to one another as the wellpath progresses. As Wisting is very shallow, it is considered ideal for seismic reservoir monitoring from the surface (Veire, Granli, et al. 2018). A passive seismic monitoring system was installed during the construction of Wisting Central III, the most recent well drilled on the discovery. The information gathered by the system is used to detect and determine the position of seismic events in the subsurface. As the drill bit acts as a source of seismic signals while drilling, the passive seismic event positioning method is evaluated in the next chapter for its use in drill bit positioning.

To summarize, the shallow depth of the Wisting discovery does not permit the construction of an S-shaped trajectory, therefore relief wells have to be designed as J-shapes. To keep both the DLS and the inclination as low as possible, the trajectory should be designed with a DLS in the range of 10°/30m. This high DLS requirement made it necessary to drill the build section on Wisting Central II in complete slide mode with a PDM. Drilling with a RSS would be preferable both for the drilling performance and because RSS can have integrated MWD tools and near bit inclination measurement, thereby providing information on the wellbore position closer to the drill bit compared to MWD tools run behind a PDM. However, there is one RSS that is advertised as being capable to build 10°/30m in the required hole size, but this has not been field tested in Wisting. In a relief well it is therefore better to rely on the proven DLS capacity of a PDM.

The wellbore position derived from survey measurements while drilling is known with only a limited certainty that decreases along the length of the wellbore, due to the nature of surveying and errors in the survey measurements. The lateral position is affected more than the vertical depth in deviated wellbores, yet the certainty of the lateral position is crucial the direct intersection of a vertical target well by a J-shaped trajectory as proposed in this chapter. One suggestion to improve the wellbore positioning accuracy is a passive seismic event positioning method. This method is evaluated for its applicability in relief well drilling.

Chapter 4 Evaluation of a Passive Seismic Drill Bit Positioning Method

Downhole surveying introduces a considerable amount of uncertainty into positioning the wellbore. Wisting's shallow reservoir requires high accuracy in positioning the wellbore to facilitate direct intersection. This chapter evaluates a passive seismic method for seismic event positioning, with regards to its application in wellbore positioning. The basic idea behind positioning the drill bit from a drilling point of view is to triangulate and find the position based on the seismic signals the receivers on the surface record. The following sections provide an assessment of subsurface seismic wave propagation, the event positioning method applied to the data gathered in the seismic study in Wisting, and finally a discussion of this method from a wellbore placement point of view.

4.1 Subsurface Wave Propagation

During drilling, energy is expended in the form of string rotation and mud circulation to overcome the reactive torque between drill bit and formation and thereby destroy the rock. However, some of this energy is dissipated in form of heat generated by the friction in the borehole. Another part of the energy is converted to vibration that radiates into the borehole environment as seismic waves. As the drill bit is known to generate vibrations when it drills, it can act as a seismic source that is located directly at the bottom of the wellbore. The amount of energy that radiates away from the bit depends on the force amplitude and frequency that it exerts on the formation (Poletto and Miranda 2004, 103-106, 129).

Haldorsen et al. (2006) describe three types of waves that are associated with boreholes: compressional waves, shear waves, and Stoneley waves.

Compressional waves are body waves that travel through media in a longitudinal fashion. Since they rely on the compression of the medium and this compression is passed from particle to particle, they can propagate through fluids and solids alike. This means they oscillate in their direction of propagation, perpendicular to the wavefront.

Shear waves are transversal body waves. They spread through a medium by deflecting particles perpendicular to their direction of propagation. To transport energy in this way, a medium must be capable of supporting shear stresses. As fluids do not support shear stresses, shear waves can only propagate in solids.

In general, compressional waves propagate faster through the same solid medium than shear waves. For this reason, compressional waves that are emitted in a seismic event reach the detectors first. These are referred to as primary waves while shear waves are referred to as secondary waves.

Like any kind of wave, these body waves are subject to refraction in dependence of their incidence angle and velocity ratio when they cross over between media of different propagation velocity. Layers of rock in the overburden constitute such media of different

wave velocity. Consequently, the waves' ray paths from source to receiver are not linear. The following Figure 31, taken from Simm and Bacon (2014), illustrates this in a simple model.

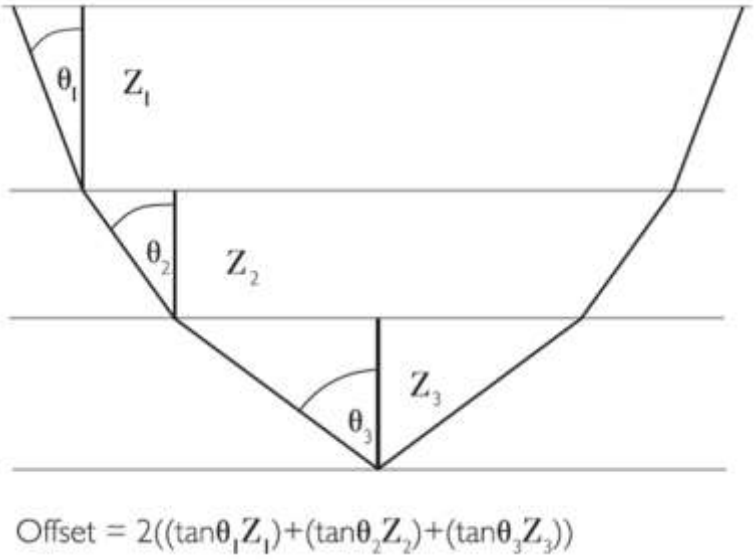

Figure 31: Ray path in layered medium. From Simm and Bacon (2014, 21)

The example calculates the offset between source and receiver by retracing the ray path to its original lateral position. It is pointed out that linear ray paths are assumed within the single layers, which is not necessarily true in a real rock. Furthermore, the wave velocities, thickness, and dip of each layer must be known. In this example, the layers are homogenous and isotropic (Haldorsen, et al. 2006), horizontal, and flat (Simm and Bacon 2014). This suggests that tracing a ray back to its position of origin is unpractical in a real overburden since many of these parameters are uncertain.

The model in Figure 32 was constructed by Octio and presented by Bergfjord et al. (2018). It displays the ray paths of an event in the Wisting discovery, approximately at the depth of the Realgrunnen subgroup. The colour scale indicates the velocities assigned to the layers of the model. In the upper picture, the model includes a thin, high velocity layer (presumably Klippfisk) that causes the rays that hit it above a certain angle to be refracted above the critical angle. These rays are completely reflected at the next boundary and no part of the wave is transmitted further to reach the detectors on the seabed. The model in the lower picture does not include this layer; a larger part of the wave reaches the detectors.

Bergfjord et al. (2018) go on to state that Stoneley waves, as stated also by Haldorsen et al. (2006), are to be expected in the wellbore. Contrary to primary or secondary waves, Stoneley waves propagate along the interface of two media of different wave velocity. They are therefore surface waves, which are similar to Rayleigh waves, in that they excite particles to move in an ellipse around their mean position (Stoneley 1924). Thus, the wave propagates along the wellbore, similar to fluid waves along a liquid-gas interface. When the Stoneley wave encounters an obstacle, such as a casing shoe, some of its energy is converted into a body wave that radiates into the formation (Poletto and Miranda 2004, 326), (Bergfjord, et al. 2018).

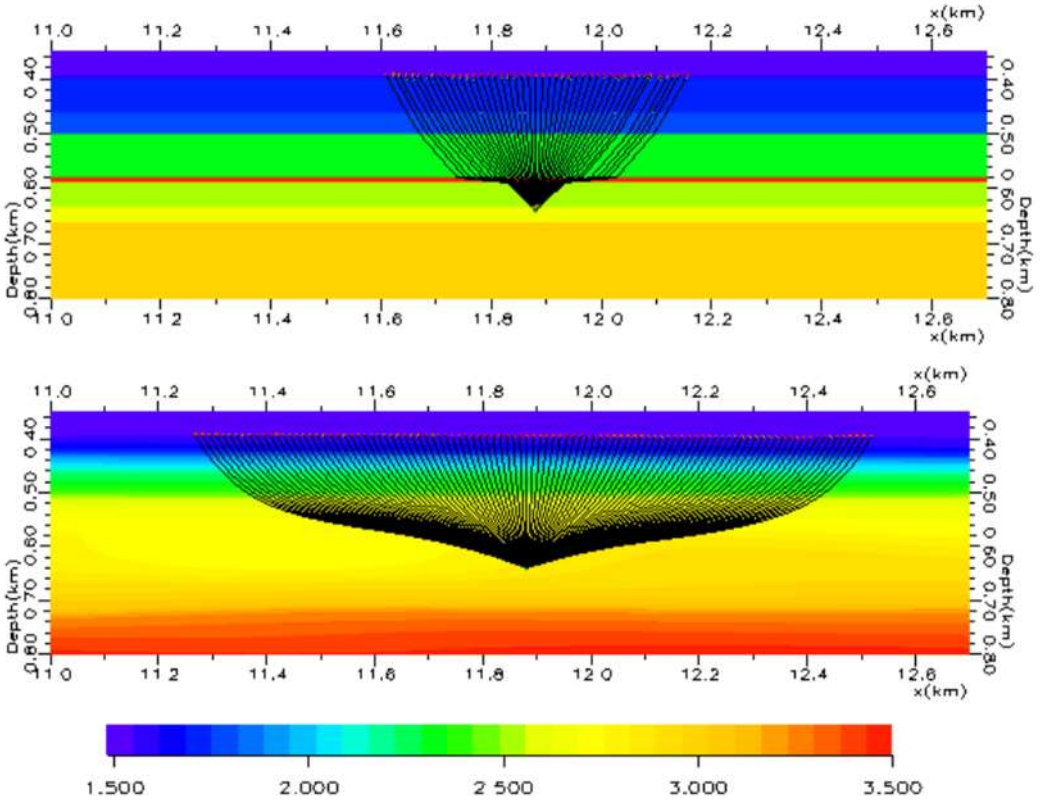

Figure 32: Ray path modelled for a seismic event in Wisting. From Bergfjord et al. (2018).

Stoneley waves propagate at a slower velocity than primary and secondary waves. Therefore, compressional or shear waves that are converted from Stoneley waves at some point along the wellbore reach the surface after the primary and secondary waves that propagate through the formation directly from the source and are referred to as direct arrivals. Stoneley waves that reach the surface can then travel along the seabed and reach the detectors as surface waves. Thus, they interfere with the direct arrivals from the drill bit (Bergfjord, et al. 2018).

Other interference is generated along the wellbore in the form of these three types of waves. In deviated wellbores, the part of the drillstring that is in contact with the borehole wall produces noise at the contact point (Poletto and Miranda 2004, 197). Another possible source of seismic waves are pressure pulses in the drilling mud that are converted to body and surface waves when they reach the liquid-solid interface of the borehole wall (Haldorsen, et al. 2006).

The subsurface acts as an attenuating filter on seismic waves (Simm and Bacon 2014, 26). Low frequency waves are transmitted better than high frequency signals (Bergfjord, et al. 2018) and it is therefore necessary for seismic drill bit detection that the drilling action produces seismic waves in the right frequency range so that they reach the surface before they are attenuated (Poletto and Miranda 2004, 140). The concept of the subsurface as attenuating filter further suggests that signals are more easily detected if they come from a shallow depth and have less distance to travel between source and receiver. This makes

the shallow Wisting reservoir ideal for studying passive seismic signals (Veire, Granli, et al. 2018).

4.2 Octio's DrillWatch Project on Wisting Central III

The most recent well drilled on the Wisting discovery is Wisting Central III. It is a vertical appraisal well that drilled to a total depth of 775 m in the Fruholmen formation. Its main purpose was to conduct injection tests in the Stø formation. During the entire construction and testing of the well, a microseismic field study was carried out by the company Octio AS. The main motivation for this study, termed the DrillWatch project, was to monitor the reservoir and the cap rock for fractures that are being induced by the drilling activity and the injection tests. Developing fractures are sought to be recorded on a receiver array placed on the seabed around the wellhead, via the microseismic signals the rock emits when it cracks. Wisting is especially suitable for such an application. Because it is shallow, few layers of overburden that refract and attenuate seismic waves separate the zone of interest, that is, the wellbore, from the surface (Veire, Granli, et al. 2018).

Based on the recorded seismic data, Octio aims to determine the subsurface location of induced fractures. Similar to the developing fractures, any source of noise in the subsurface that propagates to the receiver array is recorded. Since the drill bit creates noise when it drills, it can be positioned in the same way fractures and other signals are positioned, based on their seismic signals. The advantages of this way of bit positioning would be that the drill bit's path could be traced continuously while it drills. This would reduce the uncertainty of the well's trajectory in between survey stations and result in a less uncertain well path. Furthermore, the point of measurement would be at the drill bit and not further back in the drill string. This would facilitate making steering decisions and enhance the direct intersection of a blowing wellbore. In the following, the system setup on Wisting Central III is described and the event positioning method that is applied to the seismic data collected during the construction of the well is analysed.

The recording system on Wisting Central III consits of 100 receiver nodes that are connected together by the cable at a spacing of 25 m (Bergfjord, et al. 2018). The number of the receiver nodes and the distance between the receivers is variable and needs to be selected individually for each application. The receivers are placed on the seafloor as they need to be in contact with the sediment to be able to record secondary waves. Each receiver node contains a hydrophone and three accelerometers. The hydrophone records the magnitudes of primary waves, while the accelerometers are orthogonal to each other and measure the magnitude and direction of primary and secondary waves (Fageraas 2012).

Figure 33 shows the pattern in which the cable was laid at the well site. The circular grid lines mark the radial distance from the wellhead. The same scale is displayed on the ordinate of Figure 34. On the abscissa, the nodes are sorted by number. This needs to be compared to Figure 33, which depicts the number of each node along the cable.

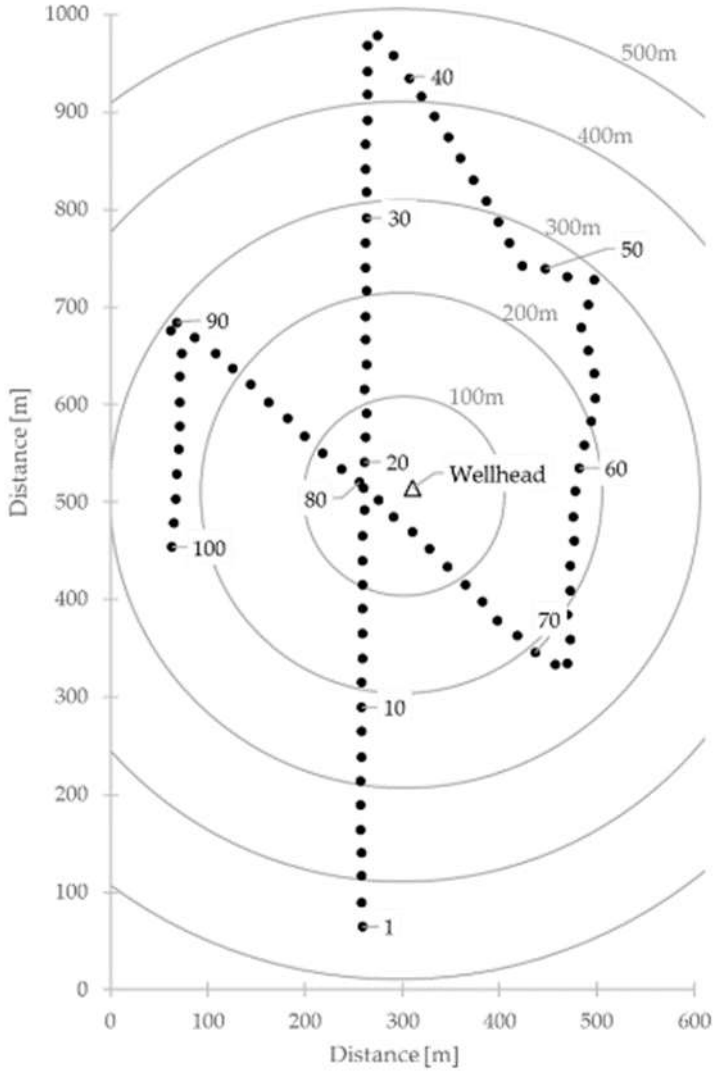

Figure 33: Cable layout around wellhead of Wisting Central III. (After Bergfjord, et al. (2018))

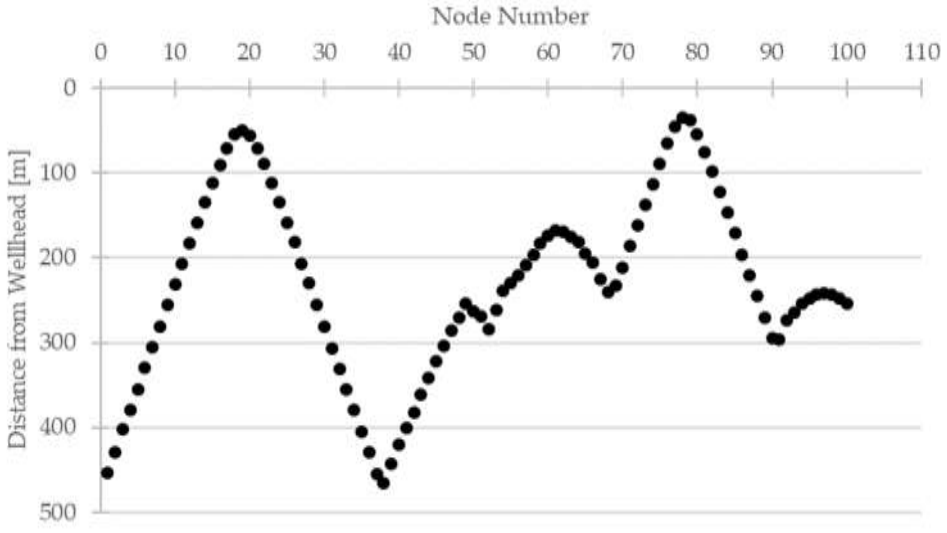

Figure 34: Distance of nodes from wellhead

In this way, each node is identified by its number. The pattern in Figure 34 is the result of the nodes' distance to the wellhead. It is therefore dependent on the pattern in which the cable is laid around the wellhead and the key to the seismic event positioning method employed by Octio.

After cable deployment and before the monitoring process starts, the position of each receiver node is determined. This is done by surveying with a remotely operated vehicle (ROV) and by conducting a positioning shot with an active seismic source in the water (Bergfjord, et al. 2018). Since the position of the active source is known and the primary waves propagate linearly through the water column at a known velocity, the time of arrival at each receiver node allows to determine its position. If the position of the receivers on the seabed are known, then their respective distances to a defined point, such as the wellhead, is also known. The shape that results from plotting the receiver nodes sorted by their number as a function of their distance to that point results in a characteristic curve, such as the one displayed for the wellhead in Figure 34.

If a signal is emitted at the wellhead that propagates radially through the water at a fixed velocity, it reaches the receiver nodes after a certain time, depending on their distance from the source of the signal. If the receivers are sorted by their number along the cable and the time of the signal arrival is plotted for each receiver, this would result in a curve similarly to the one displayed in Figure 34. The ordinate would measure time from the start of recording, instead of distance from a specific point. If the arriving signal's velocity is known, the distance to the origin of the signal can be determined by the time of arrival and the resulting shape that shows up on the receiver array. This shape is then referred to as arrival time curve.

A high velocity signal that arrives at the nearest receiver at one point in time arrives at the furthest receiver a short time afterwards. A low velocity signal that arrives at the nearest receiver arrives at the furthest receiver with a greater time delay. Therefore, the arrival time curve appears more compressed for fast signals and more distorted for slow signals.

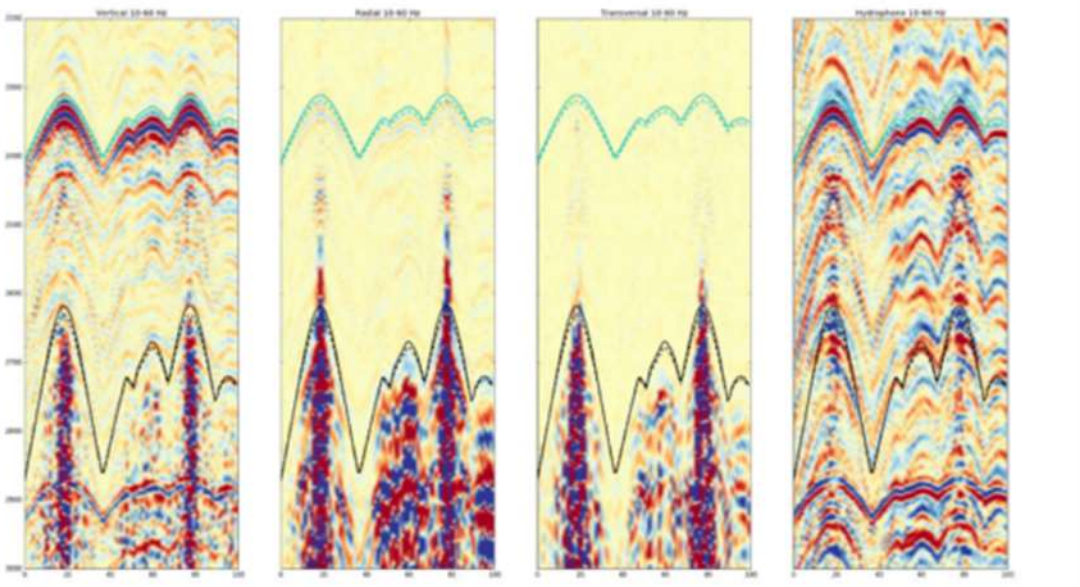

Figure 35: Perforation shot at 642m in Stø Formation. From Bergfjord, et al. (2018)

This can be observed in the example in Figure 35. The panels show the data that was recorded on the receiver array during a perforation shot on Wisting Central III. There are four sets of data since each receiver contains a hydrophone (right panel) and three accelerometers. The signals that are recorded by each accelerometer depend on the orientation of the respective receiver node. One accelerometer sits along the length of the receiver axis; the other two are oriented perpendicular to it so that the three of them are orthogonal (Fageraas 2012). Since the position and orientation of the accelerometers in the receiver nodes are known from their response to the survey shot, the accelerometers' recordings can be combined to transform the signal arrival to any coordinate system. In the figure below, the data is shown as vertical, radial, and transversal signal components in reference to the wellhead (from left to right).

The turquoise curve that is laid on the data is an artificial arrival time curve for the primary wave that was generated by Octio for this event. The black line below it is the artificial arrival time curve for the secondary wave generated by Octio. Due to its lower velocity, the secondary wave arrives later on the receiver array and is more distorted than the primary wave arrival time curve.

Octio generates the artificial arrival time curves based on a model of the subsurface. The model is comprised of layers, each of which is assigned a primary wave propagation velocity for the primary wave velocity model or a secondary wave propagation velocity for the secondary wave velocity model. Based on the velocity model, the ray paths of a signal that is emitted from a location in the subsurface model are calculated. The combination of the calculated distance and the velocity in the different segments results in the artificial arrival time curve for the receiver array.

Note how the shape of the artificial arrival time curve generated by Octio for the perforation shot looks very similar to the receiver nodes plotted as a function of their distance to the wellhead in Figure 34. This indicates that the ray paths of the perforation shot signal originating approximately 240 m below the wellhead are uniformly refracted around the well by the layers they propagate through. In fact, Octio finds that the rays in their model propagate almost vertically from the source to the receivers (Bergfjord, et al. 2018).

Furthermore, the artificial arrival time curve fits the actual recorded arrival time curve well. This is the confirmation that the velocity model is correct and the principle of event positioning. In the displayed example, the position of the seismic event is known. The event is the perforation shot that was fired in the wellbore at a depth of 642 m. Since the perforation shot is easily detectable on the recorded data because the signal is strong and the time at which the signal is emitted is known, it is used to calibrate the model. This is done by adjusting the velocities that are assigned to the individual layers of the subsurface model so that the arrival time curve that is generated for the position in the model where the seismic event takes place fits the real arrival time curve of the event.

For positioning an event of an unknown position, for example the drilling bit, the subsurface model is divided into grid cells of a cube length of 10 m. For each grid cell, an artificial arrival time curve is generated. An algorithm compares these artificial arrival time curves to the actual arrival time curves recorded on the receiver array. If

there is a match, the grid cell of the matching artificial arrival time curve is identified as the position of the event. In this way, seismic events are detected and positioned.

Bergfjord et al. (2018) report that the perforation shots that were used to confirm the accuracy of the subsurface velocity model are positioned within several metres of the vertical position of the event and at the exact lateral position of the shot, that is, in the wellbore. (Octio 2018)

The primary wave velocity model resulted in a more accurate position than the secondary wave velocity model, which leads the authors to the conclusion that the shear wave velocities in the model are less accurate and require further calibration. An increased accuracy of the subsurface model and its parameters results in an increased event positioning accuracy. In their report, Bergford et al. point out that an inaccurate model can lead to a seismic event being positioned in the wrong grid cell, if another grid cell's artificial arrival time curve results in a better match for the actual arrival time curve. Further, if no artificial arrival time curve matches an actual arrival time curve well enough, the algorithm can fail to detect an event. A seismic event that would otherwise show up as a clear signal is then missed.

The detection of seismic events that are of interest, such as the noise of the drill bit, can further be hindered by the overburden's attenuation of propagating waves and other noise that overlies the signal. It is found that low frequency signals are transmitted better through the overburden than high frequency signals. To reach the receiver array, the drill bit signal must be in a transmissible frequency range. According to Berfjord et al. (2018), the drill bit generates mainly secondary waves in shallow sections. However, it is not clear if the signals that are identified as the drill bit are direct arrivals of secondary waves or if they are converted Stoneley waves. As there are other sources of seismic signals present in the wellbore, such as the mud being circulated, they can mask the signal of the drill bit. It is therefore crucial to filter the noise from the data. In Wisting, the drilling rig was identified as the major source of noise. Since the noise pattern is similar to the signal pattern, it is difficult to filter the noise and detect weaker signals. It is pointed out however, that a common method of filtering noise is to identify its pattern and subtract it from the data, leaving the signals of different shape intact.

It might be concluded that continuous drill bit detection is dependent on the frequency range the source emits during drilling and the signals interaction with the overburden on the way to the receiver array. It is further dependent on the ability of filtering algorithms to pick the drill bit signal from the data. Therefore, it is possible that the signal might be lost at times of elevated noise in the wellbore that masks the signal, or if there is ambient noise whose signal shape is similar to that of the signal. If event detection is successful, sources of inaccuracy in positioning the event are the subsurface model and the velocities assigned to the subsurface model. Additional uncertainty is introduced by the position on the receiver nodes. They are surveyed prior to and after the operation. It was found that two receiver nodes shifted their orientation on the seabed during the operation, probably due to external influences. Aside from uncertainties, the event positioning accuracy is limited by the grid size, into which the model is divided. For their first assessment, Octio used a cube length of 10 m in the model, which resulted in a vertical offset of several metres, with the closest match being positioned 6,5 m from the

events position. Further processing of the data yielded a positioning accuracy of 2-5 m (Helene Veire, personal communication, 15.06.2018). Work is ongoing to improve the detectability and positioning of events.

4.3 Application of Seismic Event Positioning Method in Relief Well Placement

Based on the method's procedure that was analysed in the previous section it is believed that seismic event positioning cannot improve the accuracy of the known wellbore position in the subsurface compared to surveying the wellbore with MWD or gyroscopic tools.

This is mainly because the seismic event positioning method relies on subsurface velocity models that are calibrated based on events of known position in the subsurface, such as perforation shots. However, the subsurface position of these events is known from the survey data gathered in the wellbore. Therefore, this is not the true position of the event and the positional uncertainty is equal to the survey uncertainty. A velocity model based on the survey data will have the same uncertainty even if it was otherwise entirely realistic.

In vertical wells, such as Wisting Central III, the lateral position is relatively certain, as the well does not deviate. However, the depth of the event is subject to uncertainty because it is measured by the length of the drillstring or wireline that is run into the hole. The suspended string deforms elastically under its own buoyant weight and the weight of the tool run on it, making the measured depth an approximation rather than the true depth (Poletto and Miranda 2004, 245). In a deviated relief well, the positional uncertainty is larger and this can be expected to translate into the subsurface model.

Furthermore, it needs to be considered that the real subsurface cannot be rebuilt in a computer model with absolute accuracy. Formation thickness, dip, and properties are likely to change with lateral offset, which will alter the ray paths of direct body waves in an unknown way. To control the lateral position of the wellbore, it is suggested to lay a receiver cable along the surface projection of the well trajectory. Poletto and Miranda (2004, 402) point out that this can only yield an approximation of the lateral deviation from the planned trajectory, as geological structures can cause the seismic signal to arrive asymmetrically at the receivers. Further, if such an approach was chosen to control the lateral deviation of a relief well, the critical section would be close to the intersection point. However, in the case of a blowout, the immediate area around the target well is likely not accessible and a cable could be deployed only up to a certain distance to the target surface projection.

A possible alternative use of a receiver array in relief well operations that is not investigated in this work is to employ a form of pattern recognition when the relief well is approaching the target. In this scenario, the receiver array is deployed during the construction of the target well. The receivers would have recorded the shape of the real arrival time curve while the intersection point was drilled before the incident. An approaching relief well could then be steered to result in the arrival time curve becoming

gradually more similar to the arrival time curve observed at the intersection point in the target well (John Even Lindgård, personal communication, 07.09.2018).

However, it is not known how much noise a blowout would produce in and around the target wellbore and if the drill bit signal could be detected above this noise. Further, the seafloor might be affected by the blowout and damage or interfere with the cable and its connection to the surface.

In conclusion, alternative options, such as further improving the accuracy of wellbore surveying or the use of alternative, independent systems such as the suggested seismic pattern recognition, need to be explored for the Wisting discovery.

Chapter 5 Conclusion

Relief well drilling is expected to be challenging on the Wisting discovery, as the shallow reservoir requires difficult trajectories, which also limit the chances of fast target well intersection. S-shaped and J-shaped well trajectories were analysed concerning the DLS and sail angle in the profiles to find the most effective combination of these two parameters so that both are kept as low as possible. Under the depth constraints in the shallow Wisting discovery, this yielded a DLS and sail angle in the range of 18°/30m at 92° for S-shaped profiles and 11°/30m at 86° for J-shaped profiles. The DLS requirement for S-shaped profiles is out of the achievable build rate in the planned hole size of 12 1/4". Furthermore, it was found that the minimum DLS requirement in an S-shape would be 12°/30m at 140°. Therefore an S-shaped profile cannot be constructed and relief wells have to be planned as J-shaped trajectories.

The build rate that was found to be most effective in J-shaped profiles in Wisting results in a profile similar to the high DLS relief well strategy (10°/30m) devised for the discovery. Additionally, such a trajectory would land out horizontally in the cap rock and not penetrate the reservoir formations. A further reduction in the sail angle would require a disproportional increase in the DLS. Thus, the high DLS design was identified as the most beneficial trajectory for relief wells.

Positive displacement motors and rotary steerable systems were compared concerning their working principle and impact on the drilling performance. This showed that where applicable, rotary steerables have an advantage over motors and could bring an improvement to constructing the profile build section. However, for the section hole size, only one rotary steerable system is advertised whose maximum build rate capacity as per manufacturer specifications equals the requirements of the high DLS relief well design. Therefore, it is safer to construct the build section of a relief well with a motor, unless field experience in comparable well sections in Wisting show that the RSS is capable of delivering the high build rate. The development of large high build rate capacity RSS should be investigated.

To enhance the intersection of the target well with the proposed J-shaped profile, the wellbore positioning accuracy needs to be enhanced. For this reason, a passive seismic event positioning method that was applied in reservoir and cap rock monitoring in Wisting was evaluated. The evaluation showed that the method is not independent of the survey measurements, in that it uses survey data for calibration and thus positions the signals relative to the survey data. It is therefore not suitable to reduce the wellbore positioning uncertainty compared to wellbore survey measurements. Other methods that provide independent positional measurement need to be developed and the accuracy of the wellbore position based on survey measurements needs to be further improved.

Chapter 6 Discussion

The relationship between DLS and sail angle for S-shaped and J-shaped trajectories developed in this thesis are limited to 2-dimensional profiles that do not experience a change in azimuthal direction. This is a special theoretical case that allows those profiles to be planned with the additional consideration of build rate effectiveness, but it limits the further application of the concept to modern, 3-dimensional profiles. In the author's opinion, the concept can be expanded to other trajectories or sections of trajectories that require a change in inclination and azimuth, where the rate of change is a limiting factor. Such a trajectory section could be a slide – rotate section when correcting the wellpath with a PDM, resulting in a "mini-J-shape" in the well. While this action is performed based on the experience of the directional driller, the most effective DLS can offer a key performance indicator (KPI) for the individual sections and provide an additional input in planning the length of the slide and rotate interval for inexperienced personnel. This application requires the generalization of the relationship to the 3-dimensional case, which could be part of future research.

The evaluation of the passive seismic event positioning method yielded no improvement for wellbore positioning. The examined method converts the arrival time curves from the seismic domain to the depth domain, thereby requiring survey data as input for the subsurface model. Without this conversion, it is believed that arrival time curves resulting from sources in the subsurface would be identical for identical positions of the source in unaltered conditions. This opens the possibility of drilling in the depth-independent seismic domain if the drilling activity is tracked continuously on a fixed receiver array. To the author's knowledge, geophysical investigation is ongoing in Wisting and could provide the potential for "drilling in the seismic domain" in the future.

Appendix A

A.1 Relationship between lower and upper sail angle limit

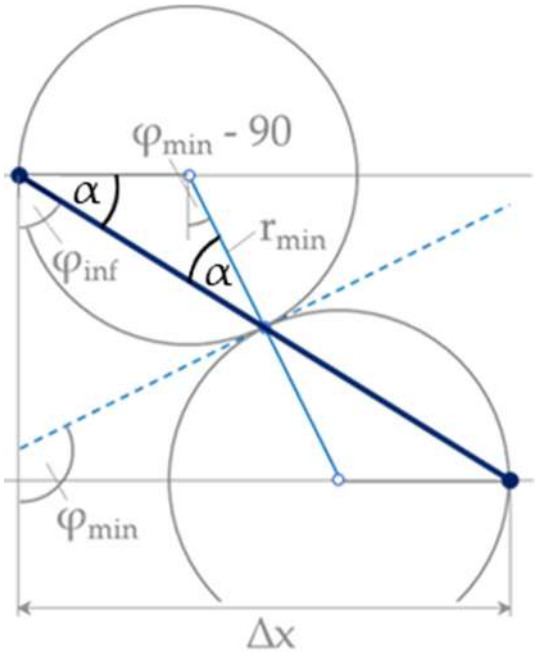

$$\alpha = 90 - \varphi_{inf}$$

$$\varphi_{min} = 180 - 2\alpha = 180 - 2(90 - \varphi_{inf})$$

$$\varphi_{min} = 2\varphi_{inf} \quad (4)$$

A.2 Minimum DLS

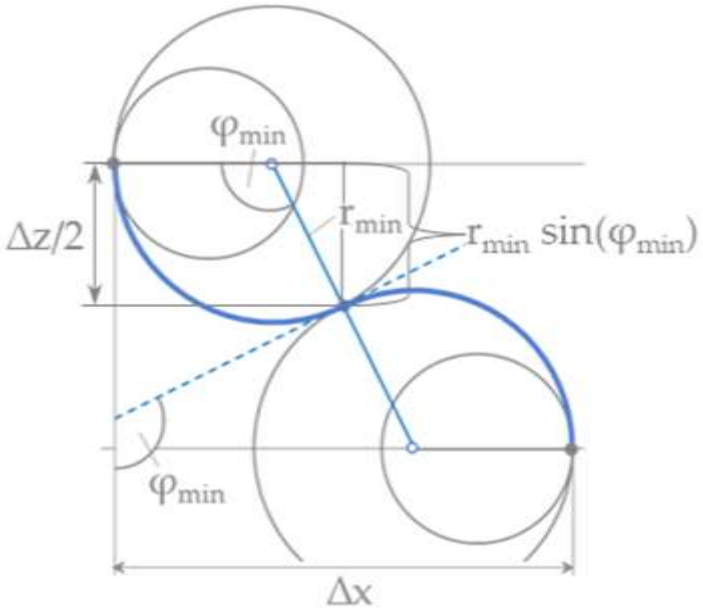

$$r = \frac{180}{\pi\ DLS} \tag{2}$$

$$r_{min} = \frac{180}{\pi\ DLS_{min}} = \frac{30 * 180}{\pi\ \delta_{min}}$$

$$\frac{\Delta z}{2} = r_{min} \sin(\varphi_{min})$$

$$\frac{\Delta z}{2} = \frac{30 * 180}{\pi\ \delta_{min}} \sin(\varphi_{min})$$

$$\delta_{min} = \frac{2 * 30 * 180 \sin(\varphi_{min})}{\Delta z\ \pi} = \frac{10800 \sin(\varphi_{min})}{\Delta z\ \pi} \tag{6}$$

A.3 Relationship between dogleg and sail angle

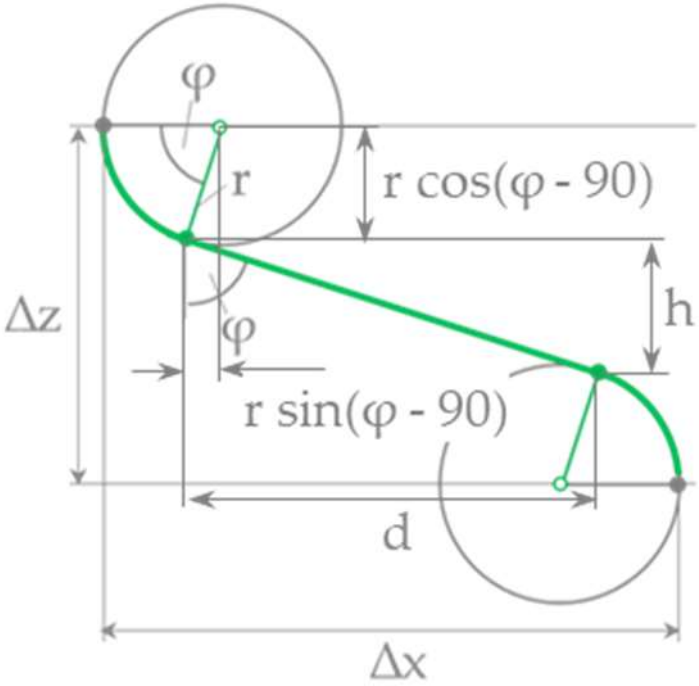

$$d = \Delta x - 2r - 2r\ sin(\varphi - 90)$$

$$h = \Delta z - 2r\ cos(\varphi - 90)$$

$$\tan(\varphi) = \frac{d}{h} = \frac{\Delta x - 2r - 2r\ sin(\varphi - 90)}{\Delta z - 2r\ cos(\varphi - 90)}$$

$$\Delta x - 2r - 2r\ sin(\varphi - 90) = \tan(\varphi)\ (\Delta z - 2r\ cos(\varphi - 90))$$

$$2r(1 + \sin(\varphi - 90) - \cos(\varphi - 90)\tan\varphi) = \Delta x - \Delta z \tan\varphi$$

$$r = \frac{\Delta x - \Delta z \tan\varphi}{2(1 + \sin(\varphi - 90) - \cos(\varphi - 90)\tan\varphi)} = \frac{30 * 180}{\delta\ \pi}$$

$$\delta = \frac{10800\ (1 + \sin(\varphi - 90) - \cos(\varphi - 90)\tan\varphi)}{\pi\ (\Delta x - \Delta z \tan\varphi)} \quad (8)$$

A.4 Derivative of dogleg with respect to sail angle

$$\delta = \frac{10800}{\pi}\left[(1 + \sin(\varphi - 90) - \cos(\varphi - 90)\tan\varphi)(\Delta x - \Delta z \tan\varphi)^{-1}\right] \tag{8}$$

$$\delta' = \frac{10800}{\pi}\left[\frac{\cos(\varphi - 90) - \frac{\cos(\varphi - 90)}{cos^2(\varphi)} - \sin(\varphi - 90) * \tan(\varphi)}{(\Delta x - \Delta z \tan\varphi)} - \frac{\frac{\Delta z}{cos^2(\varphi)}(1 + \sin(\varphi - 90) - \cos(\varphi - 90)\tan\varphi)}{(\Delta x - \Delta z \tan\varphi)^2}\right]$$

$$\delta' = \frac{10800}{\pi}\left[\frac{(\sin(\varphi - 90) * \tan\varphi - \cos(\varphi - 90) * \cos^{-2}\varphi + \cos(\varphi - 90))}{(\Delta x - \Delta z \tan\varphi)} + \frac{\Delta z \cos^{-2}\varphi\,(1 + \sin(\varphi - 90) - \cos(\varphi - 90)\tan\varphi}{(\Delta x - \Delta z \tan\varphi)^2}\right] \tag{9}$$

Bibliography

Amundsen, P A, S Ding, B K Datta, T Torkildsen, und A Saasen. 2008. „Magnetic Shielding during MWD Azimuth Measurements and Wellbore.“ *Indian Oil and Gas Technical Conference.* Mumbai: Society of Petroleum Engineers.

Arsentiev, Anatoly, David H Hathaway, and Rodney W Lessard. 2013. “Blowing in the Solar Wind: Sun Spots, Solar Cycles and Life on Earth.” *Oilfield Review*, Autumn: 48-60.

Bergfjord, Endre, Tatiana Thiem, Hugo Ruiz, and John Even Lindgård. 2018. *Report of the DrillWatch operation at well 7324/8-3.* Report, Octio AS.

Bryan, Sonny, Joe Cox, Dennis Blackwell, Fred Slayden, and Siva Naganathan. 2009. “High Dogleg Rotary Steerable System: A Step Change in Drilling Process.” *SPE Annual Technical Conference and Exhibition.* New Orleans: Society of Petroleum Engineers.

Buchanan, Andrew, Carol A Finn, Jeffrey J Love, William E Worthington, Fraser Lawson, Stefan Maus, Shola Okewunmi, and Benny Poedjono. 2013. “Geomagnetic Referencing - The Real-Time Compass for Directional Drillers.” *Oilfield Review*, Autumn: 32-47.

Bugge, Tom, Geir Elvebakk, Stein Fanavoll, Gunn Mangerud, Morten Smelror, Hermann M Weiss, John Gjelberg, Stein Erik Kristensen, and Kåre Nilsen. 2002. “Shallow stratigraphic drilling applied in hydrocarbon exploration of the Nordkapp Basin, Barents Sea.” *Marine and Petroleum Geology 19* 13-37.

Carden, Richard S, and Robert D Grace. 2007. *Horizontal and Directional Drilling.* Tulsa: PetroSkills, LLC.

Clement, William P. 2008. *Writting and Thinking Well.* 2 February. Accessed July 13, 2016. http://cgiss.boisestate.edu/~billc/Writing/writing.html.

de Wart, John P, Steve Mullin, John L Thorogood, John Wright, and Robert Bacon. 2013. “Well Bore Collision Avoidance and Interceptions - State of the Art.” *SPE/IADC Drilling Conference and Exhibition.* Amsterdam: SPE/IADC Drilling Conference and Exhibition.

Edvardsen, I, E Nyrnes, M G Johnsen, T L Hansen, U P Løvhaug, and J Matzka. 2014. “Improving the Accuracy and Reliability of MWD/Magnetic-Wellbore-Directional Surveying in the Barents Sea.” *SPE Drilling & Completion* 215-225.

Esketh, Roger, and John Weston. 2010. “Wellbore Positions Obtained While Drilling by the Most Advanced Magnetic.” *2010 IADC/SPE Drilling Conference and Exhibition.* New Orleans: IADC/SPE Drilling Conference and Exhibition.

Fageraas, Bjarte. 2012. “Ethernet on the seabed.” *Oilfield Technology.*

Flores, Vanessa, Penny Dailey, David Todd, Rohit Mathur, and Brian Donadieu. 2014. “Relief Well Planning.” SPE Conference Paper.

Gharib, Hossam, and Kennedy Kirkhope. 2017. "A Modified Three-Point Contact Approach for Dogleg Severity Modeling." *SPE Middle East Oil & Gas Show and Conference.* Manama: Society of Petroleum Engineers.

Goobie, Roger B, William T Allen, Barbara M Lasley, Kent Corser, and Jose Patino Perez. 2015. "A Guide to Relief Well Trajectory Design using Multidisciplinary Collaborative Well Planning Technology." London: SPE/IADC Drilling Conference and Exhibition.

Gyrodata. n.d. "Product Spec Sheet Wellguide RSS Point-the-Bit Rotary Steerable System." *Wellguide RSS Point-the-Bit Rotary Steerable System.* Accessed October 2018, 8. http://www.gyrodata.com/services/drilling-services/well-guide-rss/.

Haldorsen, Jakob B U , David Linton Johnson, Tom Plona, Bikash Sinha, Henri-Pierre Valero, and Kenneth Winkler. 2006. "Borehole Acoustic Waves." *Oilfield Review* 18 (1): 34-42.

Halliburton. 2018. *Halliburton Rotary Steerable Systems.* Accessed October 8, 2018. https://www.halliburton.com/en-US/ps/sperry/drilling/directional-drilling/rotary-steerables/rotary-steerable-solutions.html?node-id=hfvq7ixu.

Heisig, G, G Cavallaro, P Jogi, J Hood, and I Forstner. 2004. "Continuous Borehole Curvature Estimates While Drilling Based on Downhole Bending." *SPE Annual Technical Conference and Exhibition.* Houston: Society of Petroleum Engineers.

Hollinger, Gerald, Stephan Trauner, Christoph Dupuis, Anke Simone Wendt, Dag Helge Breivik, and Odd Helege Myrvoll. 2017. "Transformation of Mindset - Cost Effective Collaborative Well Engineering & Operation Delivers Record Horizontal Appraisal Well in the Barents." *SPE/IADC Drilling Conference and Exhibition.* The Hague: SPE/IADC.

Janwadkar, S, O Hummes, Peter M Freeman, S Privott, D Greene, and C Loesel. 2011. "Overvoming Challenges for Drilling High-Dogleg-Severity Curves." *SPE/IADC Conference and Exhibition.* Amsterdam: SPE/IADC Drilling Conference and Exhibition.

Kabirzadeh, Hojjat, Elena Rangelova, Gyoo Ho Lee, Jaehoon Jeong, Ik Woo, Yu Zhang, and Jeong Woo Kim. 2017. "Varianle In-FIeld Geomagnetic Referencing for Improved Wellbore Positioning in Directional Drilling." *Abu Dhabi International Petroleum Exhibition & Conference.* Abu Dhabi: Society of Petroleum Engineers.

Lubinski, Arthur, and H B Woods. 1953. "Factors Affecting the Angle of Inclination and Dog-Legging in Rotary Bore Holes." *Spring meeting of the Mid-Continent District, Division of Production.* Tulsa: American Petroleum Institute. 222-250.

Malcore, Eric, and Bruce Murray. 2010. "Do You Really Need That Rotary Steerable? An Evaluation of Applications and Comparisons with High Performance Mud Motors." *Abu Dhabi International Petroleum Exhibition & Conference.* Abu Dhabi: Society of Petroleum Engineers.

Marchand, Nicholas, and Masoud Kalantari. 2013. "A New Approach for Build Rate Estimation of Downhole Motors." *SPE Annual Technical Conference and Exhibition.* New Orleans: Society of Petroleum Engineers.

Mathis, Wolfgang, Harald Strand, and Gerald Hollinger. 2017. "Case History: How to Enable the Horizontal Development of Shallow Reservoirs." *SPE/IADC Drilling Conference and Exhibition.* The Hague: SPE/IADC.

Menand, S, K A Mills, and R Suarez. 2016. "Micro Dogleg Detection with Continuous Inclination Measurements and." *Abu Dhabi International Petroleum Exhibition & Conference.* Abu Dhabi: Society of Petroleum Engineers.

Monterrosa, Leida C, Marina Ferreira Rego, Erica Zegarra, and Ross Lowdon. 2016. "Statistical Analysis Between Different Surveying Instruments to Understand the Reliability of MWD/RSS High Resolution Surveys and its Effect in Well Trajectory Characterization." *IADC/SPE Drilling Conference and Exhibition.* Fort Worth: IADC/SPE Drilling Conference and Exhibition.

Moody, Mike, and Paul Boonen. 2005. "Borehole Quality Analysis Comparing Rotary Steerable Tools to Conventional Directional Drilling Assemblies." *AADE 2005 National Technical Conference and Exhibition.* Houston: American Association of Drilling Engineers.

Nedrum, Jack. 2015. *7324/7-3S Wisting Central II PL537: Blowout Contingency Plan - Volume 2.* OMV Document, Wild Well Control.

NORSOK. 2013. "NORSOK Standard D-010 Rev. 4." *Well integrity in drilling and well operations.* NORSOK, June.

Norwegian Petroleum Directorate. 2015. *NPD Factpages Wellbore / Exploration.* 17 September. Accessed April 30, 2018. http://factpages.npd.no/factpages/default.aspx?culture=en.

—. 2014. *The Barents Sea.* 13 November. Accessed May 14, 2018. http://www.npd.no/en/Publications/Reports/Compiled-CO2-atlas/6-The-Barents-Sea/.

Octio. 2018. "OCTIO DrillWatch Wisting." Presentation.

Oskarsen, Ray T, Ole B Rygg, Mike Cargol, and Brett Morry. 2016. "Challenging Offshore Dynamic Kill Operations Made Possible With the Relief Well Injection Spool." *SPE Deepwater Drilling & Completions Conference.* Galveston: Society of Petroleum Engineers.

Pedersen, Rune, Hans Peter Dahlslett, Anne Wenke, Sønnøve Mclvor, und Svein Olav Drangeid. 2016. „Development of a Robust and Cost Efficient Solution for Oil Spill Response for Barents Sea Exploration." *SPE International Conference and Exhibition on Health, Safety, Security, Environment, and Social Responsibility.* Stavanger: Society of Petroleum Engineers. 2.

Petroleum Safety Authority Norway. 2014. *Drilling and well technology: Bit of a rough ride.* 20 February. Accessed July 05, 2018. http://www.ptil.no/disciplined-issues/drilling-and-well-technology-bit-of-a-rough-ride-article10452-1144.html.

Poletto, Flavio, and Francesco Miranda. 2004. *Seismic While Drilling Fundamentals of Drill-Bit Seismic for Exploration.* 1st. Elsevier Ltd.

Ripperger, Georg. 2015. *Enhanced Rig Classification System: Impact and Limitations of Torque and Drag, Buckling, and Hydraulics on the Drilling Envelope.* Leoben.

Schlumberger. 2011. "PowerDrive Archer High Build Rate Rotary Steerable System." 28 March. Accessed October 9, 2018. www.aade.org.

—. 2018. *PowerDrive Xceed Ruggedized Rotary Steerable System.* Accessed October 8, 2018. https://www.slb.com/services/drilling/drilling_services_systems/directional_drilling/powerdrive_family/powerdrive_xceed.aspx.

—. 2004. "PowerPak Steerable Motor Handbook." *Schlumberger.* December. Accessed October 1, 2018. https://www.slb.com/~/media/Files/drilling/brochures/directional_drilling/powerpak_handbook.pdf.

—. 2018. *Video: PowerDrive Archer High Build Rate Rotary Steerable System.* Accessed October 8, 2018. https://www.slb.com/resources/VideoListingPage/video.aspx?id=83276661-2720-454B-B62E-EB1FF1469EF5.

Simm, Robert, and Mike Bacon. 2014. *Seismic Amplitude: An Interpreter's Handbook.* Cambridge University Press.

Sivertsen, Trond, and Harald Strand. 2011. "New Well Foundation Concept, As Used at a Norwegian Sea Well." *SPE Arctic and Extreme Environments Conference & Exhibition.* Moscow: Society of Petroleum Engineers.

Smelror, Morten, Alte Mørk, Eric Monteil, David Rutledge, and Han Leereveld. 1998. "The Klippfisk Formation - a new lithostratigraphic unit of Lower Cretaceous platform carbonates on the Western Barents Shelf." *Polar Research 17(2)* 181-202.

Society of Petroleum Engineers. 2014. "Society of Petroleum Engineers Style Guide 2014-2015."

Stoneley, R. 1924. „Elastic Waves at the Surface of Separation of Two Solids." *Proceedings of the Royal Society of London Series A* 416-428.

Sugiura, Junichi. 2008. "Systematic Testing with Push- and Point-the-Bit Rotary Steerable Systems Leads to the Optimal BHA Design for Stability, Steerability and Borehole Quality." *AADE Fluids Conference and Exhibition.* Houston: American Association of Drilling Engineers.

Swiss Academic Software. n.d. *Citavi - Organize your knowledge. Reference management, knowledge organization, and task planning.* Accessed May 24, 2016. https://www.citavi.com/.

Tipu, Imran, Eman Alawadhi, R Kumar, Batyr Amanov, Mohamed A El Gebaly, A M Al-Hammadi, A M Bin Shamlan, et al. 2015. "Bending Rules with High Build Rate RSS." *Abu Dhabi International Petroleum Exhibition and Conference.* Abu Dhabi: Society of Petroleum Engineers.

Trauner, Stephan. 2017. *Blowout Contingency Plan - Wisting Central III.* OMV Document, OMV (Norge) AS.

Trauner, Stephan. 2016. *Wisting Central II.* Presentation, Stavanger: OMV Norge (AS).

Tribe, I R, L Burns, P D Howell, and R Dickson. 2003. "Precise Well Placement With Rotary Steerable Systems and Logging-While-Drilling Measurements." *2001 SPE Annual Technical Conference and Exhibition.* New Orleans: Society of Petroleum Engineers. 42-49.

Ulaeto, Ubong, Zimuzo Nwobi, Hamza Ibrahim, Emmanuel Ubadigha, and Ndidi Asiodu. 2018. "Reducing TVD Uncertainties Using Dual Inclination and SAG Model." *Nigeria Annual Conference and Exhibition.* Lagos: Society of Petroleum Engineers.

Veire, Helene Hafslund. 2017. *Introduction to Wisting.* Presentation, OMV Upstream.

Veire, Helene Hafslund, John Reidar Granli, Eirik Stueland, Kjetil Ivar Krathus-Larsen, and Erika Angerer. 2018. "Preparing for Geophysical Surveillance at Wisting." *80th EAGE Conference and Exhibition 2018.* Copenhagen: EAGE.

Warren, T. 2006. "Steerable Motors Hold Out Against Rotary Steerables." *SPE Annual and Technical Conference and Exhibition.* San Antonio: Society of Petroleum Engineers.

Weatherford. 2018. *Revolution® Rotary Steerable System.* Accessed October 8, 2018. https://www.weatherford.com/en/products-and-services/drilling/drilling-services/rotary-steerable-systems/point-the-bit-rss/.

Wolf, Adrian. 2016. *Relief well strategy: Barents Sea Exploration Collaboration BaSEC.* OMV Document, OMV.

Wu, M, and D C-K Chen. 2006. "A Generic Solution to Bottomhole-Assembly Modeling." *SPE Annual Technical Conference and Exhibition.* San Antonio: Society of Petroleum Engineers.

Acronyms

DLS	Dogleg severity
EOB	End of build
EOD	End of drop
EOT	End of tangent
KOP	Kick off point
NPD	Norwegian Petroleum Directorate
PDM	Positive displacement motor
ROP	Rate of penetration
RSS	Rotary Steerable System
SOD	Start of drop

Symbols

DLS	dogleg severity	[°/30 m]
δ	curvature	[rad]
φ	sail angle	[°]
r	radius	[m]
Δx	horizontal offset between KOP and EOD/EOT	[m]
Δz	vertical depth between KOP and EOD/EOT	[m]

List of Figures

Figure 1: Production Licence 537 in the Norwegian Barents Sea. (Modified after Norwegian Petroleum Directorate n.d.). 3
Figure 2: Schematic of Wisting Central. After Norwegian Petroleum Directorate (2015). 5
Figure 3: High-resolution seismic cross section in Wisting. From Veire (2007). 6
Figure 4: Wisting Central II trajectory profile 7
Figure 5: Inclination and azimuth survey data from Wisting Central II 8
Figure 6: Schematic of Wisting Central II. After Norwegian Petroleum Directorate (2016). 10
Figure 7: Planned relief well surface locations for Wisting Cental II and Wisting Central III. After Nendrum (2015) and Trauner (2017). 16
Figure 8: Schematic of J-shaped relief well profile and contingency solution. After Wolf (2016) 17
Figure 9: Schematic of S-shaped and J-shaped relief well trajectory 18
Figure 10: Relief well trajectories for high, medium, and low DLS strategy. After Wolf (2016). 20
Figure 11: S-shaped profiles at different Δx/Δz intersecting a vertical target wellbore 22
Figure 12: Possible trajectory parameters at fixed Δx/Δz. 23
Figure 13: Sheave model for S-shaped trajectory 25
Figure 14: Upper and lower limit for sail angle as function of Δx/Δz. 26
Figure 15: Low, medium, and high relief well strategy visualised as S-shape trajectories. 26
Figure 16: Minimum DLS in S-shape for vertical depth of Δz = 175 m and Δz = 500 m. 27
Figure 17: DLS vs sail angle behaviour and most effective DLS in S-shaped trajectory under conditions in Wisting. 29
Figure 18: Sheave model for J-shaped trajectory 30
Figure 19: Minimum DLS and most effective DLS in J-shape for vertical depth of Δz = 175 m and Δz = 500 m. 31
Figure 20: Upper and lower limit for sail angle and most effective sail angle in J-shape for vertical depth of Δz = 175 m and Δz = 500 m as function of Δx/Δz. 31
Figure 21: DLS vs sail angle behaviour and most effective DLS in J-shaped trajectory under conditions in Wisting. 32
Figure 22: DLS vs sail angle for J-shaped trajectories for low, medium, and high DLS relief well startegy 33
Figure 23: Most effective sail angle and upper and lower limit sail angle for Wisting Central II and III. 35
Figure 24: Most effective DLS and minimum DLS for Wisting Central II and III. 35
Figure 25: DLS vs sail angle for Wisting Central II potential relief well spud locations. 36
Figure 26: Most effective J-shaped relief well trajectories for Wisting Central II. 36
Figure 27: DLS vs sail angle for Wisting Central III potential relief well spud locations. 37
Figure 28: Most effective J-shaped relief well trajectories for Wisting Central II. 37
Figure 29: Maximum DLS capability as per tool specifications of various service providers' RSS 44
Figure 30: Effect of well trajectory between subsequent survey stations 48
Figure 31: Ray path in layered medium. From Simm and Bacon (2014, 21) 54
Figure 32: Ray path modelled for a seismic event in Wisting. From Bergfjord et al. (2018). 55
Figure 33: Cable layout around wellhead of Wisting Central III. (After Bergfjord, et al. (2018)) 57
Figure 34: Distance of nodes from wellhead 57
Figure 35: Perforation shot at 642m in Stø Formation. From Bergfjord, et al. (2018) 58

List of Tables

Table 1: Relief well parameters for high, medium, and low DLS strategy. After Wolf (2016). 19
Table 2: Wisting relief well trajectory confining conditions. After Nedrum (2015) and Trauner (2017). 34
Table 3: Most effective DLS and sail angles for J-shaped trajectory; DLS to build to 90°. 38